

EVALUATION AND
QUANTIFICATION OF ENGINEERED
FLOCS AND DRINKING WATER
TREATABILITY

by

Adam Arnold

A thesis
presented to the University of Waterloo
in fulfillment of the
thesis requirement for the degree of
Master of Applied Science
in
Civil Engineering

Waterloo, Ontario, Canada, 2008

© Adam Arnold

Author's Declaration

I hereby declare that I am the sole author of this thesis. This is a true copy of the thesis, including any required final revisions, as accepted by my examiners.

I understand that my thesis may be made electronically available to the public.

Adam Arnold

Abstract

The provision of safe drinking water requires adequate inactivation of pathogenic organisms. Common drinking water disinfection technologies become decreasingly effective as levels of additional particulate matter in waters to be treated increases. Therefore, solids removal processes must always precede drinking water disinfection assuming there is enough particulate matter to warrant them, and chemical pre-treatment techniques enhance their efficiency. A treatment plant must be robust or resilient to challenge. With the coming changes in climate, there will be a heightened need to respond to increased variability (Cromwell *et al.*, 2007).

Jar tests are performed to simulate full-scale pre-treatment and particle removal processes. Operators typically conduct them in an effort to attempt alternative treatment doses and strategies without altering the performance of the full-scale drinking water treatment plant. However, information obtained from these tests must be evaluated judiciously, as they currently focus on reduction of specific water quality parameters (i.e., ultraviolet absorption at 254 nm and turbidity), and measuring and understanding the significance of coagulant dose on floc size. Consideration of aggregate structure has been less explored due mainly to a lack of appropriate theories to describe the complex random floc structure. Improving the predictive capacity of bench-scale protocols commonly used for optimizing conventional chemical pre-treatment in full-scale drinking water treatment plants is required.

Using protocols and raw water from the Mannheim Water Treatment Plant (MWTP) in Kitchener, Ontario, Canada, twelve (12) jar tests were performed throughout this investigation. The ultraviolet absorption at 254 nm (UV_{254}) and turbidity of the supernatant were evaluated during each jar test to investigate potential relationships between these parameters and floc settling rates and structure. Six (6) jar tests were conducted to generate aggregates for settling tests. Samples were collected after a period of settling from the bottom of the jars so that it could be determined whether or not the settling rates and/or sizes of the aggregates that had settled would correspond to the UV_{254} and turbidity of the supernatant. The six (6) jar tests were then repeated to characterize the fractal structure of the flocs by digital image analysis with microscopy. Structural characteristics were calculated from samples of aggregates that were collected prior to settling. This was done to predict particle removal performance (i.e., based on turbidity reduction) by using the floc structural information of the aggregates generated during coagulation and flocculation. Samples of aggregates generated at full-scale at the MWTP were then collected and compared to the results of the bench-scale testing. This analysis was conducted to determine the extent to which bench-scale tests truly simulate full-scale coagulation and flocculation processes.

At the conditions investigated, either alum or polyaluminum chloride (PACl) coagulation at a dose of ~ 30 mg/L in conjunction with 0.2 mg/L of cationic polyelectrolyte can achieve the lowest levels of UV_{254} and turbidity (i.e., 0.02 to 0.05 AU and 0.3 to 1.0 NTU, respectively) after flocculation and a period of settling. Results from the settling tests indicated that the

production of larger and more settleable flocs could not be described by floc settling velocities and floc sizes. Settling velocities were not directly related to either UV_{254} or turbidity reductions. Results of the floc characterization tests indicated that measured values of UV_{254} and turbidity of the supernatant were generally inversely proportional to aggregate D_{90} ; that is, the residual UV_{254} and/or turbidity decreased as the value of D_{90} increased, which may have been indicative of flocculent settling. No direct relationship could be discerned between D_1 (i.e., floc shape) and the UV_{254} and turbidity of the supernatant; however, the turbidity after flocculation and a period of settling appeared to be inversely proportional to D_2 (i.e., porosity). Overall, the results of the experiments have demonstrated that grain size distributions and fractal dimensions might be used to assess and/or predict pre-treatment and/or particle removal performance. Specifically, the relationship between D_{90} values calculated from samples of flocculated water prior to settling and UV_{254} and turbidity values of that water after a period of settling may be a simple tool that can be utilized to describe and potentially better predict flocculent settling performance. At present, this appears to be the first such tool of its kind that has been reported.

Full-scale sampling at the MWTP, however, indicated that the size and structure of aggregates generated at bench-scale at the MWTP were clearly not indicative of the size and structure of those produced at full-scale. The aggregates that were generated at full-scale were much smaller and denser than those that were produced in any of the tests (i.e., under all conditions considered). At the MWTP at present, the only reliable indicator of full-scale performance is full-scale data because jar tests are not indicative of full-scale performance (i.e., floc formation). Additional experimentation at the MWTP is required that focuses primarily on optimizing the bench-scale tests utilized to improve full-scale performance predictability.

Acknowledgements

First and foremost, I would like to thank my supervisor, Dr. Monica Emelko for her guidance, advice and support. Throughout the past six years, she has truly been a mentor to me and I don't even think that dinner at Charbries every day for the coming six years would sufficiently express my gratitude. I would also like to thank her husband, Dr. Mike Stone, for his counsel; I do not believe that I would have been able to grasp the concept of a fractal dimension if it was not for him.

To Tim Walton and Snjezana Kozomara at the Mannheim Water Treatment Plant; Tim for his interest in the project and aid in coordinating various stages and Snjezana for assisting with sampling and jar test preparation- thank you both for everything! A very special thank you, as well, to Ian Droppo and his group (Christine Jaskot, Brian Trapp and Samantha Deignan) at the Canadian Center for Inland Waters for the use of their settling column and for taking the time to ensure that the tests were done correctly and efficiently. And if it was not for Erin Harvery at the Statistics Help Desk and Lisa Tomalty-Crans in the Graduate Studies Office, it might have taken me an additional two years to analyze the data and format this document.

To the undergraduate students who spent countless hours in the laboratory measuring the properties of floc and/or conducting water quality analysis; Kim Thomas, Kate Geng, Emily Vance, and Jeff Ho- your hard work is truly appreciated. Of course, making sense of the laboratory equipment would not be possible without the help of the Water Resources lab technicians- Mark Sobon and Bruce Stickney. The two of them continue to make life for graduate students considerably less frustrating.

To my fellow MBE group colleagues, Phil Schmidt, Dave Scott, Ryan Snyder and Katie Higgins, specifically, for their respective contributions to my work and/or graduate student experience. Speaking of which, I doubt that I would have enjoyed my time at UW as much if it were not for my good friends Pat O'Neill, Leigh Davis, Maureen O'Connell and Paul Javor. Your friendship means a great deal to me and I cannot possibly thank you enough for the encouragement, support and most importantly- the laughs.

To my entire family, thank you for your constant reassurance and belief that I am capable of achieving anything that I put my mind to. Specifically, I want to thank my parents; two people who have recently endured tremendous adversity. Their courage and perseverance has been an inspiration to me and I dedicate this thesis to them.

Finally, and most importantly, I'd like to thank my wife, Brenda, for her unending love and support. She is a beautiful, intelligent, caring and compassionate woman and I am absolutely honored to be her husband. Words cannot describe how happy she makes me feel and how proud I am of her countless achievements. In one of my previous lives, I must have done something really fantastic to deserve this wonderful marriage.

Table of Contents

List of Tables	viii
List of Figures	ix
List of Acronyms	xi
1 INTRODUCTION.....	1
1.1 Research Motivation	3
1.2 Objectives and Scope	4
1.3 Research Approach	5
1.4 Thesis Organization	6
2 BACKGROUND.....	7
2.1 Particles in Natural Systems	7
2.1.1 Particles Derived from Atmospheric Sources	8
2.1.2 Particles Produced by Chemical and Biological Processes.....	9
2.1.3 Particles Derived from Municipal and Agricultural Waste Discharge.....	9
2.2 Particle Removal Processes	10
2.2.1 Sedimentation	11
2.2.2 Coagulation	16
2.2.2.1 Particle Destabilization Mechanisms.....	17
2.2.2.2 Types of Coagulants	19
2.2.3 Flocculation	24
2.3 Bench-Scale Testing	27
2.3.1 Ultraviolet Absorption at 254 nm (UV ₂₅₄).....	29
2.3.2 Turbidity.....	30
2.3.3 Floc Size and Shape	31
2.4 Fractal Geometry	34
2.4.1 Fractal Dimensions.....	36
2.4.2 Practical Application of Fractal Dimensions for Water Treatment	38
2.5 Methods for Characterizing Floc Structure	41
2.5.1 Light Microscopy, Photography and Image Analysis	42
2.5.2 Light Scattering	43
2.5.3 Settling	44
2.5.4 Selecting a Characterization Technique	46
2.6 Research Needs	47
3 MATERIALS AND METHODS	49
3.1 Research Rationale and Methodology	49
3.2 The Mannheim Water Treatment Plant (MWTP)	51
3.3 MWTP Jar Test Protocol.....	54
3.3.1 Reagent Preparation	55
3.3.2 Jar Testing Procedure.....	57
3.3.3 Water Quality Analyses.....	59
3.3.3.1 Turbidity.....	59
3.3.3.2 Total Organic Carbon (TOC).....	59
3.3.3.3 Ultraviolet Absorption at 254 nm (UV ₂₅₄).....	60
3.3.3.4 Conductivity.....	60
3.3.3.5 pH.....	60
3.4 Settling Experiments	60
3.5 Floc Characterization	62
3.5.1 Floc Sampling.....	62
3.5.2 Light Microscopy and Digital Image Analysis.....	64
3.5.3 Fractal Analysis.....	65
3.5.4 Calculation of Variability in the Fractal Data	66

3.5.5	Statistical Assessment of Light Microscopy and Digital Image Analysis	67
3.5.5.1	Experimental Design.....	68
3.5.5.2	Statistical Analysis of Precision	70
3.6	Full-Scale Floc Sampling at the MWTP.....	70
4	RESULTS AND DISCUSSION.....	72
4.1	Jar Test Results.....	73
4.2	Settling Test Results.....	82
4.3	Floc Characterization Results.....	89
4.3.1	Difficulties in Collecting Reliable Floc Characterization Data.....	100
4.4	Full-Scale Floc Sampling Results	107
4.4.1	The Importance of Full-Scale Performance Prediction.....	110
5	CONCLUSIONS	112
6	RECOMMENDATIONS	115
	References	117

Appendices

Appendix A	Common Equivalent Spherical Diameters for Characterizing Floc	126
Appendix B	MWTP Jar Test Protocol Sample Data Sheet	127
Appendix C	Jar Test Results: Water Quality Analyses Data	128
Appendix D	Mannheim Water Treatment Plant Operating Strategy Review: Jar Test Results	131
Appendix E	Settling Column Test Results	134
Appendix F	Particle Size Distribution Data	139
Appendix G	Fractal Regression Confidence Intervals	152
Appendix H	Fractal Analysis Results	154
Appendix I	Statistical Assessment SPSS Output.....	162

List of Tables

Table 2.1: Particle settling regimes (Gregory <i>et al.</i> , 1999).....	13
Table 2.2: Particle transport mechanisms in a destabilized suspension (Metcalf and Eddy, 2003).	25
Table 2.3: Recent publications relating to the application of fractal dimension measurements (modified from Jefferson and Jarvis, 2006).....	39
Table 2.4: Advantages and Disadvantages of floc structural characterization techniques (modified from Jarvis <i>et al.</i> , 2005).....	46
Table 3.1: Nominal raw water quality characteristics of Grand River water at the MWTP.	53
Table 3.2: Physical and Chemical Properties of Alum and PACl.	55
Table 3.3: Physical and Chemical properties of Magnafloc LT 22 S.	56
Table 3.4: Quantities of Dilute Coagulant and Polymer Solutions required for Jar Testing.	57
Table 4.1: Raw water quality data for all twelve jar test experiments (mean \pm std. deviation).	73
Table 4.2: Structural characterization data of flocs in the flocculation basin, and at the outlet of the inclined plate settlers at the MWTP.....	107

List of Figures

Figure 2.1: Suspended (left) and colloidal (right) material in the natural environment.....	7
Figure 2.2: Early patent for inclined plate settling (Barham et al., 1956).	12
Figure 2.3: The Electrical Double Layer and related potential energy (Letterman, 1999).	18
Figure 2.4: Example of interparticle bridging.	18
Figure 2.5: Solubility of $\text{Al}(\text{OH})_3$ (modified from Sawyer <i>et al.</i> , 2003).	21
Figure 2.6: Coagulation diagram for alum and PACl (Amirtharajah and Mills, 1982).	23
Figure 2.7: A typical, fundamental drinking water treatment sequence in North America.	24
Figure 2.8: A Phipps & Bird standard jar tester (Grammer, 2007).	29
Figure 2.9: Depiction of the various longest dimension (L_D) measurements.	31
Figure 2.10: Conceptual depiction of an equivalent spherical diameter (ESD).....	32
Figure 2.11: An example of a grain-size distribution curve.	33
Figure 2.12: Conceptual depiction of a fractal structure (modified from Mandelbrot, 1982).	35
Figure 2.13: Coastline of Britain measured by two different length ($a = 5$, $b = 31$) measuring sticks (modified from Jefferson and Jarvis, 2006).	36
Figure 2.14: Steps involved in digital image analysis (modified from Jarvis <i>et al.</i> , 2005).	43
Figure 2.15: Example of a settling column for characterizing flocs.	45
Figure 3.1: The Mannheim Water Treatment Plant in Kitchener, ON (Emelko <i>et al.</i> , 2006).	52
Figure 3.2: Jar testing equipment used during the MWTP jar test protocol.	54
Figure 3.3: G-values for a standard Phipps and Bird Jar Tester (Grammer, 2007).	58
Figure 3.4: 2.5 L capacity settling column with a stereoscopic microscope.	61
Figure 3.5: 25 mL plastic sampling columns for sampling of suspended particles and/or floc.	63
Figure 3.6: Engineered flocs settled onto 0.45 μm Millipore HA filters.....	63
Figure 3.7: Wild Leitz inverted light microscopy microscope fitted with a Sony XC75 CCD camera connected to a Pentium computer.	64
Figure 3.8: Systematic evaluation of the 0.45 μm Millipore HA filters.	69
Figure 3.9: Full-scale sampling sites at the Mannheim Water Treatment Plant.....	71
Figure 4.1: UV_{254} values of supernatant obtained from jar tests conducted during settling experiments ("optimal" range dependent on conditions).	74
Figure 4.2: UV_{254} values of supernatant obtained from jar tests conducted during floc characterization experiments ("optimal" range dependent on conditions).	75
Figure 4.3: Turbidity of supernatant obtained from jar tests conducted during settling experiments ("optimal" range dependent on conditions).	76
Figure 4.4: Turbidity of supernatant obtained from jar tests conducted during floc characterization experiments ("optimal" range dependent on conditions).	77
Figure 4.5: Alum flocs (left) and PACl flocs (right) produced during the jar tests.	78
Figure 4.6: UV_{254} values of supernatant obtained from additional alum and PACl jar tests (mean \pm 1 standard deviation, $n = 3$).	80
Figure 4.7: Turbidities of supernatant obtained from additional alum and PACl jar tests (mean \pm 1 standard deviation, $n = 3$).	80
Figure 4.8: Settling velocity as a function of floc size for flocs produced by alum coagulation at a temperature of 5 $^{\circ}\text{C}$	83
Figure 4.9: Settling velocity as a function of floc size for flocs produced by PACl coagulation at a temperature of 5 $^{\circ}\text{C}$	84
Figure 4.10: Settling velocity as a function of floc size for flocs produced by alum coagulation at a temperature of 25 $^{\circ}\text{C}$	85
Figure 4.11: Particle densities for alum flocs produced and settled at a temperature of 25 $^{\circ}\text{C}$	88
Figure 4.12: Photographs of flocs, taken during the settling column tests.....	88
Figure 4.13: Visual representation of the floc characterization experimental design.....	90
Figure 4.14: Depiction of flocculent settling of aggregates during jar testing.....	92
Figure 4.15: Particle size distribution of flocs produced by alum coagulation at 25 $^{\circ}\text{C}$	93

Figure 4.16: Comparing aggregate D_{90} to residual UV_{254} for alum coagulation at 15 °C.	95
Figure 4.17: Comparing aggregate D_{90} to residual turbidity for PACI coagulation at 5 °C.	96
Figure 4.18: Comparing aggregate D_1 to residual UV_{254} for PACI coagulation at 15 °C.	98
Figure 4.19: Comparing aggregate D_2 to residual turbidity for PACI coagulation at 5 °C.	100
Figure 4.20: Visual depiction of preferential settling on the 0.45 μm Millipore HA filters.	101
Figure 4.21: Images of engineered aggregates captured by a Sony XC75 CCD camera.	102
Figure 4.22: Linear regression to calculate D_1 value of flocs produced by alum coagulation at 5 °C.	103
Figure 4.23: Linear regression to re-calculate D_1 value of flocs produced by alum coagulation at 5 °C.	103
Figure 4.24: <i>RSD</i> as a function of the cumulative number of aggregates characterized ($n=9$).	104
Figure 4.25: <i>RSD</i> as a function of the cumulative number of particles characterized ($n=9$).	105
Figure 4.26: Possible variation of particle size distribution with depth in standard 2 L jars after fifteen (15) minutes of settling.	106
Figure 4.27: Particle size distribution of flocs in the flocculation basin, and at the outlet of the inclined plate settlers at the MWTP.	108
Figure 4.28: PACI flocs generated at the MWTP at bench-scale (left) and full-scale (right).	109

List of Acronyms

AE	Associated Engineering
ANOVA	Analysis of Variance
CCD	Closed-coupled Device
DAF	Dissolved Air Flotation
DI	Deionized
DOC	Dissolved Organic Carbon
epiDMA	epichlorohydrin dimethylamine
EPA	Environmental Protection Agency
ESD	Equivalent Spherical Diameter
HMS	Hydrolyzing Metal Salt
MOE	Ministry of the Environment
MWTP	Mannheim Water Treatment Plant
NOM	Natural Organic Matter
NTU	Nephelometric Turbidity Unit
ON	Ontario
PACl	Polyaluminum Chloride
PE	Percent Error
polyDADMAC	polydiallyldimethyl ammonium chloride
RMOW	Regional Municipality of Waterloo
RSD	Relative Standard Deviation
SCADA	Supervisory Control and Data Acquisition
TC	Total Carbon
THM	Trihalomethane
TIC	Total Inorganic Carbon
TOC	Total Organic Carbon
UV	Ultraviolet Irradiation
UV₂₅₄	Ultraviolet Absorption at 254 nm
UW	University of Waterloo
VFD	Variable Frequency Drive

1 INTRODUCTION

Despite advances in the development, protection, and treatment of water supplies, waterborne disease outbreaks continue to occur in North America. Between 1980 and 1996, 402 outbreaks were reported in the United States with over 500,000 associated cases of waterborne disease (Cohn *et al.*, 1999). In Canada, outbreaks of disease have occurred in cities including North Battleford, Kitchener-Waterloo and Walkerton within the past fifteen (15) years. Triggered by the occurrence of specific organisms, waterborne illness is usually acute in healthy individuals and is typically characterized by gastrointestinal symptoms. For the immunocompromised, however, the effects are often more severe.

Pathogens are disease-causing organisms that have been implicated in many outbreaks of waterborne disease. They include bacteria (e.g., *Escherichia coli O157:H7*), viruses (e.g., Norovirus) and protozoa (e.g., *Cryptosporidium parvum*) (Feachem *et al.*, 1993; Madigan *et al.*, 2000; Crook, 1998). The provision of safe drinking water requires adequate inactivation of pathogenic organisms. At present, the most common drinking water disinfection technologies are conventional chemical oxidation with chlorine and/or ozone and UV irradiation.

Despite proper disinfection of an unfiltered water supply with chlorination, in June 1986 more than 3000 residents of Penticton, British Columbia were impacted by an outbreak of waterborne giardiasis (Hrudey *et al.*, 2002). Such incidents underscore that pathogens and other organisms can be partially protected against the action of UV and chemical disinfection by attachment to or enmeshment in nonviable particles present in water (Stagg *et al.*, 1978; Hejkal *et al.*, 1979; Boardman and Sproul, 1977; Sproul, 1972 and Gehr *et al.*, 2003). For this reason, drinking water disinfection is typically preceded by one or more solids removal processes (e.g., sedimentation, filtration, etc.).

To maximize particle removal, coagulation and flocculation are often employed to encourage the interaction of small particles to produce larger aggregates or 'flocs'. These chemical pre-

treatment methods are often designed and operated based upon information derived from bench-scale protocols (i.e., jar tests) that are used to simulate full-scale treatment performance. By regularly performing such tests, water treatment operators can assess alternative treatment strategies without altering plant performance. Additionally, bench-scale tests are used to determine the optimum dose of coagulant which "... in most cases, saves money and in many cases a lot of money- so much money, in fact, that the initial cost of the equipment is often recovered in less than one year. In many plants where testing is not done, there is a tendency to dose a little extra 'just to be sure.' This overdosing can result in ongoing, unnecessarily high, coagulant expenses" (Satterfield, 2005).

Although bench-scale testing does typically provide a reasonable estimate for coagulant dosing, it is commonly acknowledged that the associated procedures can often be improved to better predict full-scale performance. For example, an understanding of the physical characteristics of flocs formed during water treatment is important in determining the efficiency, operation and robustness of the separation processes used to remove them (Jefferson and Jarvis, 2006). Bench-scale protocols currently focus on measuring and understanding the significance of coagulant dose on floc size. Consideration of floc structure has been less explored due mainly to a lack of appropriate theories to describe its complex random structure.

In the late 1970s, Benoit Mandelbrot of Poland introduced the concept of fractal geometry. Generally, he defined a fractal structure as "a fragmented geometric shape that can be subdivided into parts, each of which is a reduced-size copy of the whole." The development of this geometric concept has subsequently enabled demonstrations that engineered aggregates are fractal (Gorczyca and Ganczarczyk, 2001). Fractal geometry is often used to characterize wastewater sludge. In the drinking water treatment industry; however, the practical applications of fractal theory are relatively unexplored. Quantitative assessment of floc structure using particle characterization methods as a technique to improve the predictive capacity of bench-scale tests for optimizing chemical pre-treatment (i.e., coagulation,

flocculation, clarification, etc.) during conventional treatment represents one possible application.

1.1 Research Motivation

The Mannheim Drinking Water Treatment Plant (MWTP) is located in the city of Kitchener, Ontario and provides approximately 22% of the drinking water to the Regional Municipality of Waterloo (Clarke, 2007). The raw water entering the plant is surface water from the Grand River and is treated in a conventional manner (i.e., coagulation, flocculation, sedimentation, filtration and disinfection). In addition, ozone is added to control the taste and odour, oxidize any naturally occurring compounds, and to assist in disinfection. The primary disinfection processes are ultraviolet (UV) irradiation, followed by chlorination. Continuous analyzers observe levels of turbidity prior to the water being discharged. The MWTP has a design capacity of 72 MLD (i.e., 19 U.S. MGD) (Clarke, 2007).

Like many conventional plants, the MWTP has not been able to reach its operational capacity due to a variety of reasons including floc build-up on the surface of and within their filters. One possible explanation for this observation is that the pre-treatment processes are not optimized to ensure adequate solids removal in the sedimentation basins. Furthermore, data from bench scale tests have indicated better settled water turbidities and values of ultraviolet absorption at 254 nm (UV_{254}) than those being achieved at full-scale. A key limitation of the bench scale protocols used to make these preliminary assessments is that they do not consider the structure of the flocs that are produced; rather, they focus only on floc size and a settling period that can often seem arbitrary because full-scale performance can be difficult to reproduce. The need to achieve low settled water UV_{254} values and turbidities while increasing plant capacity, and the important and frequently overlooked need to improve the predictive capacity of bench-scale protocols for optimizing conventional chemical pre-treatment provided the motivation for this research.

1.2 Objectives and Scope

The primary goal of this thesis research was to improve the predictive capacity of bench-scale protocols commonly used for optimizing conventional chemical pre-treatment in full-scale drinking water treatment plants. More specifically, the objectives were to:

1. critically evaluate the limitations of traditional bench-scale tests for evaluating chemical pre-treatment performance of coagulation/flocculation/sedimentation processes;
2. investigate one or more floc characterization technique(s) that might be relevant to characterizing aggregates generated during drinking water treatment;
3. quantify the variability in floc characterization data and assess the accuracy and/or precision of the floc characterization technique(s); and
4. identify floc characterization techniques that will contribute to optimizing the predictive capacity of traditional bench-scale tests for evaluating chemical pre-treatment performance of coagulation/flocculation/sedimentation processes.

The secondary goal of this research was to provide recommendations and strategies for further optimizing conventional chemical pre-treatment at the MWTP. More specifically, the objective was to evaluate the developed pre-treatment optimization techniques at the MWTP and demonstrate opportunities for improvement. The practical contributions of this work are:

1. a state-of-the-art review of particle characterization techniques relevant to characterizing aggregates generated during drinking water treatment;
2. demonstration of the limitations of traditional bench-scale protocols commonly used to optimize conventional chemical pre-treatment during full-scale drinking water treatment and articulation of the reasons why data obtained from these tests must be evaluated judiciously; and
3. development of practical strategies for integration of key aspects of advanced particle characterization techniques into common bench-scale chemical pre-treatment protocols.

The research contributions of this work are:

1. a state-of-the-art review of particle characterization techniques relevant to characterizing aggregates generated during drinking water treatment;
2. development and demonstration of essential guidance for determining how to characterize floc populations in a statistically significant manner;
3. development and validation of techniques to quantify the variability in fractal floc characterization data; and
4. preliminary development of approaches for integrating advanced particle characterization techniques with bench-scale protocols commonly used to optimize conventional chemical pre-treatment during full-scale drinking water treatment.

1.3 Research Approach

Twelve (12) jar tests using the MWTP protocol were performed throughout this investigation. The UV_{254} and turbidity of the supernatant were evaluated during each jar test to investigate potential relationships between these parameters and floc settling rates and structure. Six (6) jar tests were conducted to generate aggregates for settling tests. Three (3) jar tests were conducted at 5, 15 and 25 °C using alum as the primary coagulant and three (3) jar tests were conducted at 5, 15 and 25 °C using PACl as the primary coagulant. Samples were collected after a period of settling from the bottom of the jars so that it could be determined whether or not the settling rates and/or sizes of the aggregates that had settled would correspond to the UV_{254} and turbidity of the supernatant.

The six (6) jar tests were then repeated to characterize the fractal structure of the flocs by digital image analysis with microscopy. Structural characteristics were calculated from samples of aggregates that were collected prior to settling. This was done in order to predict particle removal performance (i.e., based on turbidity reduction) by using the floc structural information of the aggregates generated during coagulation and flocculation.

All of the tests were conducted at varying temperatures because an original objective of the study was to evaluate the temperature effects on floc structure and/or settling velocity. It was decided after the experiments were performed, however, that the primary focus of this thesis would be on the general development and application of floc characterization techniques to water treatment. The initially proposed temperature-floc analysis will be presented elsewhere.

Variability in the characterization data was quantified using commonly utilized statistical tests. A simple approach for quantifying the uncertainty in floc characterization data was also developed. Samples of aggregates generated at full-scale at the MWTP were then collected and compared to the results of the bench-scale testing. This analysis was conducted to determine whether or not bench-scale tests truly simulated full-scale coagulation and flocculation processes.

1.4 Thesis Organization

A review of relevant clarification, coagulation, and flocculation theory, as well as floc structural characteristics and characterization techniques relevant to this research is presented in Chapter 2. Chapter 3 provides details regarding the research approach utilized herein. Experimental results are provided and synthesized in Chapter 4. Overall thesis conclusions and recommendations are presented in Chapters 5 and 6, respectively.

2 BACKGROUND

2.1 Particles in Natural Systems

Impurities in the natural aquatic environment can be distinguished as either “dissolved” or “particulate”. The operational distinction between dissolved and particulate is often made on the basis of a standard procedure: microfiltration (Gregory, 2006). Essentially, a water sample is filtered through a membrane with a pore size of 0.45 μm . Impurities that pass through the filter are regarded as dissolved and those that are retained by the filter are defined as particulate.

Particulate material can be categorized further as either “colloidal” or “suspended”. Conventionally, colloids range from 1 to 1000 nm; particles larger than this are classified as suspended solids. Particles in the colloidal size range are often “unstable”, meaning that forces of attraction between the particles might cause them to aggregate on contact and form clusters typically referred to as “aggregates” or “floc”. Particles in the natural environment often contain both suspended and colloidal material and vary extensively in origin, concentration and size. Figure 2.1 depicts the difference between suspended material and colloidal material as aggregates.

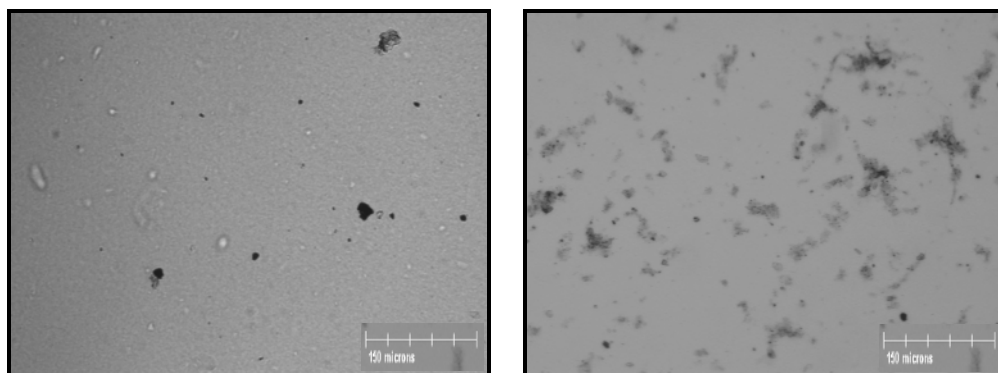


Figure 2.1: Suspended (left) and colloidal (right) material in the natural environment.

The majority of particles in surface waters: silts, clays and other products of weathering, for instance, are derived from atmospheric sources (Letterman, 1999). Chemical and biological processes occur in natural waters and produce particles such as algae and organic exudates of aquatic organisms. Aquatic organisms can also include pathogenic microorganisms derived from municipal and agricultural waste discharge, and can also be described as particulate matter. Atmospheric sources, chemical and biological processes, and waste discharge are the three principal origins of particles in the natural aquatic environment.

25 °C

2.1.1 Particles Derived from Atmospheric Sources

The primary source of rocks, soil and debris found in natural water systems in urban and agricultural areas is runoff during periods of heavy precipitation or snow melt. Resuspension of previously introduced settled bottom sediments can also occur during these episodes. Other sources of particles derived from atmospheric sources include stream bank erosion, construction activity and mining operation (Hroncich, 1999).

Both biological and non-biological suspended solids have the potential to be key vectors for the transport of toxic substances such as heavy metals (e.g., lead, mercury, cadmium, etc.). Heavy metals are naturally present in the environment and if regularly ingested, can be a threat to human health (Metcalf and Eddy, 2003). Long-term exposure to lead, for example, can cause kidney damage, anemia and nerve damage (Goyer, 1993). Mercury poisoning can result in insomnia, diarrhea, memory loss and brain damage (Ratcliffe *et al.*, 1996). Sediment-associated heavy metals have the potential to be transported by particles typically less than 63 µm in a water body, both naturally occurring and biologically or chemically produced (Ongley *et al.*, 1992). Several factors including land use, climate change, flow conditions, sediment source and availability, redox conditions and water chemistry contribute to the transport of sediment-associated metals and other compounds of concern.

2.1.2 Particles Produced by Chemical and Biological Processes

Organic materials in the natural environment include algae and precipitates of calcium carbonate (CaCO_3), manganese dioxide (MnO_2) and goethite (FeOOH). The majority of organic constituents in natural waters; however, are derived from biological degradation of plant and animal remains. Collectively, these substances are known as natural organic matter (NOM); much of which is dissolved. It has been suggested that the characteristics of dissolved organic materials in natural systems promote flocculation and influence the behavior of those flocs (Droppo, 2001). As well, like rocks and soil, these NOM-associated flocs can absorb and transport trace quantities of heavy metals, as well as potentially pathogenic microbial communities.

2.1.3 Particles Derived from Municipal and Agricultural Waste Discharge

Disease-causing microorganisms (i.e., pathogens) that are found in surface waters are most commonly classified as bacteria, protozoa or viruses. Infectious agents potentially present in drinking water sources in North American include various toxic strains of *Escherichia coli*, *Cryptosporidium parvum*, *Giardia lamblia* and Hepatitis A virus, to name a few (Feachem *et al.*, 1983; Madigan *et al.*, 2000; Crook, 1998). The aforementioned organisms are excreted by human beings or animals who are infected with disease or who are carriers of a particular infectious disease and can enter water bodies through domestic sewage from wastewater discharges and most commonly by runoff from various land uses such as animal husbandry and manure spreading on agricultural lands. In places where wastewater treatment processes are effectively utilized, most pathogens are contributed by livestock wastes (Mawdsley *et al.*, 1994). Other sources of pathogenic microorganisms include septic systems, urban runoff, and waterfowl droppings (Hroncich, 1999).

When discharged into the natural environment, pathogens have the potential to be transported to drinking water treatment plant source water intakes. If ingested, bacterial pathogens typically cause diseases of the gastrointestinal tract, such as diarrhea. Protozoans are of

particular concern because of resilience to common chemical disinfectants and their significant impact on immunocompromised individuals, including very young children, the elderly and persons undergoing treatment for cancer (Lisle and Rose, 1995). Viruses can also cause diarrheal disease, respiratory illness and gastroenteritis.

The provision of safe drinking water requires sufficient inactivation of these pathogens by processes such as ultraviolet irradiation (UV), ozone, or oxidation with chemicals such as chlorine. All of these disinfection processes, however, become decreasingly effective as levels of particulate matter in waters to be treated increase (Stagg *et al.*, 1978, Sproul, 1972). For example, it has been found that pathogens may be partially shielded against the action of UV, ozone and chlorine by attachment to or enmeshment in other particles present in the water. Moreover, organic materials, such as NOM-associated flocs, may serve as precursors in the formation of potentially carcinogenic by-products [e.g., trihalomethanes (THMs) and haloacetic acids] when oxidants are applied to the water (Cohn *et al.*, 1999). For these reasons, particle removal processes must always precede drinking water disinfection assuming there is enough particulate matter to warrant them.

2.2 Particle Removal Processes

There are a variety of techniques employed by utilities and suppliers of drinking water to remove particles from water. The choice of technique depends upon factors that include the quality of the water being treated, the cost of the process and the expected quality of the processed water. The three most common processes for separating particles from water are (Bratby, 2006):

1. Dissolved Air Flotation (DAF);
2. Sedimentation; and
3. Filtration.

DAF is the process by which particles become attached to air bubbles that rise to the water surface, thus removing the particles from suspension. Sedimentation, quite simply, is the deposition by gravity settling of a suspended material. Filtration for solid-liquid separation can be divided into two broad classes: gravity and deep bed filtration in which a suspension flows through a bed of granular material, and membrane filtration, which is primarily a size exclusion process by a thin layer of material with pores of a particular size.

Granular media filtration processes are further categorized as either direct or in-line filtration, or conventional filtration. Direct, or in-line filtration refers to filtration preceded by chemical pre-treatment of the water. When sedimentation is employed prior to the filter, the process is known as conventional filtration.

Of the available methods for particle removal, sedimentation followed by filtration (i.e., conventional filtration) is currently the most commonly practiced particle removal process in North America due to its ease of operation, cost effectiveness and high solids removals, especially microorganisms (i.e., 99% to 99.5% removals) (Cleasby and Logsdon, 1999). Bench-scale protocols commonly used to optimize conventional chemical pre-treatment during full-scale drinking water treatment often incorporate settleability of particles, and therefore particle removal by sedimentation was the primary focus of this thesis research. A detailed theoretical discussion of sedimentation is presented in the following section.

2.2.1 Sedimentation

Sedimentation for the improvement of water quality has been practiced for hundreds of years. The basic theory that water stored undisturbed and then poured or ladled out with little agitation will improve water quality has been used throughout the development of societies around the world (Gregory *et al.*, 1999). Basic surface water impounding reservoirs are even thought to have been constructed as early as 600 B.C. (Ellms, 1928).

As the need for safe, clean drinking water increased during the industrial age, so too did sedimentation technology. Modern sedimentation equipment typically consists of either a conical, circular or rectangular basin with agitators, pipes and pumps for settled solids collection (Swamee and Tyagi, 1996). In rectangular tanks, the water to be settled flows horizontally in one end, and the treated water flows out at the other end. The inlet flow arrangement must provide a flow distribution that maximizes the opportunity for particles to settle. In circular tanks, flow is usually from a central feedwell radially outward to peripheral weirs. The tank floor is occasionally conical to a center sludge well. These types of sedimentation basins were predominant for many years until the development of inclined plate settlers in the late 1950s (Kapoor and Acrivos, 1995).

Inclined plate settlers (Figure 2.2) were established for drinking water treatment in Sweden and are now widely used in water treatment plants across North America. The primary advantage of these systems is that they can be designed and constructed to increase sedimentation efficiency by increasing the area available for settling and decreasing the vertical distance that particles must travel (Kapoor and Acrivos, 1995). An additional benefit of inclined plate settling is the self-cleaning of the surfaces, and therefore optimal performance, when the angle of inclination of the plates is more than 50° (Yao, 1973).

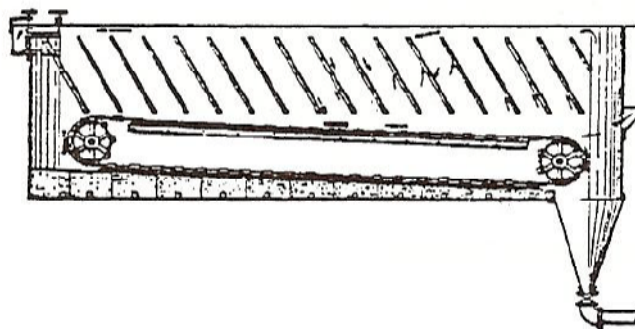
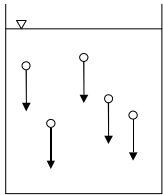
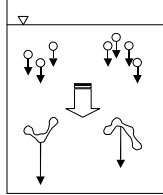
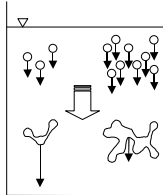
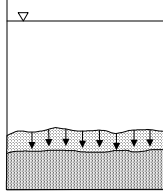


Figure 2.2: Early patent for inclined plate settling (Barham et al., 1956).

Regardless of which type of sedimentation basin is selected as the preferred alternative for any particular treatment train, they are all designed and operated to achieve high levels of particle removal in the shortest amount of time. For all varieties of sedimentation equipment, the design equations typically used to describe and model particle settling are generally and universally based upon two assumptions (Valioli and List, 1984):

1. Impermeable, spherical particles; and
2. Type 1 settling behavior (Table 2.1), which is the settling of individual, separate and distinct particles by gravity.

Table 2.1: Particle settling regimes (Gregory *et al.*, 1999).

<p>Type 1</p>	<p>Settling of discrete particles in low concentration.</p>	
<p>Type 2</p>	<p>Settling of particles in low concentration but with coalescence or flocculation. As coalescence occurs, particle masses increase and particles settle more rapidly.</p>	
<p>Type 3</p>	<p>Hindered, or zone, settling in which particle concentration causes interparticle effects, which might include flocculation, to the extent that the rate of settling is a function of solids concentration.</p>	
<p>Type 4</p>	<p>Compression settling or subsidence develops under the layers of zone settling. The rate of compression is dependant on time and the force caused by the weight of solids above.</p>	

The settling velocity of a single, impermeable spherical particle that settles discretely can readily be predicted according to Stokes' law, which is based upon a force balance. There are three forces, gravity (F_g), buoyancy (F_b) and drag (F_d) [$\text{kg}\cdot\text{m}/\text{s}^2$], acting upon the particle. Equating these forces produces:

$$F_d = F_g - F_b \quad (2.1)$$

The drag force exerted on a particle can be expressed as a function of the fluid density (ρ) [kg/m^3] and the particle's terminal settling velocity (v) [m/s] (Prandtl and Tietjens, 1957):

$$F_d = \frac{\rho v^2 A C_d}{2} \quad (2.2)$$

where A_c is the projected cross-sectional area of the particle [m^2] and C_d is an empirical drag coefficient. Since gravitational and buoyant forces can be expressed as $\rho_p V g$ and $\rho V g$, respectively, where ρ_p is the density of the particle [kg/m^3], V is the effective volume of the particle [m^3] and g is the gravitational constant of acceleration [m/s^2], then *Equation 2.1* can be written as:

$$\frac{\rho v^2 A_c C_d}{2} = \rho_p V g + \rho V g \quad (2.3)$$

When rearranged to isolate for settling velocity, *Equation 2.3* becomes:

$$v = \sqrt{\frac{2g\Delta\rho V}{C_d \rho A_c}} \quad (2.4)$$

where $\Delta\rho$ is the difference between the particle and fluid densities. In a typical drinking water treatment plant, fluid flow through a sedimentation tank is laminar; that is, water flows in parallel layers with no disruption between layers (Swamee and Tyagi, 1996). When this type of flow is assumed, the empirical drag coefficient for spheres is:

$$C_d = \frac{24}{R_e} \quad (R_e \lll 1) \quad (2.5)$$

where R_e is the Reynold's number which can be expressed as vd/μ ; μ being the kinematic viscosity [m^2/s] and d being the particle diameter [m]. Assuming that the particles are spherical, geometric relationships ($V = \pi d^3/3$ and $A_c = \pi d^2/4$) will simplify *Equation 2.4* to Stokes' law:

$$v = \frac{g\Delta\rho d^2}{18\mu} \quad (2.6)$$

Equation 2.6 reveals that the settling velocity of a particle is proportional to the diameter squared. This relationship is true, but only for objects that are impermeable and spherical. In most natural and engineered systems, particles are often not characteristic of either parameter (Droppo *et al.*, 2005). Several investigators have examined the settling velocities of such particles by including a shape factor, ϕ , into Stokes' law in the form:

$$v = \frac{g\Delta\rho d^2}{\phi 18\mu} \quad (2.7)$$

Engineered aggregates (i.e., flocs), however, have been found to settle at rates that are four (4) to eight (8) times higher on average than those predicted by Stokes' law (Johnson *et al.*, 1996). Several investigators have ascertained that the explanation for Stokes' law (*Equation 2.6*) being irrelevant for engineered flocs is because aggregate porosity is not constant (Li and Ganczarczyk, 1989) and because flocculent settling (i.e., Type 2) likely occurs. Furthermore, the shape factors that are necessary to describe these types of particles are practically impossible to determine because their physical characteristics are complicated, often being linked to the mechanics of their formation and disruption resulting from the flow of water around them. Without methods to determine shape factors in a manner that has physical significance, they essentially become fitting parameters.

Despite the development of simple modeling approaches that rely on fitting parameters for estimating the flocculent settling velocity of suspended particles (Je and Chang, 2004), at present there are no practical tools that have been reported to describe and/or predict flocculent settling as it relates to water quality parameters such as turbidity and ultraviolet

absorption at 254 nm (UV₂₅₄). The ability to predict the settling velocities of engineered particles would be a considerable contribution to the water treatment industry because particle settling velocities are widely used in calculations for the design and maintenance of water treatment processes. Research efforts have mainly focused on settling simulated flocs, often with controlled primary particle size distributions prior to flocculation, to enhance the theoretical relationships between settling velocity and particle characteristics. Studies that validate these concepts for practical application are lacking, both at bench-scale and full-scale.

Johnson *et al.* (1996) investigated aggregates that were generated by coagulation and flocculation of latex microspheres in paddle mixers and then analyzed their size, porosity and settling velocity individually. In engineered systems, pre-treatment processes such as coagulation and flocculation typically precede sedimentation to produce flocs; which are formed particles with characteristics that make them more likely to settle than the particles that they are comprised of (i.e., primary particles). The structure of the flocs can be altered and manipulated based on operator-controlled parameters in the coagulation stage, such as coagulant type and dose, and mixing speed and time.

2.2.2 Coagulation

A primary particle is generally considered to be stable in the natural aquatic environment if it has a negative charge (Letterman, 1999). Since the majority of particulate matter in surface waters has a negative charge, it is kept in suspension because it naturally repels particles with the same charge. Coagulation essentially refers to the destabilization of those particles by the addition of appropriate additives (i.e., coagulants), as well as the removal of dissolved organic carbon (DOC). Altering the surface charge of particles increases the probability that they will aggregate to form flocs. Historically, four (4) mechanisms of particle destabilization have been recognized:

1. Double Layer Compression;

2. Surface Charge Neutralization;
3. Interparticle Bridging; and
4. “Sweep” Flocculation.

2.2.2.1 Particle Destabilization Mechanisms

Double layer compression is a phenomenon that has been well studied and is mechanistically well understood. When a colloid or particle surface is charged in a suspension, ions of opposite charge (i.e., counterions) accumulate at the particle surface and are held there through attractive and electrostatic forces. The compact and fixed region of counterions is known as the “Stern Layer”. Surrounding this is the “Diffuse Layer” of ions resulting from electrostatic attractions of ions of opposite charge to the particle and electrostatic repulsion of ions of the same charge as the particle (Lyklema, 1978). Together, the two (2) layers form the “Electrical Double Layer”.

Because counterions adsorb from the suspension, the potential energy (ψ) at a particle’s surface decreases exponentially with increasing distance making particle-particle interactions difficult (Deryagin and Landau, 1941) (Figure 2.3). By adding a suitable electrolyte to the suspension, ions that are opposite to the charge on the surface of the particle enter the diffuse layer. If enough of these ions are added, the diffuse layer is compressed, reducing the energy required to move two (2) particles of like surface charge into close contact (Letterman, 1999).

Similar to double layer compression, surface charge neutralization involves reducing the net surface charge of particles in suspension, therefore decreasing the thickness of the diffuse layer and minimizing the energy required to move particles into contact. This process, however, is accomplished by the surface adsorption of coagulants that carry the opposite charge to the net surface charge of the particles. These coagulants usually have a strong tendency to adsorb surfaces (Licsko, 2004).

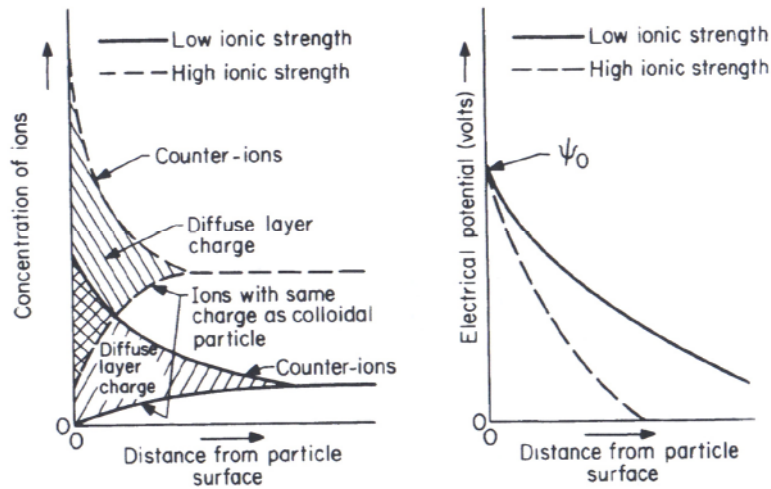


Figure 2.3: The Electrical Double Layer and related potential energy (Letterman, 1999).

Interparticle bridging occurs when segments of polymers, or polyelectrolytes, attach to multiple particle surfaces, effectively linking the particles together (Figure 2.4). Specifically, when polymer comes into contact with a particle, some of the reactive portion of that polymer attaches to the particle surface and other portions extend into the suspension. If a second particle is able to adsorb the extended portion of the polymer, then an interparticle bridge will have formed. Bridges can then become entangled with other bridges forming even larger aggregates (Metcalf and Eddy, 2003).

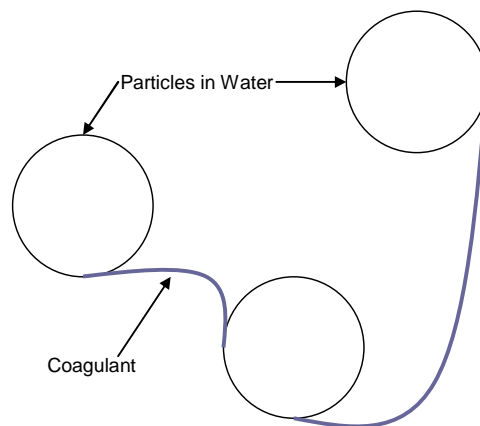


Figure 2.4: Example of interparticle bridging.

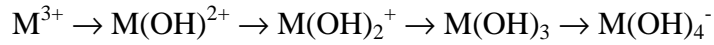
“Sweep” flocculation has been separately described as occurring:

- a. when particles are “swept” out of the water by an amorphous hydroxide precipitate (Gregory, 2006); and
- b. due to an increase in contact opportunities. As amorphous hydroxide precipitation occurs, there are more particles in the suspension, which increases the chance that particles will aggregate to form flocs (O’Melia, 2007).

As evidenced from these recent works, the description of the “sweep” flocculation mechanism of particle destabilization continues to evolve both quantitatively and qualitatively. An accurate understanding of coagulation theory is essential for the design, optimization and operation of water treatment coagulation processes. It is also crucial for the selection of a coagulant since it is generally recognized that the each type of coagulant will each behave in a distinctive manner (Wesolowski and Palmer, 1992; Flynn, 1984). Regardless of the coagulation mechanism, addition of metal salt coagulants such alum ($\text{Al}_2(\text{SO}_4)_3$) or polyaluminum chloride ($\text{Al}_x(\text{OH})_{3x-2y-z}(\text{SO}_4)_y\text{Cl}_z$) to water at appropriate doses will likely increase the chances of particle aggregation. Adding a polymer will generally increase the size of the aggregates formed. Descriptions of widely used coagulants are presented in the following section.

2.2.2.2 Types of Coagulants

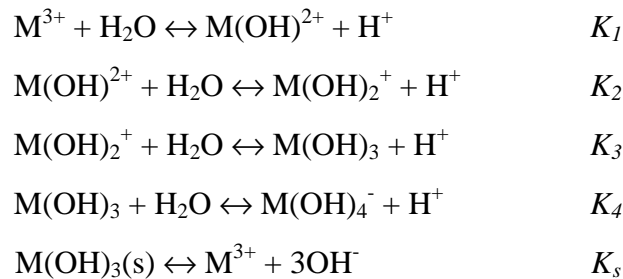
The most commonly used coagulants in water treatment are hydrolyzing metal salt (HMS) coagulants; more specifically, sulfate and chloride salts that contain metal ions Al^{3+} or Fe^{3+} . These positively charged ions form such strong bonds with the oxygen atoms of six (6) surrounding water molecules that the oxygen-hydrogen association in the water molecules is weakened, and hydrogen atoms are released. This process is known as hydrolysis and the resulting aluminum and ferric hydroxide species are known as hydrolysis products. Hydrolysis is often signified as a sequential replacement of water molecules by hydroxide ions and can be represented for Al^{3+} and Fe^{3+} as:



As hydrolysis proceeds, simple mononuclear products can form complex polynuclear species, which in turn forms the amorphous hydroxide precipitate that causes “sweep” flocculation. Hydrolysis products can adsorb, and continue to hydrolyze on many types of particulate surfaces (Letterman, 1999). The solubility of the metal precipitate is an important factor in achieving optimal coagulation performance and for minimizing the concentrations of Al^{3+} and Fe^{3+} in treated water.

Hydroxide precipitates are rapidly formed at higher concentrations of Al^{3+} and Fe^{3+} salts (Sawyer *et al.*, 2003). Figure 2.5 illustrates the effect of pH on the hydrolysis of aluminum hydroxide (i.e., $Al(OH)_3$). Because of the many products that aluminum and iron can form with hydroxide ions, these metal salts are more soluble at both higher and lower pH values. At low pH, the dissolution of the metal-hydroxide precipitate produces the metal ion (Al^{3+}). At high pH, the negatively charged, soluble hydrolysis products $Al(OH)_4^-$ are formed. Coagulation is usually best carried out at the pH of minimum solubility (pH_{min}), which increases with decreasing temperature (i.e., pH_{min} of $Al(OH)_3 \approx 6.3$ when the temperature is 25 °C, but increases to 6.8 as the temperature is lowered to 4 °C).

Hydrolysis constants (K) may be defined for each of the stages in the hydrolysis process in terms of the following equations (Gregory and Duan, 2001):



Calculation of K and pK are completed in the following manner, for example:

quickly than compression of the diffuse layer (Hahn and Stumm, 1968; Letterman *et al.*, 1973). Notwithstanding, coagulation research efforts have traditionally focused on understanding the science and mechanisms of HMS coagulants. They are inexpensive and robust and therefore, are still the most predominant coagulants used by water treatment plants (Bratby, 2006).

HMS coagulants used for water treatment can be categorized into two (2) product groups: simple metal salts and prehydrolyzed metal salts. The simple HMS coagulants include aluminum sulfate (alum), ferric sulfate, and ferric chloride. They are sold as dry crystalline solids and as concentrated aqueous solutions. Prehydrolyzed HMS coagulants are manufactured to contain significant quantities of hydrolysis products after having been partially neutralized by a base and are becoming increasingly prevalent due to their effectiveness (i.e., higher rate of settling) at low temperatures (i.e., ≤ 5 °C) (Letterman *et al.*, 1999) and because the primary coagulant species are preformed, and are immediately available for coagulant reactions. Polyaluminum chloride (PACl), a prehydrolyzed metal salt made with aluminum chloride, is a frequently used prehydrolyzed HMS coagulant and is typically sold as a concentrated aqueous solution. Prehydrolyzed iron solutions exist but are still a relatively uncommon and expensive commercial product.

Coagulation diagrams are often used to select an appropriate HMS coagulant product for a given application. A coagulation diagram outlines the regions of coagulant performance on a stability diagram for the metal hydroxide precipitate. Figure 2.6 is an alum and PACl coagulation diagram for coagulation when there are negligible concentrations of NOM (Amirtharajah and Mills, 1982). The minimum alum concentration and pH to achieve optimum “sweep” flocculation (referred to as “sweep” coagulation in the figure), for example, would be 24 mg/L and 7.5, respectively. Alternatively, charge neutralization will begin to occur when the alum concentration is less than 1 mg/L, if the pH is less than 7.

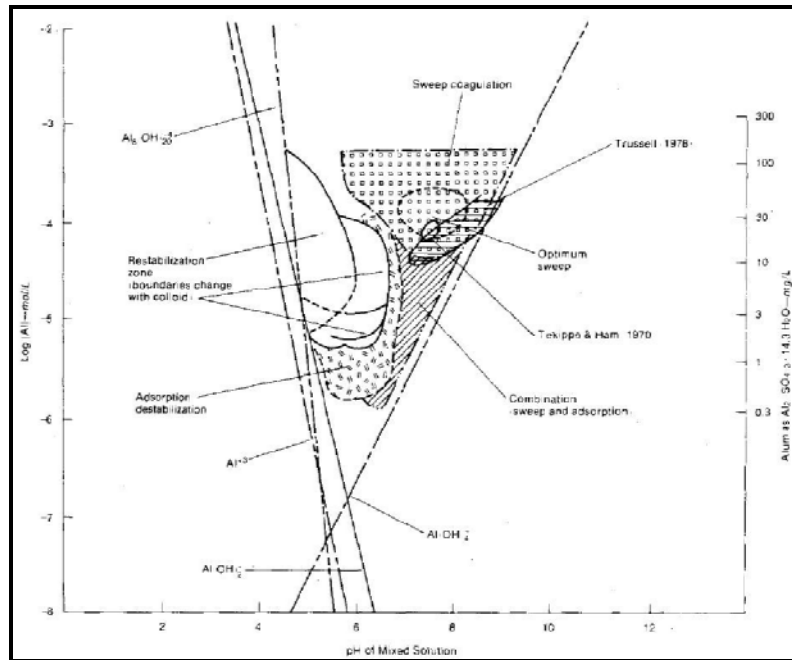


Figure 2.6: Coagulation diagram for alum and PACI (Amirtharajah and Mills, 1982).

Typically used as a supplement or aid to HMS coagulants, polyelectrolyte coagulants, or polymers, are high molecular weight, synthetic organic compounds that have a strong tendency to adsorb to the surfaces of most naturally occurring particles in aqueous suspensions (i.e., interparticle bridging). Polymers that are negatively charged are anionic; those that are positively charged are called cationic. Two (2) of the most widely used polyelectrolyte coagulants in water treatment are cationic polydiallyldimethyl ammonium chloride (polyDADMAC) and cationic epichlorohydrin dimethylamine (epiDMA); both of which are sold as concentrated aqueous solutions (Bratby, 2006).

In addition to coagulation diagrams, coagulant selection typically depends upon cost and raw water quality because certain characteristics other than pH (e.g., turbidity, temperature, and concentration of NOM) have been found to influence coagulation performance (Hanson and Cleasby, 1990; Pernitsky and Edzwald, 2006). It should be noted that coagulation could also be optimized to remove NOM; such an application is termed “enhanced coagulation”.

Regardless, no matter which coagulant is chosen as the preferred alternative, the actual treatment processes are generally the same (Figure 2.7). First, a flash mix step used to disperse the coagulant(s) for particle destabilization and to initiate the particle aggregation process occurs in a rapid mix basin. A slow-mix flocculation basin typically follows.

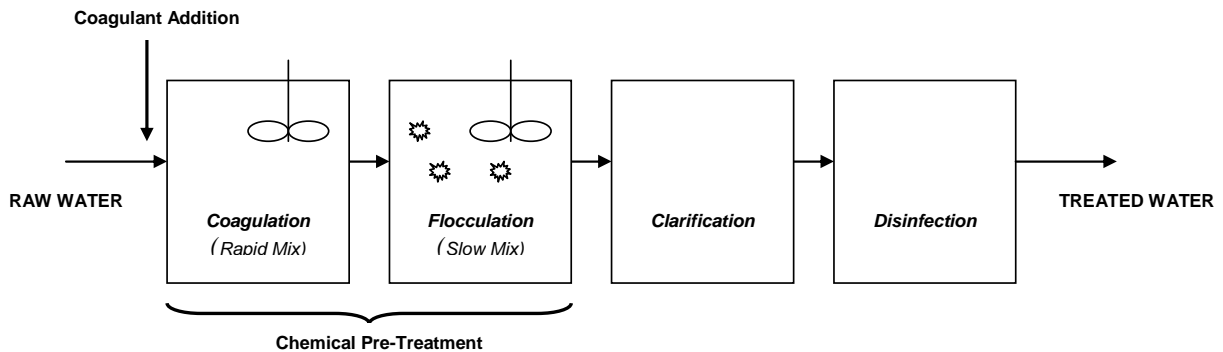


Figure 2.7: A typical, fundamental drinking water treatment sequence in North America.

2.2.3 Flocculation

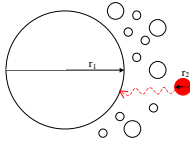
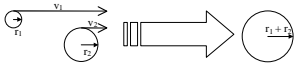
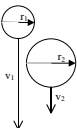
During water treatment, the purpose of the flocculation process is to promote the interaction of particles to form floc that can be readily removed in subsequent clarification processes. Flocculation basins are typically placed in close proximity to the clarification basin(s) so that the flocs are not damaged or broken during transportation. They are also mixed slowly so as to promote efficient flocculation.

The temperature of water can have a considerable effect on flocculation performance. Generally, it has been found that the rate of floc formation is slower, flocs are smaller and particle removal efficiency is decreased at lower temperatures (Hanson and Cleasby, 1990; Fitzpatrick *et al.*, 2004). Fitzpatrick *et al.*, (2004) noted that although warmer temperatures produced larger flocs, they were not as strong and broke more easily. Morris and Knocke (1984) have presented evidence that physical factors of floc are behind the effect of

temperature on flocculation performance, observing significant temperature effects on the size distribution of alum floc.

For efficient flocculation to occur, suspensions must be initially be destabilized by a coagulant so that particle collisions can take place (Letterman *et al.*, 1999). There are three (3) primary mechanisms that cause these collisions in a destabilized suspension: perikinetic flocculation, orthokinetic flocculation and differential settling (Table 2.2). Thermal energy and fluid velocity are the driving forces of perikinetic and orthokinetic flocculation, respectively; differential settling is driven by gravity. Flocculation rate equations have been derived for each of these mechanisms by assuming that the aggregation process is a second-order rate process in which the rate of collision between two (2) particles is proportional to the product of the concentrations of the two (2) colliding objects.

Table 2.2: Particle transport mechanisms in a destabilized suspension (Metcalf and Eddy, 2003).

<p>Perikinetic Flocculation (Brownian Motion)</p>	<p>Aggregation of small particles that move about in a random way due to the thermal motion of the surrounding fluid molecules.</p>	
<p>Orthokinetic Flocculation (Transport in Laminar Shear)</p>	<p>In a laminar flow field, particles located at a point with a higher fluid velocity will overtake particles located at a point with lower fluid velocity. If they are close enough together or collide, they may aggregate.</p>	
<p>Differential Settling</p>	<p>When aligned in a vertical direction, particles that have unequal settling velocities will collide when one overtakes another.</p>	

The orthokinetic flocculation rate constant (k_o), for example, is given by:

$$k_o = \left[\frac{(d_1 + d_2)^3}{6} \right] \left(\frac{du}{dz} \right) \quad (2.8)$$

where d_1 and d_2 are the particle diameters [m] and du/dz is the velocity gradient [s^{-1}]. Most water treatment flocculators; however, are mechanically mixed, continuous-flow reactors, and the fluid motion is turbulent. Particle interaction through laminar velocity gradients and unequal settling velocities tends to be insignificant. In the 1940s, a flocculation rate equation for turbulent flow was developed after it was determined that a root-mean square (rms) velocity gradient (G) [s^{-1}] can be used in place of du/dz in turbulent conditions (Camp and Stein, 1943). The modified orthokinetic flocculation rate constant ($k_{o,c-s}$) is given by:

$$k_{o,c-s} = \left[\frac{(d_1 + d_2)^3}{6} \right] G \quad (2.9)$$

The rms velocity gradient is given by:

$$G = \sqrt{\frac{P}{V_w \mu}} \quad (2.10)$$

where P is the power input to the fluid (i.e., through, for example, blades of rotation) [$m^2 \cdot kg/s^3$] and V_w is the volume of water in the vessel [m^3]. The limitations of the G value concept have been discussed elsewhere (Cleasby, 1984; McConnachie, 1991; Hanson and Cleasby, 1990; Clark, 1985). It is generally believed that its use as a design and operating parameter in flocculation is limited because the rate of flocculation is affected not only by the intensity of the fluid motion but also the distribution of that energy. Three (3) other considerations make application of the G value problematic, which are:

1. the local rate of energy dissipation in a mechanically mixed vessel varies widely with location in the vessel (Schwartzberg and Treybal, 1968; McConnachie, 1991);
2. some of the energy supplied to the rotating impeller shaft is dissipated directly as heat at the surfaces of the impeller and does not produce turbulent fluid motion (Letterman, 1999); and

3. fluid shear, and therefore the G value, is a controlling factor in flocculation kinetics only when the interacting particles are larger than $1\ \mu\text{m}$ and approximately the same size (Han and Lawler, 1992).

Studies have shown, however, that when G is multiplied by the mean residence time of the fluid in the reactor compartment (T), the dimensionless product GT can be utilized to predict the effectiveness of a flocculation performance to some extent (Argaman, 1970; Letterman, 1999). In other words, flocculator performance is a function of the GT . Unfortunately, it has also been shown that GT itself is not an adequate parameter for describing the effects of mixing on flocculation efficiency, as there is a minimum residence time below which that performance cannot be attained regardless of G .

Until there is a more clear understanding of turbulent flow in mechanically agitated vessels, the development of sensitive and practical methods for measuring flocculation performance, especially the performance of full-scale units, will be precluded. Because of this, water treatment practitioners continue to use the G value for flocculator design, operation and scale-up from bench-scale testing.

2.3 Bench-Scale Testing

Bench-scale tests, specifically jar tests, are performed to simulate full-scale coagulation and flocculation processes. They are typically performed by plant operators to provide a reasonable indication of the way a coagulant might behave at various operational conditions (e.g., variable water quality, temperature, etc.). More specifically, the objectives of jar testing are often to:

1. determine the coagulant that will perform the best at current and anticipated operational conditions;
2. attempt alternative treatment doses and strategies without altering the performance of the full-scale treatment plant and compare the results of several different

chemical treatments for time of aggregate formation, floc size, and settleability (Pask, 1993); and/or

3. optimize full-scale chemical pre-treatment processes.

There is no standard frequency for which jar testing should be conducted at any particular water treatment plant. It can be performed seasonally, monthly, daily, or whenever a coagulant is being changed, or new pumps or motors have been installed. Recommendations for jar test regularity are typically made on a plant-by-plant basis; water quality may vary daily at one plant but only seasonally at another, for example. It is generally acknowledged, though, that the more often the tests are conducted, the more efficiently the pre-treatment processes will operate.

If bench-scale tests of pre-treatment are not utilized adequately, sub-optimal clarification and/or disinfection resulting from coagulant underdosing might be one possibility. In contrast, one of the most common problems encountered during drinking water treatment is coagulant overfeeding or overdosing, which can result in unnecessarily high coagulant expenses and sludge production. It has been suggested that "... the initial cost of jar testing equipment is often recovered in less than one (1) year. In many plants where jar testing is not done, there is a tendency to dose a little extra 'just to be sure'" (Satterfield, 2005).

Typical jar testing equipment (Figure 2.8) is often comprised of a stirring machine with six (6) paddles, and six (6) cylindrical or cubic plastic jars. A standard jar test procedure entails dosing fixed volumes of raw water with increasing dosages of coagulant. Water quality parameters, such as pH, turbidity and alkalinity are initially measured. The water is then mixed for a period of time based upon full-scale conditions to produce "representative" floc. This is followed by a settling period that is based upon full-scale specifications and practice. The optimum coagulant dose is typically established from the reduction in ultraviolet absorption at 254 nm (UV_{254}), an indicator of dissolved organic material, and/or turbidity. Most water treatment plants will select a coagulant dose based on simultaneously reducing

both parameters to an optimum level. This is often a difficult task because a lower pH is typically required for the removal of dissolved organic material; a pH that could hinder the process of removing suspended particles.



Figure 2.8: A Phipps & Bird standard jar tester (Grammer, 2007).

2.3.1 Ultraviolet Absorption at 254 nm (UV_{254})

Ultraviolet Absorption at 254 nm (UV_{254}) is the intensity of a light passing through a sample (I) compared to the intensity of light before it passes through the sample (I_o). The ratio of I to I_o is referred to as the transmittance, which is usually expressed as a percentage ($\%T$). Most techniques to quantify UV_{254} will determine the $\%T$ and calculate UV_{254} using the following equation:

$$A = -\log(\%T) \quad (2.11)$$

where A is the UV_{254} absorbance in absorbance units (AU). An increase in UV absorbance of 1 AU corresponds to a reduction in transmittance by a factor of ten (10). Research efforts have shown that at a wavelength of 254 nm, dissolved organic compounds will absorb light. In water treatment, therefore, UV_{254} has been used as an indicator of dissolved organic carbon (DOC) (Pernitsky and Edzwald, 2006). In general, as the quantity of DOC decreases, A decreases, as well (Letterman, 1999).

Coagulation is a process that is commonly used to remove dissolved organic compounds. Coagulant-NOM interaction typically occurs immediately after chemical dispersal in rapid mixing if the pH is low (Letterman, 1999). The nature of the flocs that are in suspension following coagulation will be highly influenced by the quantity and constituency of organic materials that have been removed from solution.

2.3.2 Turbidity

Turbidity is an indirect measurement of suspended particle (e.g., floc) concentrations in water. The most common technique for measuring turbidity is the nephelometric turbidity method, quantified by nephelometric turbidity units (NTU), and is based on the theory that light scattering intensifies as particle concentration increases. Since the intensity of scattered light at an angle of 90° to the beam is proportional to the total scattering, turbidity can be used to estimate suspended particle concentration (Van de Hulst, 1957). As the concentration of particles decreases, the NTU decrease, as well. The method requires establishing an empirical relationship between known particle concentrations and NTU.

To obtain accurate concentration estimates, the properties of the particles within the measured water must be consistent with those of the standard curve. This is often a difficult task because turbidity is thought to be affected by many factors; primarily the size, distribution and shape of the particles in suspension. Thus, samples with equivalent quantities of particles could provide turbidity values that do not correspond to each other due

to varying particle characteristics (ie. size and shape). Smaller particles, for example, have been found to scatter shorter (blue) wavelengths more intensely while larger particles tend to scatter longer (red) wavelengths more intensely (Sadar, 1998). In water treatment, flocs may range in size from a few nanometers to several millimeters in diameter depending on the properties of the water and the type of coagulant(s). They will also have various shapes, with many variations in between, which make accurate particle characterization and distribution somewhat challenging.

2.3.3 Floc Size and Shape

The simplest measure of the size of particles, including flocs, is the particle longest dimension (L_D), or the longest line through an object that is parallel to its orientation (i.e., it does not necessarily cross the center of mass). This measurement is of limited use, however, as it only provides a description of floc size in one (1) dimension. A more practical approach might be to measure the longest dimension in both the horizontal (L_{Dh}) and the vertical directions (L_{Dv}) [m]. Figure 2.9 illustrates various longest dimension measurements.

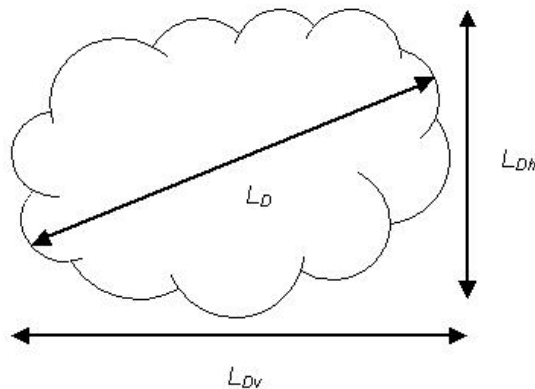


Figure 2.9: Depiction of the various longest dimension (L_D) measurements.

The discussion of floc size is greatly simplified, however, if all of the particles in a sample are considered to be spherical (Gregory, 2006; Cousin and Ganczarczyk, 1998). ‘Equivalent

spherical diameter' (*ESD*) [m] defines a floc as a sphere or a circle that is in some way equivalent to that floc (Figure 2.10). These *ESD* values can be calculated using various quantifiable properties of the aggregate, including the perimeter, area, volume or settling velocity. Unless the floc is a perfect sphere, the computed *ESD* value will vary depending on which property was measured. *ESDs*, therefore, are used for comparative purposes (e.g., floc to floc, sample to sample) rather than as absolute values describing floc diameter.

The most commonly used equivalent spherical diameters for characterizing aggregates have been summarized elsewhere (Jarvis *et al.*, 2005) (Appendix A). One- or two-dimensional *ESDs* (i.e., based upon the area of perimeter of the particle), rather than those that are three-dimensional (i.e., based upon the volume of the particle), are the most frequently utilized. Although more dimensions would likely result in a more accurate description of floc size, current capabilities of three-dimensional measurement techniques are limited.

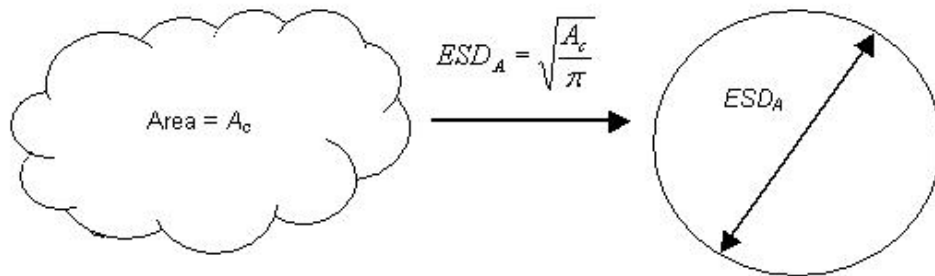


Figure 2.10: Conceptual depiction of an equivalent spherical diameter (*ESD*).

The measurement of one- and two-dimensional parameters is also statistically complicated. For example, the projected area diameter (ESD_A), described below by Equation 2.12, is the diameter of a circle with the same projected cross-sectional area (A_c) as the floc measured in a stable orientation. It is often calculated because the area of a floc can be readily measured. The use of this area, however, is problematic because particles have a tendency to orient themselves on surfaces (e.g., microscope slides or filters) such that they present their maximum area (Allen, 1997). The dimension perpendicular to the viewing plane, which is

neglected, will therefore be the smallest. Accordingly, measurements of floc area in two-dimensions are likely frequently biased. The simplest way to manage these types of errors may be to calculate a value that is based on entire distributions of particles.

$$ESD_A = 2\sqrt{\frac{A_c}{\pi}} \quad (2.12)$$

A size distribution of particles dispersed in a fluid is a mathematical function that defines the relative quantities of particles present, sorted according to their size (e.g., ESD_A). A typical particle size distribution is presented in Figure 2.11 as a curve, the ordinates being the percentage by number of volume of particles smaller than the size range given by the abscissa (Craig, 1997). The flatter the distribution curve the larger the range of particle sizes in the sample; the steeper the curve the smaller the size range. The particle size corresponding to any specified value on the “percentage smaller” scale can be read from the curve. For example, the size such that 50% of the particles are smaller than that size is denoted by D_{50} .

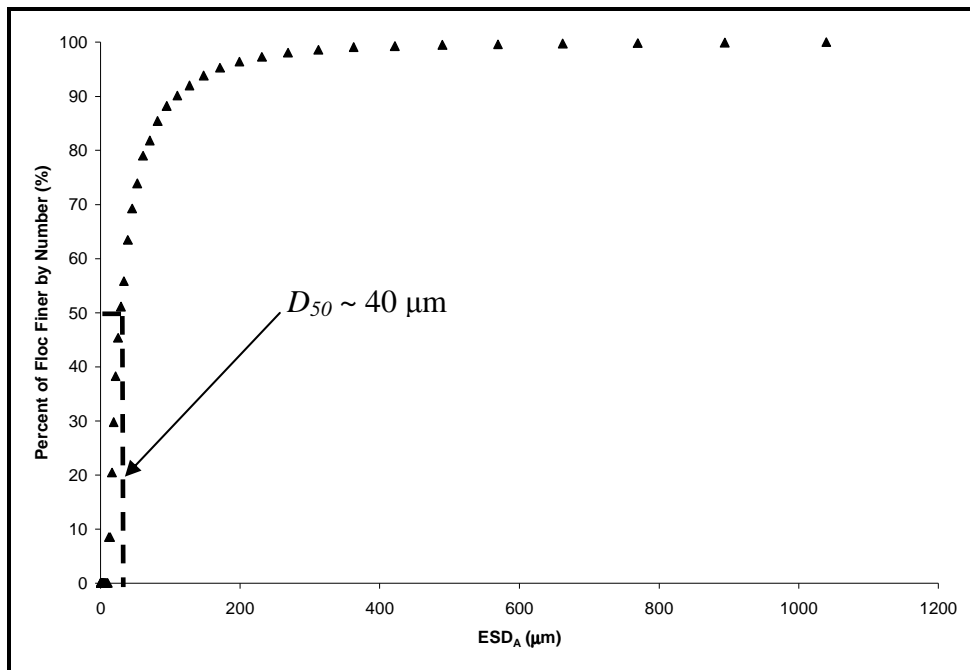


Figure 2.11: An example of a grain-size distribution curve.

Although evaluating an entire population of particles might reduce the error associated with the individual measurements, biases in calculated floc characteristics will still exist. These biases will be consistent for all parameters based on the perimeter, area and/or volume, both size and shape descriptors. Shape descriptors, or factors, are often based on a ratio of two (2) or more dimensions and are calculated to provide a description of a flocs shape by indicating how much their profile varies from a perfect sphere or circle (Craig, 1997). For example, the circularity (C) of a two-dimensional object, or a three-dimensional object projected in two (2) dimensions, is defined as:

$$C = \frac{p^2}{4\pi A_c} \quad (2.13)$$

where p is the perimeter of the particle [m]. A circularity value of 1 indicates that the shape is a perfect circle, as it has the greatest area to perimeter ratio. A thin, thread-like object would have a shape factor approaching 0.

Until recently, significant attention has focused on measuring and understanding the impact of aggregate size and shape on water quality (e.g., turbidity, particle counting); specifically during bench-scale tests for optimizing chemical pre-treatment during conventional water treatment. Consideration of floc structure has been less investigated due mainly to a lack of appropriate theories to describe the complex random structure of the flocs (Jefferson and Jarvis, 2006). Mandelbrot's (1982) text on fractal geometry enabled the application of these theories to description of floc structure.

2.4 Fractal Geometry

Mandelbrot (1982) generally defined a fractal structure as “a fragmented geometric shape that can be subdivided into parts, each of which is a reduced-size copy of the whole” (Figure 2.12). Because they appear similar at all levels of magnification, fractals are often considered to be infinitely complex. This self-similarity is the first of three (3)

characteristics that define a fractal object; the other two (2) are non-integer dimensions and a power law relationship between two (2) variables. That is, measured properties of fractal structures do not scale with size raised to integer values of two (2) and three (3) for area and volume, respectively, but to fractional or fractal powers. As a consequence, fractal dimensions relate size to some property of the object in n dimensions by a power function, where $n = 1, 2, 3$ and D_n is the fractal dimension in the n^{th} dimension (Stone and Krishnappan, 2003).

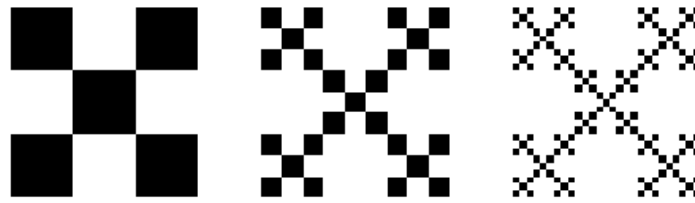


Figure 2.12: Conceptual depiction of a fractal structure (modified from Mandelbrot, 1982).

The concept of fractal geometry is perhaps best explained by examining the coastline of an island such as Britain, which exhibits the characteristics of a fractal object (Figure 2.13). When the perimeter of the coastline is measured with a fixed length measuring stick, there is a relationship between the size of the stick and the measured property. This occurs as smaller sized sticks ($a = 31$) can resolve details (e.g., bays and inlets) that the larger sticks ($b = 5$) cannot (Jefferson and Jarvis, 2006).

The geometric power law relationship illustrated in Figure 2.13 can be defined by:

$$X \propto R^{D_n} \quad (2.13)$$

where X is the measured property (e.g., perimeter) and R is a linear measure of size. For Euclidean objects (e.g., squares or cubes), the dimensional values of D_n will be integers; fractal objects show non-Euclidean dimensionality. It is commonly recognized that particle aggregates, both natural and engineered, are fractal (Gorczyca and Ganczarczyk, 2001;

Gregory, 2006). The fractal dimension of floc can be determined based on a number of measurable properties. However, they all rely on the same basic concept that a geometric power law scaling relationship applies between each dimension. Mass (M) [kg] or V , A_c and p are proportional to the characteristic length scale (L) [m] of the aggregate (Jefferson and Jarvis, 2006) in one (1), two (2) and three (3) dimensions, respectively.

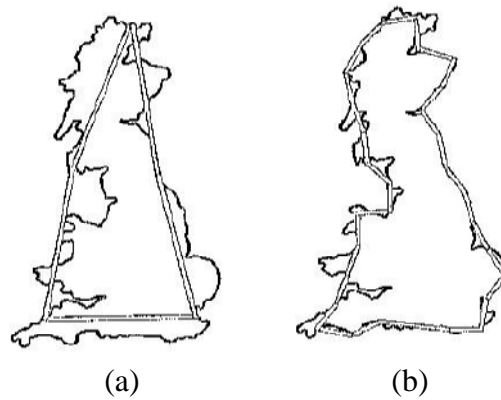


Figure 2.13: Coastline of Britain measured by two different length ($a = 5$, $b = 31$) measuring sticks (modified from Jefferson and Jarvis, 2006).

2.4.1 Fractal Dimensions

A three-dimensional fractal dimension (D_3) for a single floc, or for a population of flocs, can be determined from the following expressions:

$$M \propto R_g^{D_3} \quad \text{or} \quad V \propto L^{D_3} \quad (2.15, 2.16)$$

where R_g is the radius of gyration [m], or the standard deviation of the floc from its center of mass. In other words, R_g is a distance where, if the entire mass of the object were centered at that radius, would give the same moment of inertia as the original object. For Euclidean objects, $D_3 = 3$. Higher values of D_3 indicate lower aggregate porosities, higher densities and faster settling velocities (Jiang and Logan, 1996).

A two-dimensional fractal dimension (D_2) for a single floc, or for a population of flocs, can be determined from the following expression:

$$A_c \propto L^{D_2} \quad \text{or} \quad p \propto A_c^{\frac{D_2}{2}} \quad (2.17, 2.18)$$

For Euclidean objects, $D_2 = 2$. Values of $D_2 > 2$ indicate that as the object size increases, the projected area increases slower than the square of the length scale (deBoer and Stone, 1999). In this case, the projected area of larger objects is less than that of Euclidean objects of the same scale because of elongation of the larger objects or because the larger objects surround or partially surround regions that are not part of the object. Densely packed aggregates have a high two-dimensional fractal dimension, while lower values of D_2 result from large, highly branched and loosely bound structures (Chakraborti *et al.*, 2000).

Fractal dimensions D_3 and D_2 essentially illustrate how porous an object is. For particles, porosity quantitatively describes the fraction of void spaces in the material, where the void spaces may contain air or water, and is defined by (Craig, 1997):

$$\phi = \frac{V_v}{V_t} \quad (2.18)$$

where V_v is the volume of the void space [m^3] and V_t is the total volume of the aggregate [m^3]. Standard values for many types of particles in natural systems have been determined. For sand, porosity ranges between 0.20 and 0.50; for clay, it is generally between 0.50 and 0.70 (Craig, 1997). It is generally accepted that the porosity of most natural suspended material (i.e., non-flocculated) decreases as particle size increases.

Floc porosity, however, is very complex and difficult to measure. Traditional models (i.e., ϕ) regard porosity as continuous and uniformly distributed, failing to account for irregularities caused by aggregation. Fractal dimensions do not make these assumptions and offer a more accurate and quantifiable approach for describing aggregate structure.

A one-dimensional fractal dimension (D_1) for a single floc, or for a population of flocs, can be determined from the following expressions:

$$p \propto L^{D_1} \quad (2.20)$$

For Euclidean objects, $D_1 = 1$. Values of $D_1 > 1$ indicate that with increasing object size, the perimeter increases faster than the object length scale so that the object becomes more complex for larger objects (deBoer and Stone, 1999). Higher values of D_1 signify more complex particle outlines.

In simplistic terms, D_1 has been defined as describing the complexity of the outlines of an object while D_2 and D_3 determine how well objects fill two- or three-dimensional space (Kenkel and Walker, 1996). While the significance of the actual values is not yet known (i.e., the difference in structure between an object with a D_1 value of 1.2 and another with a D_1 value of 1.25), fractal dimensions provide a more accurate description of objects where Euclidean geometry does not apply (i.e., flocs). The application of fractal dimensions in engineering crosses many disciplines from the detection, location and depth of cracking in structural supports to the characterization of wastewater sludge (Chakraborti *et al.*, 2003).

2.4.2 Practical Application of Fractal Dimensions for Water Treatment

Water treatment investigations involving fractal dimensions have traditionally focused on understanding the changes to the structural characteristics of flocs under various coagulation regimes. Attempts to make links between the fractal properties of aggregates and the performance of downstream processes such as sedimentation and filtration are limited in the literature. Most of these reported studies were conducted with idealized particles and simulated aggregation. Table 2.3 summarizes recent investigations that have used fractal dimension measurements for various water treatment applications and highlights the practical implications of those studies.

Table 2.3: Recent publications relating to the application of fractal dimension measurements (modified from Jefferson and Jarvis, 2006).

Description	Fractal Dimension	Range of Fractals Measured	How Fractals Changed	Practical Implications of the Results
Change in fractal dimension with a change in primary particle size for charged silica particles (Kim and Berg, 2000)	D_3	2.26 → 2.64	Decrease in D_3 as the primary particle size changed	N/A
The effect of increasing the ratio of organic matter on organo-ferric floc structure (Jarvis <i>et al.</i> , 2005)	D_3	1.78 → 2.20	As the ratio of organic floc decreased from 3.8 to 0 (by mass), the D_3 increased	Organic:coagulant ratio important in determining optimum floc removals
Change in floc structure from charge neutralization (CN) to 'sweep' flocculation (SF) for alum-particle flocs (Chakraborti <i>et al.</i> , 2000)	D_2	<u>Lake Water</u> 1.96 → 1.84 (CN) 1.96 → 1.65 (SF) <u>Clay Suspension</u> 1.89 → 1.81 (CN) 1.81 → 1.77 (SF)	D_2 was lower for 'sweep' flocculation than for charge neutralization	Mechanistic understanding of floc formation. Floc size was more important than fractal dimension for residual turbidity
Change in floc structure from CN to SF for alum-particle flocs (Kim <i>et al.</i> , 2001)	D_2	$\frac{A_c \propto L^{D_2}}$ 1.53 (CN) → 1.48 (SF) $\frac{A_c \propto P^{2/D_2}}$ 1.08 (CN) → 1.31 (SF)	No consistent trend between 'sweep' flocculation and charge neutralization for D_2 for both techniques	N/A
Effect of polymer dose on drinking water sludge flocs (Zhao, 2004)	D_3	1.06 → 1.77	D_3 increased with the addition of polymer, however further increases in polymer did not significantly change the value of D_3	N/A
Change in fractal dimension with aggregation time for charged silica particles (Kim and Berg, 2000)	D_3	1.79 → 1.88	Increase in D_3 as flocs grow	N/A
The effect of fractal dimension on membrane filtration for haematite flocs (Lee <i>et al.</i> , 2003)	D_3	1.83 → 2.25	D_3 increased as mixing speed increased	Specific cake resistance affected by fractal dimension for small flocs only (~ 10 μm)
Settling velocities of fractal aggregates (Johnson <i>et al.</i> , 1996)	D_3	1.78 → 2.25	When $D_3 < 2$, aggregate porosities will be overestimated and fractal dimensions will be calculated incorrectly from settling velocity data and Stoke's law	Settling velocities of these aggregates were on average 4 to 8.3 times higher than those predicted using Stoke's law

Chakraborti *et al.* (2000), for example, investigated the coagulation of lake water with alum and D_2 was seen to decrease from 1.84 to 1.65 as the destabilization mechanism changed from charge neutralization to “sweep” flocculation. The decreased fractal dimension corresponded to a reduction in turbidity. It was concluded, however, that the performance difference (i.e., change in turbidity) was related to an observable difference in floc size rather than the structure. These types of studies (i.e., the application of fractal dimension measurements to better understand water treatment processes) continue and the results of the investigations continue to vary and/or contradict each other. For example, similar work by Kim *et al.* (2001) demonstrated outcomes contrary to those from Chakraborti *et al.* (2000); flocs formed under charge neutralization had a D_2 value of 1.48 compared to 1.53 during ‘sweep’ flocculation. While further experiments are necessary to verify the results and determine the significance of these values, both studies are consistent with Jiang and Logan (1996) in that “a crucial challenge in applying fractal geometry to water treatment is that the value of these fractal dimensions is highly variable, suggesting that there is no similar universality in fractal dimensions when aggregates of different types of materials are formed by other coagulation mechanisms”. It is generally acknowledged, however, that fractal dimensions have and will continue to further our mechanistic understanding of flocculation.

Measurement of a fractal dimension has been used and is a well-established means of describing the complicated character of flocs in natural systems and wastewater treatment (Chakraborti *et al.*, 2003). For example, fractal dimensions have been used to characterize aggregate populations formed in fluid stream and marine environments to enable comparison between different floc-building materials (e.g., NOM) and flow regimes. Wastewater sludge has also been evaluated using fractal geometry to improve dewatering performance and decrease membrane fouling. As shown in Table 2.3, data supporting the use of fractal dimensions for water treatment at least as a diagnostic tool exists. From Chakraborti *et al.* (2000), the relevance of the fractal dimension to engineered processes includes effects on the properties of the aggregates formed and the coagulation rate. It is desirable to have rapid coagulation rates and also to produce floc with properties that results in efficient particle removal. Coagulation rates are reported inversely proportional to D_3 while settling velocity

is proportional to D_3 , for example. Thus for rapid coagulation, particles with a small D_3 may be desirable while for gravity settling a large D_3 is preferred

However, the true potential and exact practical significance of fractal geometry have yet to be determined. For this to occur, investigations must begin and/or continue to address the need to:

1. better understand how or why alterations in fractal dimensions are associated to changes in various other operational variables (i.e., turbidity);
2. identify a clear connection of fractal dimensions to the operation of downstream processes (i.e., clarification);
3. better understand the physical, or structural, significance in differences between values (e.g., the differences in character between a floc with a D_2 of 1.20 compared to one with a D_2 of 1.24);
4. develop techniques to quantify uncertainty when comparing similar fractal values obtained by different floc characterization methods;
5. develop techniques to quantify variability in fractal floc characterization data; and
6. develop essential guidance for characterizing floc populations in a statistically significant manner.

2.5 Methods for Characterizing Floc Structure

Prior to floc characterization, it is initially important to ensure that the extraction, preparation and measuring technique (Jarvis *et al.*, 2005):

- a. measures a representative sample or sub-sample of the original floc suspension;
- b. does not damage, break or change the flocs; and
- c. does not encourage further aggregation.

The fractal dimensions of the flocs can then be evaluated in a number of ways. The three (3) most common methods for obtaining these values are light microscopy in combination with

photography and/or image analysis, light scattering and settling (Farrow and Warren, 1993). Though all three (3) techniques have advantages and disadvantages, characterization from magnified images captured from cameras is the most commonly reported approach.

2.5.1 Light Microscopy, Photography and Image Analysis

As discussed in Section 2.4.1, floc size and shape characteristics (e.g., A_c and V) can be used to calculate fractal dimensions. Light microscopy is one of the most widely employed techniques for measuring particle size and has been used for decades as a method for sizing and counting flocs (Allen, 1997; Droppo et al., 1996; Aguilar *et al.*, 2003). The method traditionally involved carefully dropping a small sample of the suspension onto a microscope slide, or into a measuring cell on a slide (Wang *et al.*, 2002). Aggregate size was estimated by reference to a graduated eye piece graticule or by placing flocs in cells with background grids or scales of a known size (Jarvis *et al.*, 2005). Technological advancements have simplified and increased the accuracy of light microscopy through the development of image analysis and digital cameras. Modern microscopy is often combined with image analysis by mounting a CCD or digital camera onto the microscope (Li and Ganczarczyk, 1986).

Image analysis is the manipulation of information within an image to turn it into a more useful form; digital image analysis is the manipulation of digital images on a computer. The basic stages and requirements of performing digital image processing and analysis are presented in Figure 2.14. Digital image analysis typically requires elements for image processing, or enhancement to improve the quality of the image for analysis (e.g., a blurry background between two images could cause them to be sized as one).

The primary components of a typical digital image analysis system are an image capture device (e.g., a close-coupled device (CCD) camera or digital camera) connected to a computer with an image grabber. Computer software is usually required for the image processing and analysis and an assortment of commercial products are available for this

purpose. Digital image analysis is perhaps the most accurate floc characterization method; examination of single flocs allows detailed information on variation in floc structure. Unlike light scattering and settling, however, it is often a time consuming procedure.

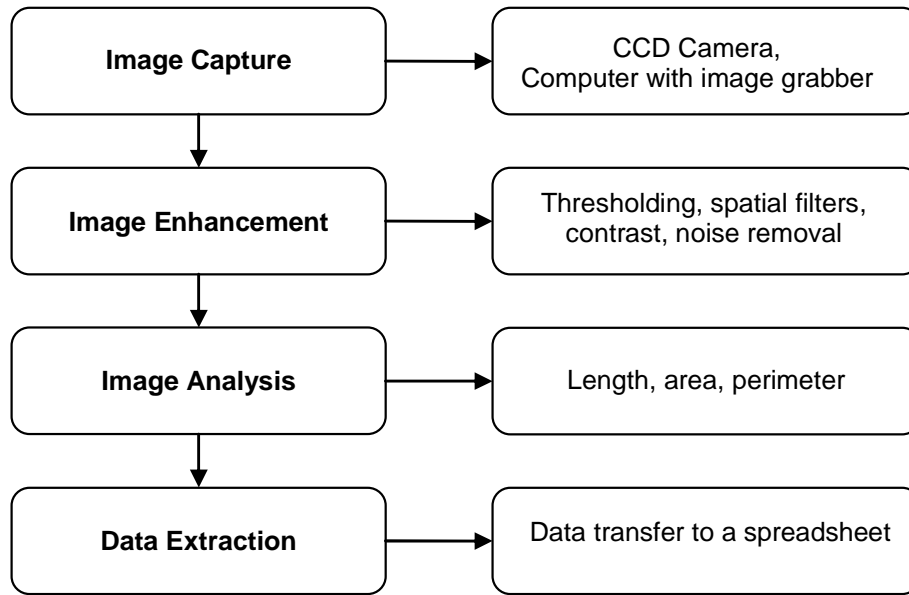


Figure 2.14: Steps involved in digital image analysis (modified from Jarvis *et al.*, 2005).

2.5.2 Light Scattering

The pattern in which an aggregate scatters incoming radiation gives information about the aggregate structure as a function of a length scale (Bushell *et al.*, 2002). To generate various particle characteristics (e.g., fractal values) using a light scattering particle sizing technique, the measured scattering pattern of a light that is passed through a suspension of particles is compared to the predicted settling pattern. This predicted settling pattern is based upon an optical power-law model and can only be utilized if enough is known about the scattering properties of the material contained within the aggregate. If this information is not known, standard optical models will assume that the primary particles that compose the aggregate are uniform in both shape and size. Therefore, most application of scattering has been systems where information is known about primary particle size and the scattering behavior of the particles under investigation. Examples include flocs formed by particles of latex

microspheres (Johnson *et al.*, 1996). Selecting or developing an appropriate model is likely the primary disadvantage of this technique and the method of settling.

2.5.3 Settling

Using settling columns (Figure 2.15) to determine floc structural characteristics is a well established technique that takes on additional relevance because the settling behavior of aggregates is an important parameter for designing or optimizing the sedimentation process (Jarvis *et al.*, 2005). This floc settling behavior is dependent on size, density and porosity (i.e., structural characteristics) (Tang *et al.*, 2002). The fractal nature of the floc structure can have two (2) possible consequences on settlement, which are:

1. an increase in drag on the particle when compared to a solid sphere of the same size; or
2. a reduction in drag due to advection of the suspending medium through the floc structure.

As discussed in Section 2.2.2, the structural complexities of floc contradict the assumptions inherent in Stokes' law. This presents a problem when using settling because particle characteristics are calculated from measured settling velocities. It has been suggested, though, that flocs settle slow enough in order for Stokes' derived equations to apply so long as shape factors are added to account for the irregular shape of the aggregates (Gregory, 1998). To rectify these inaccuracies, or potentially incorrect assumptions, settling velocity models have been developed that directly account for the fractal nature of flocs, but still fail to address the issue of flocculent settling behavior. For example, Wu *et al.* (2002) derived the following theoretical expression for aggregates consisting of similar primary particles:

$$v = \frac{d^{D_3} 4kg}{3A(\beta)\mu} \quad (2.21)$$

where k is a proportionality constant [kg/m^{D_3}] and $A(\beta)$ is a correction factor for advection through the floc. Johnson *et al.* (1996) developed the following relationship:

$$v = \frac{ehg\Delta\rho d^{D_3-D_2+1}}{3a\rho\mu} \quad (2.22)$$

where a is a Reynold's constant, and the constants e and h are functions of the fractal dimension. Neither of these models has been validated by actual data, though; difficulties in selecting an appropriate model should be considered when selecting settlement as a floc characterization technique.



Figure 2.15: Example of a settling column for characterizing flocs.

2.5.4 Selecting a Characterization Technique

Three (3) common techniques for measuring floc structural characteristics have been described above and their primary advantages and disadvantages were outlined in Table 2.4. Application of light scattering techniques to complex flocs, like those produced by typical water treatment processes, has been problematic (Waite, 1999; Guan *et al.*, 1998). In these instances, although the speed of analysis is rapid, scattering is affected by shadowing, scattering interactions and multiple scattering caused by large, non-uniform primary particles with varying refractive indices. For this reason, light scattering techniques are used principally in studies of more fundamental concerns, such as those that use simulated particles.

Table 2.4: Advantages and Disadvantages of floc structural characterization techniques (modified from Jarvis *et al.*, 2005).

Technique	Advantages	Disadvantages
<i>Light Microscopy, Photography and Image Analysis</i>	<ul style="list-style-type: none"> • Best for large, open aggregates • Not prone to contamination • Examination of single flocs allows detailed information on variation in floc structure 	<ul style="list-style-type: none"> • Time consuming • Requires well defined, high contrast images for accurate analysis
<i>Light Scattering</i>	<ul style="list-style-type: none"> • Rapid, non-intrusive method • Good for analysis for small aggregates with an open structure and a low refractive index • Collects many readings from many aggregates in a few seconds 	<ul style="list-style-type: none"> • Not good for aggregates made from many primary particles • Choosing an appropriate model for scattering can be difficult • Results affected by contamination from dust, etc.
<i>Settling</i>	<ul style="list-style-type: none"> • Best for measuring compact flocs • Cheap and simple • Not prone to contamination 	<ul style="list-style-type: none"> • Time consuming • Finding an appropriate drag coefficient or model can be difficult • Can get non-random orientation of falling aggregates • Careful regulation of settling column is required

Settling is generally an inexpensive, rapid method for characterizing aggregates. Careful regulation of the settling column is required (i.e., no temperature gradients can exist);

however, care is needed in transferring the flocs to the test equipment to avoid break-up (Jefferson and Jarvis, 2006). The crucial disadvantage of this procedure is that Stokes' law will not usually apply to porous, non-spherical flocs and determining an appropriate model can be complicated.

Therefore, although microscopy and image analysis is time consuming, and requires considerable sample preparation and analysis to achieve acceptable results, it is often the most preferred option of investigators performing floc characterization on engineered floc. As long as the images are well defined with a high level of contrast, aggregates can be analyzed individually providing comprehensive information of their structural detail. This also allows for exclusion or elimination of false flocs (i.e., other particles in the sample), a benefit that is not normally available to the other two (2) methods.

Regardless of which characterization technique is preferred or selected, it is important to report which of the three (3) was used in measuring a fractal dimension as each technique might provide a different answer for the same aggregate. For example, the measured value of D_3 was 1.3 from settling and 2.06 from light scattering in one particular study characterizing activated sludge (Wu *et al.*, 2002). Detailed error analysis is thus required to assess the accuracy and precision of the particle characterization techniques and to quantify the uncertainty in these types of data.

2.6 Research Needs

Through examination of the literature related to coagulation, flocculation and clarification theory, as well as the structural characteristics and characterization techniques, a number of key research needs have been identified. These include:

- demonstration of the limitations of traditional bench-scale protocols commonly used to optimize conventional chemical pre-treatment during full-scale drinking

water treatment and articulation of the reasons why data obtained from these tests must be evaluated judiciously;

- establishment of indicators of flocculent settling behavior to improve the prediction capacity of aggregate settling performance;
- better understanding of engineered floc structure to improve the prediction capacity of aggregate settling velocities;
- development and validation of techniques to quantify the variability in fractal floc characterization data and development of essential guidance for determining how to characterize floc populations in a statistically significant manner; and
- development of practical strategies for integration of key aspects of advanced particle characterization techniques into common bench-scale protocols.

3 MATERIALS AND METHODS

3.1 Research Rationale and Methodology

The provision of safe drinking water requires sufficient disinfection of pathogens by ultraviolet irradiation (UV), ozone, oxidation with chemicals such as chlorine, and/or filtration. The first three (3) alternatives, however, become decreasingly effective as levels of additional particulate matter in waters to be treated increase (Stagg *et al.*, 1978, Sproul, 1972); filtration of water with low turbidity is often not effective because a more sophisticated level of treatment is often required to mechanically remove very small particles that pass through standard full-scale filters (Al-Ani *et al.*, 1986). Particularly, it has been found that pathogens may be partially shielded against the action of UV, ozone and chlorine by attachment to or enmeshment in other particles present in the water. These particles are separated from the water by chemical pre-treatment followed by one (1) or more particle removal processes.

Many treatment plants, including the Mannheim Water Treatment Plant (MWTP) in Kitchener, ON often have difficulty reaching their operational capacity due to a floc build-up on the surface of and within their filters. One (1) possible explanation for this observation is that the pre-treatment processes are not optimized to ensure adequate solids removal in the sedimentation basins. Furthermore, data from bench scale tests will often indicate better settled water ultraviolet absorption at 254 nm (UV_{254}) values and turbidities than what are being achieved. The need to achieve low settled water UV_{254} values and turbidities while increasing plant capacity, and the opportunity to improve the predictive capacity of bench-scale protocols for optimizing conventional chemical pre-treatment provided the motivation for this research.

Specifically, the primary focus of this investigation was to develop approaches for integrating particle characterization techniques with these bench-scale protocols. The

important and frequently overlooked need to develop guidance on characterization of floc populations in a statistically significant manner and techniques to quantify uncertainty in fractal floc characterization data were necessary components of this research. As well, it was hoped that achieving those objectives would contribute to developing strategies for further optimization of chemical pre-treatment processes (i.e., coagulation, flocculation and sedimentation) at the MWTP.

Twelve (12) jar tests using the MWTP protocol were performed throughout this investigation. The UV_{254} and turbidity of the supernatant were evaluated during each jar test to investigate potential relationships between these parameters and floc settling rates and structure. Six (6) jar tests were conducted to generate aggregates for settling tests. Three (3) jar tests were conducted at 5, 15 and 25 °C using aluminum sulfate (alum) as the primary coagulant and three (3) jar tests that were conducted at 5, 15 and 25 °C using polyaluminum chloride (PACl) as the primary coagulant. Samples were collected after a period of settling from the bottom of the jars so that it could be determined whether or not the settling rates and/or sizes of the aggregates that had settled would correspond to the UV_{254} and turbidity of the supernatant.

The six (6) jar tests were then repeated to characterize the fractal structure of the flocs by digital image analysis with microscopy. Structural characteristics were calculated from samples of aggregates that were collected prior to settling. This was done to predict DOC and particle removal performance (i.e., based on UV_{254} and turbidity reduction, respectively) by using floc structural information of aggregates generated during coagulation and flocculation.

All of the tests were conducted at varying temperatures because one of the original objectives of the study was to evaluate the temperature effects on floc structure and/or settling velocity. It was decided after the experiments were conducted, however, that the primary focus of this thesis would be on the general development and application of floc characterization

techniques to water treatment. The initially proposed temperature-floc analysis will be presented elsewhere.

A simple approach for quantifying the uncertainty in floc characterization data was developed. Samples of aggregates generated at full-scale at the MWTP were then collected and compared to the results of the bench-scale testing. The following sections describe the MWTP, outline the materials and methods employed to conduct the bench-scale experiments (i.e., jar tests and settling column tests), as well as the corresponding floc characterization method and statistical analysis of the acquired data. Full-scale floc sampling at the MWTP is also discussed.

3.2 The Mannheim Water Treatment Plant (MWTP)

The MWTP in Kitchener, ON (Figure 3.1) treats raw water from the Grand River at the Hidden Valley Low Lift Station (Clarke, 2007). The Grand River flows 300 kilometers through southwestern Ontario from the highlands of Dufferin County to Port Maitland on Lake Erie. Water passes through multiple reservoirs at the Hidden Valley Station, which reduces the loading of particles derived from atmospheric sources (i.e., due to settling), and influences the type and/or quantity of microorganisms and organic particles derived by biological processes (i.e., due to attenuation).

A 9.8 km, 1,200 mm diameter raw water transmission watermain connects the Hidden Valley Pumping Station to the MWTP. Raw water entering the plant flows through two (2) treatment trains, operating in parallel. The raw water is rapidly mixed ($G \sim 1,000 \text{ s}^{-1}$) by 2.25 kW in-line blenders and hydraulic jet mixers. Polymer injection is preceded by PACl addition. Both injection points are in-line.

The water is then conveyed into four (4) concrete reinforced flocculation basins, two (2) in each treatment train, operating in series. Each basin is baffled to provide two (2) cells, which

results in a total retention time of thirty (30) minutes at the rated capacity of 72 MLD. Eight (8) vertical paddle flocculators, with variable frequency drives (VFDs), produce mean G values of 60 to 100 s^{-1} . The chemically pre-treated water then flows through two (2) 12.4 m wide x 12.4 m long x 6 m deep reinforced concrete sedimentation basins, one (1) in each treatment train, with inclined plate separators and circular sludge collectors. The water is then conveyed through ozonation and filtration processes and is then disinfected prior to entering the two clearwells, which have a combined total useable volume of 15.28 ML.

Disinfection is primarily achieved through ultraviolet (UV) irradiation, followed by chlorination. Although the process was added mainly to control taste and odour, ozonation also acts as a disinfectant. Continuous analyzers monitor the levels of chlorine, turbidity and UV dosage prior to the water being discharged. The analyzers are connected with the Mannheim Water Treatment Plant Supervisory Control and Data Acquisition (SCADA) system, which is monitored by an operator 24 hours per day.



Figure 3.1: The Mannheim Water Treatment Plant in Kitchener, ON (Emelko *et al.*, 2006).

The Mannheim Artificial Recharge Facilities and seven (7) other groundwater wells are also located on-site. Water from these sources is blended with the treated surface water and then stored at the Mannheim Pumping Station Reservoir, which has a total storage capacity of 122.7 ML. As stated above, the Mannheim Water Treatment Plant has a rated capacity of 72 MLD, or 840 L/s. Permitted water capture from the Grand River varies from season to season; runoff from snowmelt allows for the highest takings to occur in the spring months. Raw water quality varies from season to season as well, and is constantly monitored as per the Ontario Ministry of the Environment (MOE) Drinking Water Systems Regulation O. Reg. 170/03 (2003).

As summarized in the Regional Municipality of Waterloo (RMOW) 2007 Annual Water Quality Report (Clarke, 2007), 622 grab samples of raw water were collected throughout the year for microbiological testing; 156 grab samples were collected to measure turbidity. From this testing, there were twelve (12) detections of fecal coliforms (i.e., a non-sporulating microorganism used as an indicator for other pathogens that may be present in feces) and the turbidity ranged from 0.10 to 26.4 NTU. 8,760 readings from the SCADA system demonstrated that treated water turbidities ranged only from 0.00 to 1.00 NTU and based on 57 grab samples of the effluent, total coliforms were always absent. The extreme turbidity values (i.e., 0.00 and 1.00 NTU) represented only a fraction of the 8,760 values recorded. They were attributed to equipment error associated with sampling. Because the data are collected in two (2) minute intervals, which are very small, it is not uncommon to record an outlier due to an air bubble or loss of flow. Nominal raw water quality characteristics are presented in Table 3.1.

Table 3.1: Nominal raw water quality characteristics of Grand River water at the MWTP.

	Temperature (°C)	TOC/DOC (mg/L)	Turbidity (NTU)	pH	Alkalinity (mg/L as CaCO ₃)
Nominal Value	11	6.0	3.7	8.2	210
Range	1- 23	5.0- 7.0	0.9- 13.7	7.9- 8.4	160- 250

All raw water samples from the MWTP utilized during the present investigation were collected on three (3) separate occasions between May 2007 and January 2008. Raw water quality on these dates was recorded by the SCADA system. Raw water characteristics are presented and summarized in Section 4.1. The samples were collected in 20 L polyethylene carboys from a tap located prior to the coagulant injection point and refrigerated at 4 °C until required for jar testing

3.3 MWTP Jar Test Protocol

As partially depicted in Figure 3.2, the apparatus used during the procedure utilized throughout the present investigation was a Phipps & Bird Jar Standard Tester (Phipps & Bird Inc., Richmond, VA); a stirring machine with six paddles that can operate at variable speeds [i.e., 0 to 300 revolutions per minute (rpm)], a floc illuminator for observing floc formation and six 2 L square acrylic jars. Jar test experiments are conducted at the MWTP whenever there are changes in the water quality and/or quantity (e.g., due to snowmelt or rainfall) and/or any of the treatment processes.

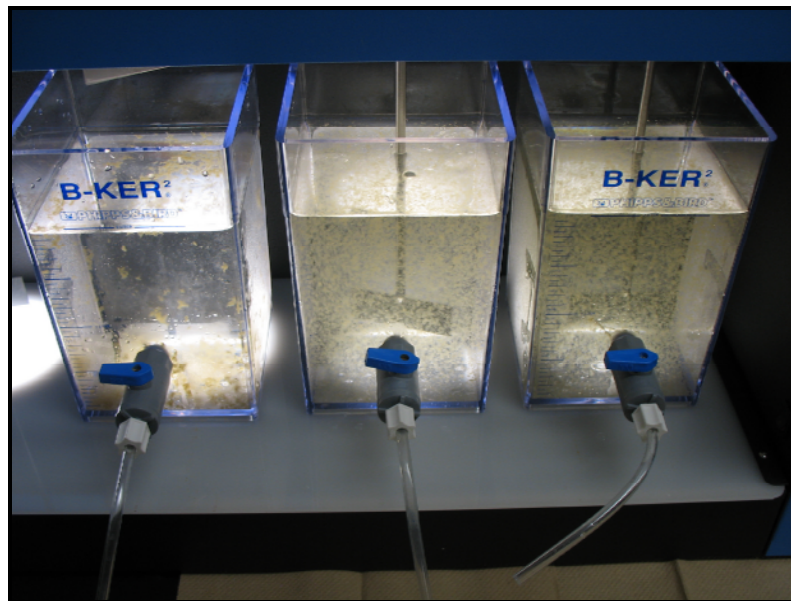


Figure 3.2: Jar testing equipment used during the MWTP jar test protocol.

The protocol describe herein was a procedure that the RMOW had previously developed to simulate full-scale coagulation and flocculation at the MWTP, which was based on reproducing the G value in the full-scale basins. The exact values of G are provided in Section 3.3.2. Using the method prescribed by the RMOW was essential in achieving the first objective of this thesis, which was to “critically evaluate the limitations of traditional bench-scale protocols”. Design of an original, and potentially “optimal” jar test protocol could have been time consuming and outside the scope of this research.

3.3.1 Reagent Preparation

At the time of this investigation, the MWTPs coagulation regime consisted of ~ 16 to 28 mg/L PACl (Kemira Water Solutions Inc., Brantford, ON) and ~ 0.2 mg/L of cationic polyelectrolyte (Magnafloc LT 22 S, Ciba Specialty Chemicals Canada Inc., Mississauga, ON). Alum (Kemira Water Solutions Canada Inc., Brantford, ON) was previously the primary coagulant, and was used in this investigation for comparative purposes. Both coagulants were concentrated aqueous solutions; the polymer was a free-flowing granular powder. Coagulant and polymer specifications are presented in Tables 3.2 and 3.3.

Table 3.2: Physical and Chemical Properties of Alum and PACl.

Physical or Chemical Property	Alum	PACl
Chemical Family	Inorganic salts	Polynuclear inorganic salts
Formula	$Al_2(SO_4)_3$	$Al_x(OH)_{3x-2y-z}(SO_4)_yCl_z$
Appearance	Clear	Clear amber to colorless
Odor	Slight acidic	Slight
Form	Liquid	Liquid
pH as is	< 2.5	3.0 ± 0.5
Vapor Pressure (mm Hg)	40 at 35 °C	17 at 20 °C
Boiling Point (°C)	106	102
Freezing Point (°C)	Concentration dependent	-5 ± 2 °C
Specific Gravity (at 20 °C)	1.2 to 1.35	1.27 ± 0.05
Solubility	Soluble	Soluble in water
Vapor Density (Air=1)	N/A	1.3
Percent Volatile by Volume	N/A	N/A

The diluted alum solution was prepared in the laboratory by pipeting 8 mL of the full-strength alum stock solution (i.e., 50% $\text{Al}_2(\text{SO}_4)_3$ concentration) into a 100 mL volumetric flask and adding 90 mL of deionized (DI) water. The flask was then swirled to completely mix the solution. 1 mL of the prepared solution contained ~ 40 mg of alum. This diluted mixture was used for a period of 48 hours. At this time, the mixture was discarded and a new solution was prepared.

Table 3.3: Physical and Chemical properties of Magnafloc LT 22 S.

Physical or Chemical Property	Magnafloc LT 22 S
<i>Form</i>	White granular solid
<i>Bulk Density (g/cm³)</i>	0.7
<i>pH of 1% Solution</i>	~ 5.4
<i>Viscosity at 25 °C</i>	Concentration dependent

The diluted PACl solution was prepared in the laboratory by pipeting 10 mL of the full-strength SternPAC stock solution (i.e., 40% $\text{Al}_x(\text{OH})_{3x-2y-z}(\text{SO}_4)_y\text{Cl}_z$ concentration) into a 100 mL volumetric flask and adding 90 mL of DI water. The flask was then swirled to completely mix the solution. 1 mL of the prepared solution contained ~ 40 mg of PACl. This diluted mixture was used for a period of 48 hours. At this time, the mixture was discarded and a new solution was prepared.

The polymer solution was prepared at the MWTP by pipeting 10 mL of the 0.2% plant stock solution into a 100 mL volumetric flask and adding 90 ml of DI water. The flask was then swirled to completely mix the solution. 1 mL of the prepared solution contained ~ 0.2 mg of polymer. This diluted mixture was used for a period of 24 hours. At this time, the mixture was discarded and a new solution was prepared.

Once the dilute reagents were prepared, the quantity of these solutions to be added to each jar was calculated for a 2 L sample of raw water. These quantities, summarized in Table 3.4, are based upon the typical annual operating range of dosages the MWTP. Twelve (12) plastic syringes, six (6) filled with the appropriate volume of coagulant solution and six (6) filled

with the appropriate volume of polymer solution, were then placed in front of the corresponding jar.

Table 3.4: Quantities of Dilute Coagulant and Polymer Solutions required for Jar Testing.

	Jar #1	Jar #2	Jar #3	Jar #4	Jar #5	Jar #6
Coagulant Dosage (mg/L)	20	30	40	50	60	70
Quantity of Dilute Solution (mL)	1.0	1.5	2.0	2.5	3.0	3.5
Polymer Dosage (mg/L)	0.1	0.1	0.1	0.1	0.1	0.1
Quantity of Dilute Solution (mL)	2.0	2.0	2.0	2.0	2.0	2.0

3.3.2 Jar Testing Procedure

Jar tests were conducted at temperatures of approximately 5, 15 and 25 °C for each of the coagulants (i.e., alum and PACl); a total of six (6) bench-scale experiments. The temperatures, which were not necessarily the temperatures of the raw water at the time of collection, represented typical raw water influent temperatures at the MWTP between the months of April and December. Operational parameters at the MWTP (i.e., coagulant dose) are variable throughout the winter due to varying water quality characteristics; the conclusions and recommendations in this thesis are for periods of stable full-scale operation (i.e., throughout the summer months). Because samples were collected during multiple seasons, a range of water qualities was investigated.

During the jar tests conducted during the present investigation, each jar was filled with 2 L of raw water, the temperature of which was measured with a mercury thermometer. The dial on the jar tester was first rotated to 300 rpm [i.e., $G \approx 300$ to 400 s^{-1} (Figure 3.3)] to induce rapid, or flash mixing. These velocity gradients represent the maximum that can be achieved with the jar test equipment; unfortunately they are lower than the 1000 s^{-1} utilized by the full-scale treatment plant.

The coagulant, in varying dosages according to Table 3.4, was then added to each of the six (6) jars at the water surface. After thirty (30) seconds, the paddle speed was lowered to 70

rpm (i.e., $G \approx 50$ to 65 s^{-1}) and the solution continued to mix for two (2) minutes. Once two (2) minutes had passed, the polymer was injected into the jars at the water surface. After an additional minute of mixing at 70 rpm, the paddle speed was lowered to 35 rpm (i.e., $G \approx 23$ to 28 s^{-1}) for ten (10) minutes, the “floculation” stage.

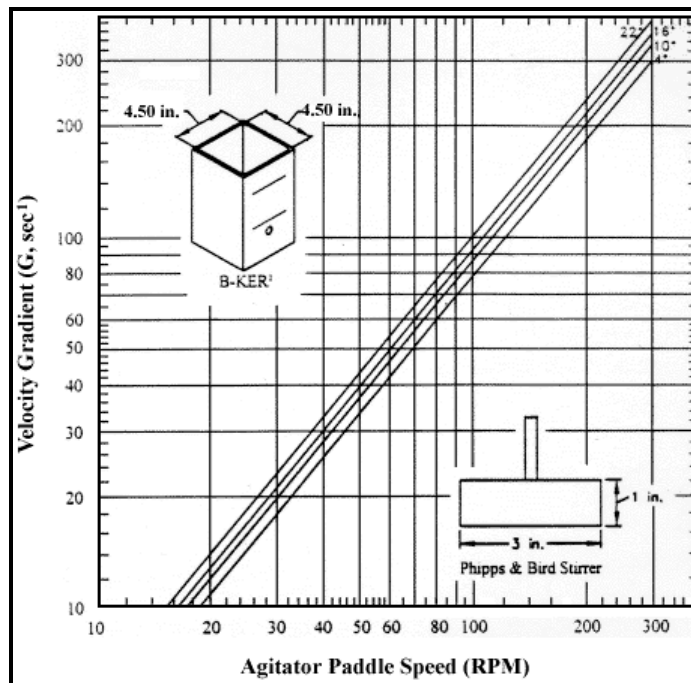


Figure 3.3: G-values for a standard Phipps and Bird Jar Tester (Grammer, 2007).

The mixers were then shut off and the particles and/or aggregates were settled for fifteen (15) minutes. Qualitative observations about the flocs and water (e.g., floc size and quantity, settleability and water quality) in each jar were made and recorded on a data sheet (Appendix B). Two (2) 40 mL grab samples of the supernatant (i.e., the clear liquid above the settled material) were collected in EPA viles from each jar at a depth of ~ 10 cm from the surface and refrigerated at 4 °C until they, along with 40 mL samples of the raw water, were processed for water quality analysis described in the following section. A drop of concentrated, 85% reagent grade phosphoric acid was added to one (1) of the 40 mL samples from each jar for preservation for Total Organic Carbon (TOC) analysis.

3.3.3 Water Quality Analyses

Five (5) water quality parameters were measured as part of the MWTP jar testing procedure: turbidity [NTU], TOC [mg/L], ultraviolet absorption at 254 nm (UV_{254}) [AU], conductivity [μ S/cm] and pH. All tests were completed in the Water Resources laboratories at the University of Waterloo (UW). All of the equipment was calibrated prior to analysis. Optimal coagulant dosages at full-scale are typically chosen based upon the settleability of the flocs and the results of these analyses, primarily the reduction in turbidity and/or UV_{254} .

It is important to note the MWTP measures UV_{254} as an indicator of dissolved organic material. In other words, DOC is not directly quantified. TOC was utilized throughout this study to approximate the organic concentration; the dissolved fraction was not measured. It could not have been assumed that DOC was equivalent to TOC because it is commonly that NOM is associated with particles, as well. It has been previously demonstrated, however, that DOC consistently comprises about 90% of the TOC in this raw water.

3.3.3.1 Turbidity

Turbidity was measured in the laboratory using a HACH 2100P Portable Turbidimeter (Fischer Scientific Company, Ottawa, ON), which provided direct digital readings in NTUs. According to the manufacturer, the resolution of the meter was 0.01 NTU on the lowest range (i.e., readings from 0 to 9.99 NTU) and 0.1 when the range was adjusted to between 0 to 99.9 NTU. A 1 NTU turbidity standard was used to calibrate the equipment.

3.3.3.2 Total Organic Carbon (TOC)

Samples were analyzed for TOC according to ASTM Method 5310B (1996), a high-temperature combustion method, using a SHIMADZU TOC-V Analyzer (Mandel Scientific Ltd, Guelph, ON), which analyzed the water for total carbon (TC) (mg/L) and total inorganic carbon (TIC) (mg/L) and provided TOC calculations in mg/L. The detection limit of the instrument, as stated by the manufacturer, was 5 mg/L with a measurement range between 0

and 25,000 mg/L for TC and 0 to 30,000 mg/L for TIC. Multilevel standard curves with a calibration range between 1 to 10 mg/L were run prior to sample analysis.

3.3.3.3 Ultraviolet Absorption at 254 nm (UV₂₅₄)

Samples were analyzed for UV₂₅₄ according to ASTM Method 5910B (1996) using an Agilent 8453 UV-Visible Spectrophotometer (Agilent Technologies, Mississauga, ON), which gave readings in percent and, as per the manufacturer, had a wavelength accuracy of ± 0.5 nm.

3.3.3.4 Conductivity

Conductivity readings were obtained using a HACH sensION portable conductivity meter with an electrode (Fischer Scientific Company, Ottawa, ON), which provided direct digital readings in $\mu\text{S}/\text{m}$. According to the manufacturer, the resolution of the meter was ± 0.5 % on the lowest range (i.e., readings from 0 to 199.9 $\mu\text{S}/\text{m}$) and ± 1.0 % when the range between 20 to 199.9 $\mu\text{S}/\text{m}$.

3.3.3.5 pH

pH readings were obtained using a HACH sensION pH meter with an electrode (Fischer Scientific Company, Ottawa, ON), which provided direct digital readings. The resolution of the meter was 0.001, as stated by the manufacturer.

3.4 Settling Experiments

Settling experiments, and the associated jar tests, were conducted at Environment Canada's Center for Inland Waters in Burlington, ON. They were performed following the methods of Droppo *et al.* (1997) that provide the discrete settling velocity for individual flocs. Settled flocs were collected from the bottom of the jars following the fifteen (15) minute settling

phase using a 25 mL graduated wide-mouth glass pipette cut horizontally 5 cm above the tip to minimize breakup of the aggregate. Vacuum was created using a standard rubber, 25 mL capacity pipette bulb. The flocs were then introduced into an insulated 2.5 L (i.e., 5 cm width x 10 cm length x 50 cm height) capacity settling column (Figure 3.4). The temperature of the raw water within the column was held constant at the same temperature as the jars in which the flocs were produced.



Figure 3.4: 2.5 L capacity settling column with a stereoscopic microscope.

A stereoscopic microscope Nikon SMZ-2 T (Nikon Canada Inc., Mississauga, ON) focused on a plane inside the column at a distance of 35 cm from the top of the column. The long settling distance relative to the size of the flocs is required to damp out any turbulence or

settling irregularities resulting from the initial introduction of the aggregates and to allow the flocs to reach terminal velocity prior to detection. Although all of the flocs were carefully observed throughout the tests, it is possible that further aggregation could have occurred over this distance, which would introduce difficult to quantify error into the results.

As flocs passed through the field of view, images were electronically recorded onto a Pentium computer through a CCD camera (Hamamatsu, Quorum Technologies Inc., Guelph, ON) interface. The settling velocity was derived by digitally overlaying two video frames obtained over a known time interval using Northern EclipseTM imaging software (Empix Imaging Inc., Mississauga, ON). In this way the same aggregate appears on the newly combined image twice and the settling distance can be digitized.

3.5 Floc Characterization

Since the method works well for large, open aggregates (i.e., engineered floc) and because it is regarded as the only reliable technique to determine floc shape characteristics (Jarvis *et al.*, 2005), light microscopy combined with digital image analysis was employed for characterizing the flocs examined throughout this study.

3.5.1 Floc Sampling

The MWTP jar test protocol was repeated following the methods outlined in Section 3.1, in a University of Waterloo Natural Sediment Laboratory. Three (3) samples of suspended flocs were collected directly from each of the 2 L jars at the end of the flocculation stage using sampling columns (Figure 3.5) described by deBoer and Stone (1999) for floc characterization. These sampling columns were plastic tubes with an internal diameter of 25 mm and volumes of 25 mL. They were held approximately 10 cm below the water surface as flocs passed through until square sections of plastic were placed at either end for closure.

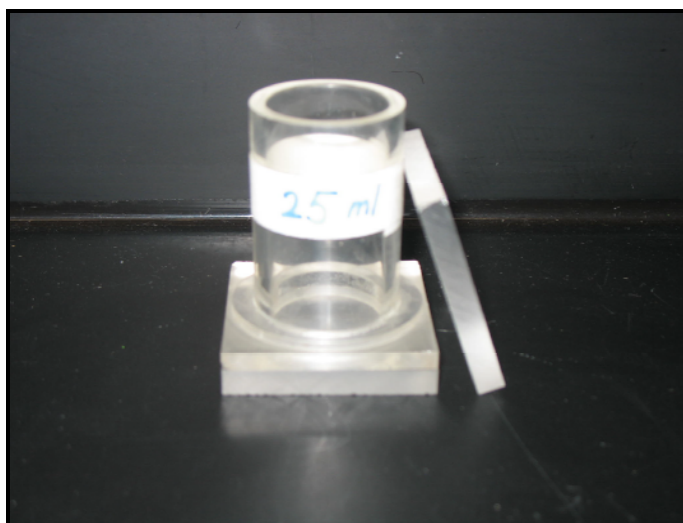


Figure 3.5: 25 mL plastic sampling columns for sampling of suspended particles and/or floc.

After sampling, a 0.45 μm Millipore HA filter was placed on a fritted glass holder and the column was inverted on the filter. A hand pump at low vacuum was used to settle flocs onto the filter (Figure 3.6). The filters were stored in a refrigerator until the characterization was performed.

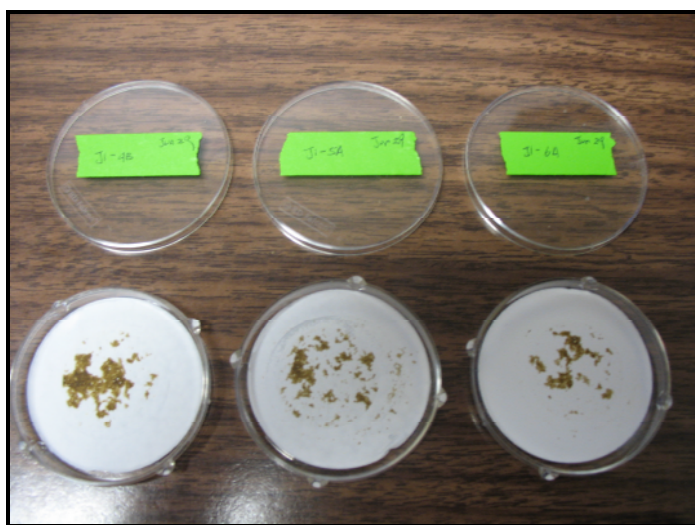


Figure 3.6: Engineered flocs settled onto 0.45 μm Millipore HA filters.

3.5.2 Light Microscopy and Digital Image Analysis

The 0.45 μm Millipore HA filters were left in the refrigerator to air-dry for approximately two (2) to three (3) weeks prior to analysis. Digital images of the particles deposited on the filters were collected using a Wild Leitz inverted light microscopy microscope fitted with a Sony XC75 CCD camera connected to a Pentium computer (Figure 3.7) running Northern Eclipse™ imaging software, according to the method described by deBoer and Stone (1999). For this method, the filters were first rendered semi-transparent by applying three (3) drops of immersion to the field of view. Collection of images began five (5) minutes after applying the immersion oil to allow for the filter to become sufficiently transparent, and image collection and particle counting typically took between twenty (20) and forty (40) minutes per sample. Between 1,500 and 20,000 aggregates or particles were enumerated, depending on the concentration of flocs on the filter.

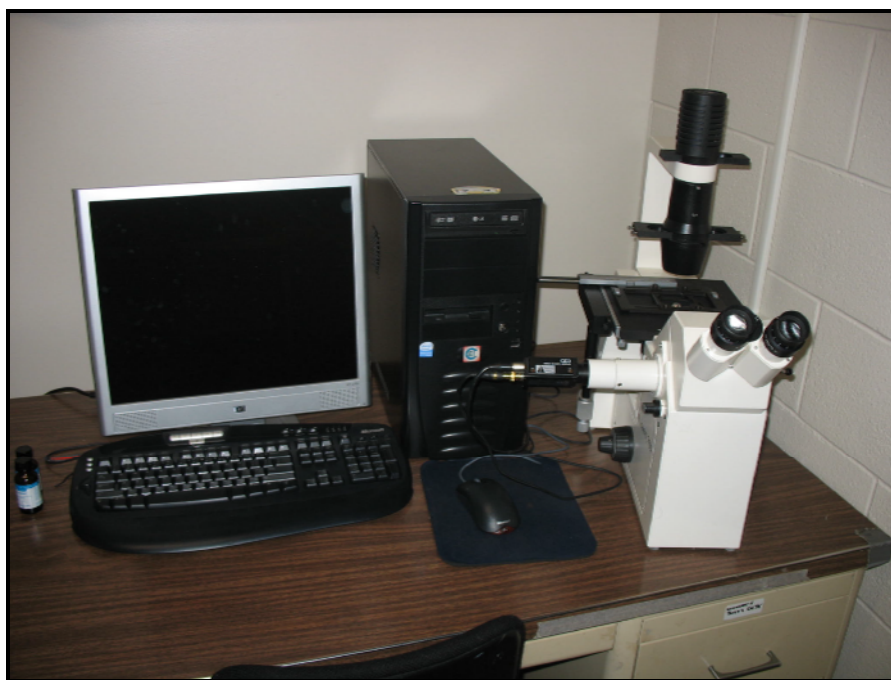


Figure 3.7: Wild Leitz inverted light microscopy microscope fitted with a Sony XC75 CCD camera connected to a Pentium computer.

Flocs were imaged at 2.5x magnification and raw water particles were imaged at 10x magnification. Background images without flocs or particles were collected for each filter and subtracted from each image taken during analysis to minimize the effect of non-uniform light levels. The image analysis software output a spreadsheet providing cross-sectional area (A_c), perimeter (p) and characteristic, or longest length (L_D) values for all aggregates or particles counted. A Visual Basic™ program was then used to calculate equivalent spherical diameter (ESD_A) and volume (V), and to perform a grain size analysis.

3.5.3 Fractal Analysis

Fractal Dimensions D_1 and D_2 were calculated from the slopes of regression lines of the relevant geometric variables (i.e., *Equations 2.15 through 2.18, 2.20*) on double-logarithm plots. D_1 was obtained from regression analysis of p versus L (i.e., *Equation 2.20*) where L was assumed to be the ESD_A . This assumption was made, as outlined in Section 2.3.2, so that populations of complex aggregates could be more accurately grouped and more accurately compared to one another. D_2 therefore, was derived from slopes of regression lines on of p and A_c (i.e., *Equation 2.18*). *Equation 2.17* (i.e., A_c versus L) was not utilized because of the assumption on L . Thus, D_2 would have been calculated from a regression analysis of the same measured parameter (i.e., A_c versus A_c) since ESD_A is derived from A_c .

Calculation of D_3 was excluded from the analysis primarily because the digital images were two-dimensional. Since V , as calculated by Visual Basic™, was also calculated assuming that the particle was spherical (i.e., from ESD_A), the values obtained from regression analysis of V versus L (i.e., *Equation 2.16*) would have been based on a hypothesis that information on three-dimensional characteristics could be extracted from a two-dimensional image. This is unlikely due to preferential settling on the filter [i.e., particles have a tendency to orient themselves on surfaces such that they present their maximum area (Allen, 1997)]. As well, *Equation 2.16* could not be utilized because of the assumption on L ; *Equation 2.15* (i.e., M versus R_g) could not be utilized because the mass of the particles was not measured.

3.5.4 Calculation of Variability in the Fractal Data

Sub-samples were considered replicates and all of the aggregates were combined if the t values calculated from both *Equations 3.1* and *3.2* (i.e., significant difference tests on the intercept and slope) were equal to 0. From these equations, a is the intercept, b is the slope and s is the standard error of the estimate.

$$t_a = \frac{a_1 + a_2}{\sqrt{s_{a1} + s_{a2} + s_{a12}}} \quad (3.1)$$

$$t_b = \frac{b_1 + b_2}{\sqrt{s_{b1} + s_{b2} + s_{b12}}} \quad (3.2)$$

Then for each regression (i.e., for each D_1 and D_2), a 95% confidence interval was calculated for both the intercept and the slope. That is, a range of intercepts and slopes that would occur for that particular sample 95% of the time. The confidence interval for the intercept is presented as *Equation 3.1*; the confidence interval for the slope is presented as *Equation 3.2*. From these equations, $t_{\alpha/2}$ is the student-t value (i.e., 1.96 at 95%), and S_{xx} is described by *Equation 3.3*.

$$A = a \pm t_{\frac{\alpha}{2}} s \sqrt{\frac{1}{n} + \frac{\bar{x}^2}{S_{xx}}} \quad (3.3)$$

$$B = b \pm t_{\frac{\alpha}{2}} s \sqrt{\frac{1}{S_{xx}}} \quad (3.4)$$

$$S_{xx} = \sum_{i=1}^n (x_i - \bar{x})^2 \quad (3.5)$$

If the confidence intervals of the sub-samples A, B and C overlapped, or intersected for both the slope and the intercept, then it was concluded that they were true replicate samples. Even if they were not true replicates, however, the sub-samples were combined because all of the

aggregates were sampled from one jar. This approach to data handling was acceptable and appropriate because the flocs were all collected from the same population and the size distribution of the combined data provided more information; thereby providing a better indication of the overall size distribution of flocs produced in a given sample. The purpose of the statistical analysis was to assess if the sampling approaches resulted in true replicates; regardless of that outcome, all of the particle data were combined to characterize the particle size distribution within the jar.

3.5.5 Statistical Assessment of Light Microscopy and Digital Image Analysis

Light microscopy with 2D image analysis, although time consuming, is a relatively inexpensive and reliable method of floc characterization (Jarvis *et al.*, 2005). This technique typically consists of using filter membranes to retain the suspended flocs and then measurement by light microscopy and computer software. Depending on the floc concentration in the water sample, the number of flocs on the filter may be low enough to permit evaluation of the entire membrane surface, which would achieve the most accurate and precise estimate of floc size and/or shape. However, floc concentrations found in characterization studies of both engineered and natural systems are often so elevated that evaluation of the entire membrane is unfeasible. In occurrences such as these, only a few images can be evaluated to estimate floc characteristics.

Approaches using combinations of microscopy with digital image analysis are based on the assumptions that flocs are uniformly distributed on the filter surface and the sample of measured aggregates is representative of the entire membrane, thereby yielding a reasonable estimate of size and/or shape. For natural system characterization studies, it has been proposed that a minimum of 3000 particles and/or flocs be counted (Stone, 2007). A general approach has not yet been suggested for engineered systems.

Floc characterization by microscopy with image analysis can be achieved by either evaluating flocs using a systematic pattern that attempts a spatially-even distribution, or by selecting aggregates randomly. Results from studies that have evaluated the effects of sample processing for direct counting methods of microorganisms (i.e., epifluorescence microscopy) have suggested that random selection has the advantage that it ensures lower statistical bias relative to systematic evaluation (Kirchman *et al.*, 1982). A lack of similar studies for floc characterization techniques suggests that the establishment of more detailed guidance regarding measurement of floc by microscopy with image analysis is necessary.

Recognizing that there can be considerable uncertainty in floc characterization data, the impact of total number of engineered flocs and particles on characterization by microscopy with digital image analysis was investigated. Specifically, the minimum number of flocs that must be measured to obtain a precise size and/or shape estimation was evaluated using statistical parameters available for use to assess the precision of particle characterization data.

3.5.5.1 Experimental Design

Three (3) samples of engineered flocs were collected from one (1) jar (i.e., one (1) coagulant dose; 30 mg/L of PACl, specifically) on three (3) separate occasions and were settled onto separate 0.45 μm Millipore HA filters. Three (3) samples of raw water particles were collected from one (1) of the carboys containing the MWTP raw water on three (3) separate occasions and were settled onto separate filters. The filters were then enumerated using a systematic evaluation (Figure 3.8), following the methods described in Section 3.5.2. The engineered aggregates were evaluated at 2.5x magnification; the raw water particles were evaluated at 10x magnification. This systematic method was utilized so that all of the aggregates or particles on the filter would be counted. The order in which the particles were counted was then randomized using a Microsoft ExcelTM random number generator to simulate a random selection approach to microscopic evaluation.

Precision was quantified by the relative standard deviation (*RSD*) of ESD_A , which is discussed in greater detail in below. A statistical software package, SPSS (SPSS Inc., Chicago, IL), was used to generate Q-Q Plots (i.e., quantile-quantile plots), which diagnose differences between the probability distribution of a statistical population from which a random sample has been taken and a comparison distribution (Michael, 1983). For this study, the normality of the population distribution was tested. For those data sets that were not normally distributed, the data was transformed by the natural logarithm.

A one-way analysis of variance (ANOVA) with repeated measures was used to analyze the data sets (i.e., three (3) separate data sets for engineered floc and three (3) separate data sets for raw water particles). The total number of aggregates and particles was investigated at six (6) levels (i.e., 50, 100, 500, 1000, 2000 and 2900). The ANOVA was conducted on the precision of the data, which was quantified by the relative standard deviation, described further in Section 3.5.5.2. The ANOVA evaluated the main effects between subjects (i.e., 2.5x and 10x magnification) and within subjects (i.e., the total number of aggregates counted). Mauchly's test of sphericity was used. When a significant difference between the main effects was observed (i.e., $p < 0.05$), Tamhane's T2, Dunnett's T3 and Games-Howell multiple comparison tests were used to determine where the difference existed.

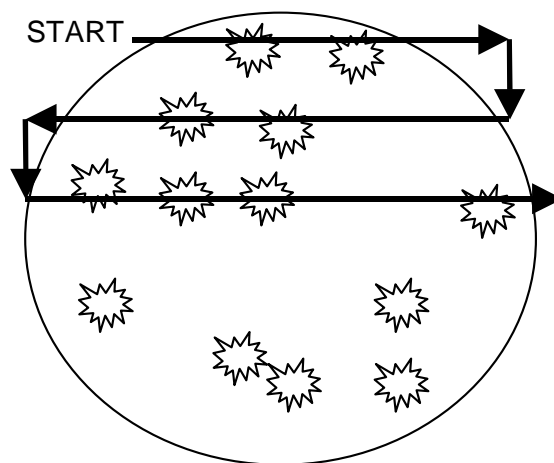


Figure 3.8: Systematic evaluation of the 0.45 μm Millipore HA filters.

3.5.5.2 Statistical Analysis of Precision

Similarly to studies that have evaluated the effects of sample processing for direct counting methods of microorganisms (Chae et al., 2008), the relative standard deviation (*RSD*) [%], or coefficient of variation was used to evaluate the precision of floc characterization data. Relative standard deviation is widely used in experimental analysis because it is useful for comparing uncertainty between different measurements of varying absolute magnitude. *RSD* is generally defined as:

$$RSD = 100 \frac{sd}{\bar{x}} \quad (3.6)$$

where *sd* is the standard deviation and \bar{x} is the arithmetic mean of a measured property of the floc (e.g., *ESD_A*). Ideally, it would be desirable to also examine the accuracy of the data. This is generally accomplished by calculating the percent error (*PE*) of the floc characteristic; defined as:

$$PE = 100 \frac{|c - z|}{c} \quad (3.7)$$

where *c* is the true value and *z* is the observed value of a measured property of the floc. Using *PE* for engineered and/or natural systems is made difficult by the lack of methods for measuring *c*. For this study, therefore, inferences will be made only for the precision of microscopy with digital image analysis techniques.

3.6 Full-Scale Floc Sampling at the MWTP

All of the full-scale floc samples from the MWTP were collected in April and May 2008. The samples were collected from the outlet of the full-scale flocculation basin (i.e., just prior to the inclined plate settling basin) and/or the outlet of the full-scale inclined plate settlers using the sampling method outlined in Section 3.1.4. The only variation is that the columns were held approximately 0.2 to 0.4 m below the surface of the water. The filters were stored in a refrigerator at 4 C until the characterization by light microscopy and digital image

analysis was performed. Raw water quality data was obtained from operators who had recorded the values based on observations from in-line meters.

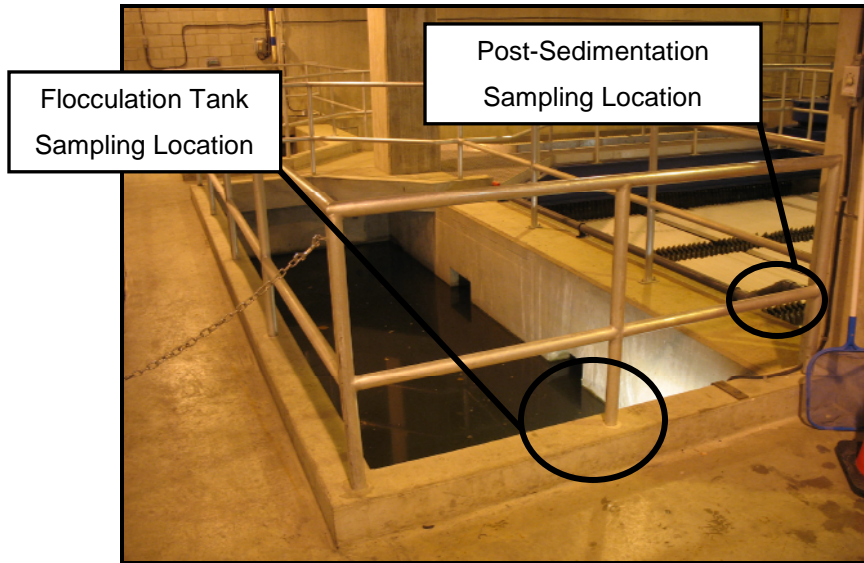


Figure 3.9: Full-scale sampling sites at the Mannheim Water Treatment Plant.

4 RESULTS AND DISCUSSION

The solids removal processes of coagulation, flocculation, and clarification remain a critical component of the drinking water treatment process for utilities that treat surface water. These processes are typically designed, operated and optimized based on information derived from bench-scale protocols (e.g., jar tests) that are used to simulate full-scale treatment performance. By regularly performing such tests, water treatment operators can assess alternative treatment strategies without altering plant performance. The primary goal of this thesis research was to improve the predictive capacity of bench-scale protocols commonly used for optimizing conventional chemical pre-treatment in full-scale drinking water treatment plants. Specifically, the primary focus was to develop approaches for integrating particle characterization techniques with these bench-scale protocols. Additional benefits that this research enabled were the opportunity to develop guidance on characterization of floc populations in a statistically significant manner and techniques to quantify uncertainty in fractal floc characterization data. In achieving these objectives, it was thought that further optimization of the MWTP would be possible.

Twelve (12) jar tests using the MWTP protocol were performed throughout this investigation. The UV_{254} and turbidity of the supernatant were evaluated during each jar test to investigate potential relationships between these parameters and floc settling rates and structure. Six (6) jar tests were conducted to generate aggregates for settling tests. Three (3) jar tests were conducted at 5, 15 and 25 °C using alum as the primary coagulant and three (3) jar tests that were conducted at 5, 15 and 25 °C using PACl as the primary coagulant. The six (6) jar tests were then repeated to characterize the fractal structure of the flocs by digital image analysis with microscopy. As well, a simple approach for quantifying the uncertainty in floc characterization data was developed. Samples of aggregates generated at full-scale at the MWTP were then collected and compared to the results of the bench-scale testing.

4.1 Jar Test Results

The raw water used during these tests was sampled from the MWTP on three (3) separate occasions. On these occasions, 80 L samples were obtained. The general water quality characteristics of the raw water treated at the MWTP are presented in Table 4.1. With the exception of UV₂₅₄ and turbidity, all values presented therein are the mean ± one standard deviation of three (3) individual 40 mL sub-samples collected from an 80 L sample. Individual UV₂₅₄ and turbidity values are based on the mean of two (2) separate readings

Table 4.1: Raw water quality data for all twelve jar test experiments (mean ± std. deviation).

	Raw Water Sample 1	Raw Water Sample 2	Raw Water Sample 3
Water Quality Parameter	Settling Tests	Floc Characterization	
		Alum Jar Tests	PACI Jar Tests
<i>Turbidity (NTU)</i>	4.4 ± 0.26	16.9 ± 0.81	33.0 ± 1.36
<i>TOC (mg/L)</i>	7.67 ± 0.06	5.65 ± 0.17	5.63 ± 0.15
<i>UV₂₅₄ (AU)</i>	0.206 ± 0.018	0.124 ± 0.022	0.172 ± 0.076
<i>Conductivity (μS)</i>	419 ± 71	530 ± 21	530 ± 9
<i>pH</i>	8.1 ± 0.22	8.3 ± 0.11	8.4 ± 0.06
<i>Temperature (°C)</i>	3.5	17	20

To reiterate, the raw water sampling events occurred over a period of six (6) months and the seasonal variations in water quality are apparent. The two (2) samples that were collected in the summer months (i.e., Raw Water Samples 2 and 3) had high turbidity values, potentially due to runoff, and high temperatures. The sample that was collected during the winter months had a lower turbidity and low temperature. The higher TOC value of the samples collected during the winter months was perhaps a measurement error, as it is typically expected that the organic concentration would be higher in the summer months because of increased biological activity. Regardless, the differences in coagulant dose requirements due to seasonal variations in water quality will be noted.

At the MWTP, in addition to filter performance, coagulant and polymer selection and dosages are typically based upon the quality of the supernatant obtained during jar tests; UV₂₅₄ values and turbidities after a period of settling (i.e., removal of dissolved organic

materials and particles) are specifically utilized for coagulant and dosage selection. UV_{254} measurements of the supernatant samples collected during the settling and floc characterization experiments are reported in Figures 4.1 and 4.2, respectively. The turbidity levels in the supernatant of those samples after a period of settling (i.e., as specified in Section 3.3.2) are presented in Figures 4.3 and 4.4. All of the detailed water quality data measured during the settling and floc characterization experiments are presented in Appendix C.

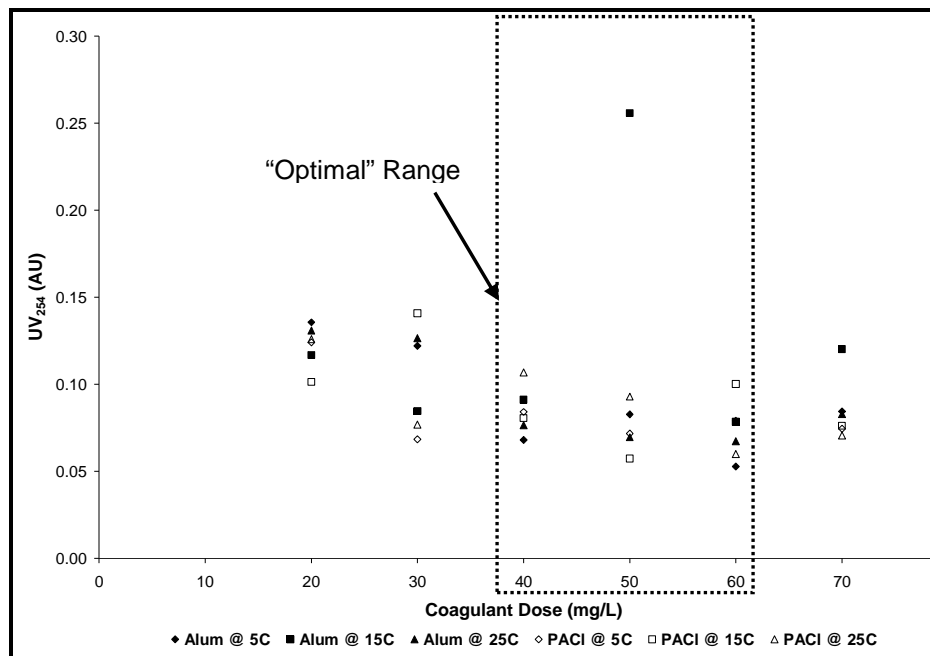


Figure 4.1: UV_{254} values of supernatant obtained from jar tests conducted during settling experiments (“optimal” range dependent on conditions).

Based on UV_{254} as an indicator, it was generally found that the highest level of organics removal occurred when the doses of both alum and PACI were between 40 and 60 mg/L; this result was generally observed for all of the samples investigated, regardless of raw water temperature. The two (2) exceptions to this otherwise consistent performance were observed during the settling experiments involving alum coagulation at 15C and PACI coagulation at

5C. During those experiments, comparable or higher levels of organic removal (i.e., lower UV_{254}) were achieved at coagulant doses of 30 mg/L.

The pH of the supernatant collected from the jar tests conducted during the settling experiments ranged only from 7.6 to 8.2 (Appendix C); no trends in the pH data were observed. Accordingly, “enhanced coagulation” was not necessarily achieved. pH was intentionally not adjusted during coagulation because pH adjustment is not practiced at the full-scale plant, in which coagulation is optimized to achieve maximal turbidity reduction, but not NOM removal.

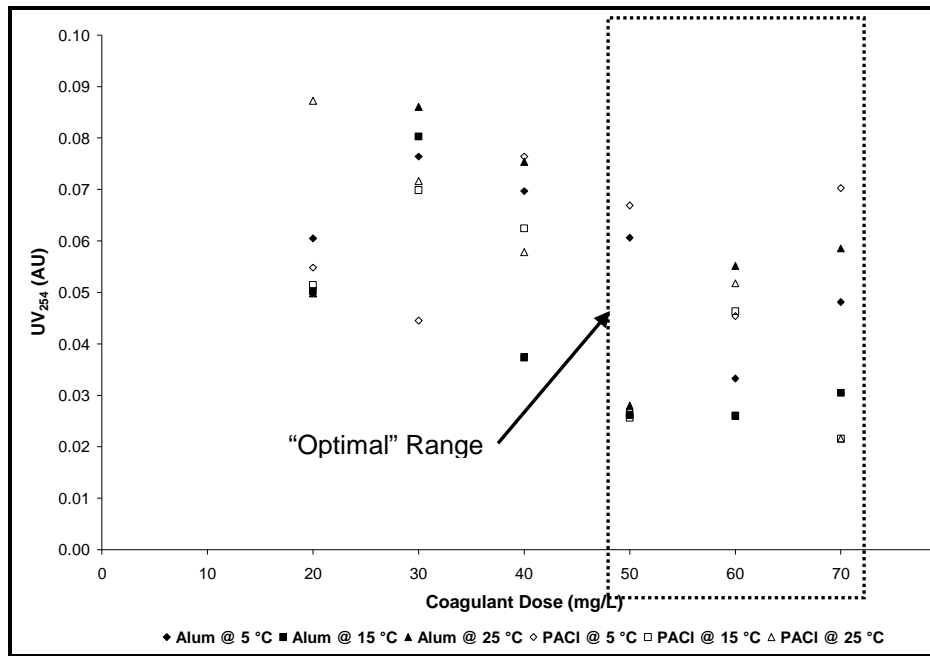


Figure 4.2: UV_{254} values of supernatant obtained from jar tests conducted during floc characterization experiments (“optimal” range dependent on conditions).

The pH of the supernatant collected from the jar tests conducted during the floc characterization experiments were slightly lower [e.g., 7.2 in one (1) instance] and as expected, organic material was best removed at higher coagulant doses. The level of removal was considerably higher than what was achieved during the previously discussed jar tests

(i.e., a minimum final UV_{254} value ~ 0.02 AU compared to ~ 0.05 AU). This result may have occurred because “enhanced coagulation” was reached as a result of a lower pH.

During a jar test conducted during the settling experiments at 15C with alum coagulation, an unexpected UV_{254} value was obtained when the dose was 50 mg/L (Figure 4.1). A second measurement of the sample’s UV_{254} confirmed the result (i.e., $UV_{254} = 0.2558$ AU) which was inconsistent with the rest of the UV_{254} data obtained during the settling experiments. This anomalous result was treated as an outlier that was likely attributable to sampling and/or instrumental error because it was inconsistent with other concurrently obtained water quality measurements; particularly the TOC, which was the lowest level (i.e., 4.58 mg/L) observed during the settling tests (Appendix C). The fact that the UV_{254} samples were filtered and the TOC samples were not, however, makes a direct comparison difficult.

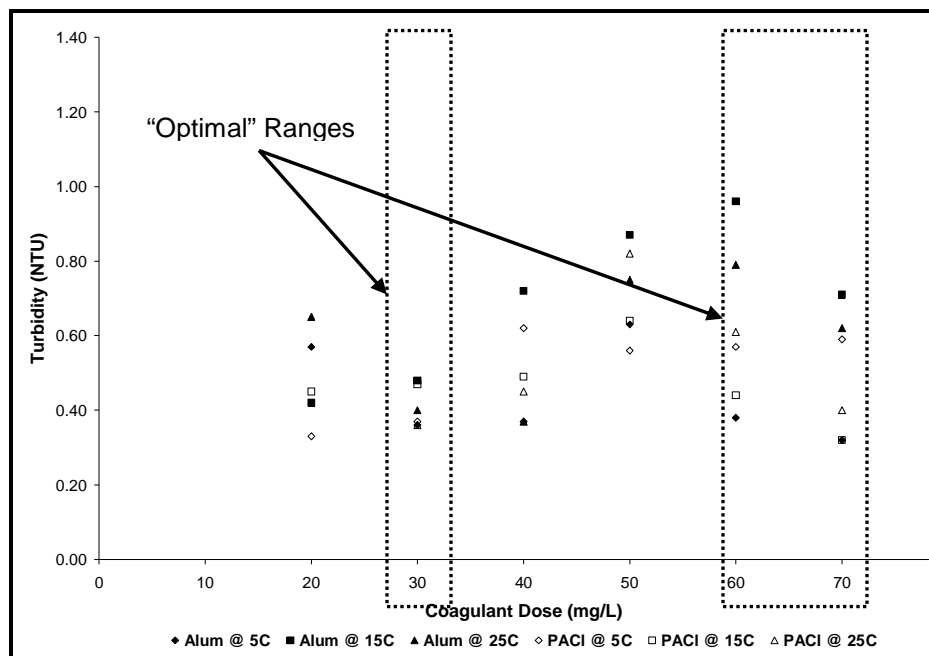


Figure 4.3: Turbidity of supernatant obtained from jar tests conducted during settling experiments (“optimal” range dependent on conditions).

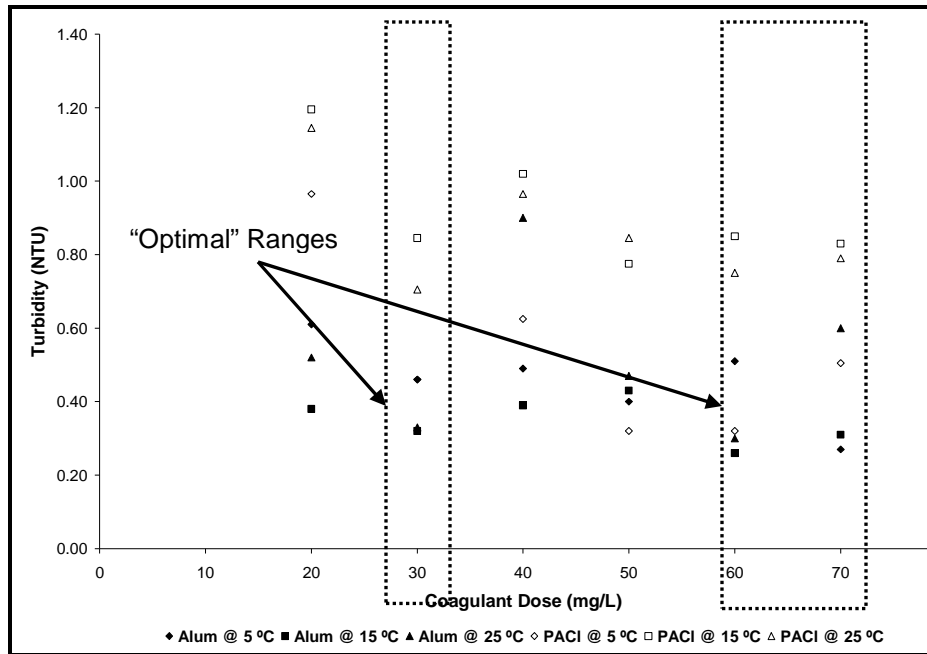


Figure 4.4: Turbidity of supernatant obtained from jar tests conducted during flocculation experiments (“optimal” range dependent on conditions).

Regardless of the raw water temperature and coagulant type investigated, all of the turbidity data collected during the present investigation indicated that coagulant doses of approximately 30 mg/L would achieve “optimal” turbidity reductions (i.e., low settled water turbidities). In some instances (i.e., alum coagulation at 15 C and PACl coagulation at 15 C), comparable or higher levels of turbidity reduction were achieved when coagulant doses were between 60 and 70 mg/L. Multiple optimal dosages can likely be attributed to a change in the principal particle destabilization mechanism; from charge neutralization to “sweep” flocculation.

The final turbidity levels measured in the supernatant during the jar tests conducted for flocculation characterization were lower when alum was used as the primary coagulant rather than PACl (Figure 4.4). This difference in settled water turbidity was likely attributable to differences in seasonal raw water quality between the two (2) experiments (i.e., mean raw water turbidities were 16.9 NTU during experiments conducted with alum and 33 NTU during

experiments conducted with PACl). Given the variations in raw water turbidity between the experiments conducted with the different coagulants, it would be premature to speculate about the performance of one coagulant relative to one another. More samples collected over a range of raw water turbidities would be required to address this issue. Additional samples were not collected; however, because that evaluation was not an objective of the present investigation.

Many investigations suggest the use of PACl over alum at temperatures of 5 °C or lower because it results in the formation of a denser floc with a higher rate of settling because of its high molecular weight (Letterman, 1999). Contrary to this expectation; however, it was qualitatively observed during both the settling and floc characterization jar tests that although alum flocs seemed smaller in size, more of them tended to settle (even during mixing). The water after the settling phase also appeared clearer. Aggregates produced by PACl coagulation were generally larger than alum flocs but more fragile and likely to float. One possible explanation is that some of the samples were collected in the summer months even though the tests were performed at low temperatures. The above noted studies used samples that would be more representative of water quality during the winter months (i.e., when the water temperature would be less than 5 °C). Figure 4.5 depicts the observable differences between the aggregates produced by alum and PACl coagulation at the same dose and temperature, and the associated difference in the clarity of the water.

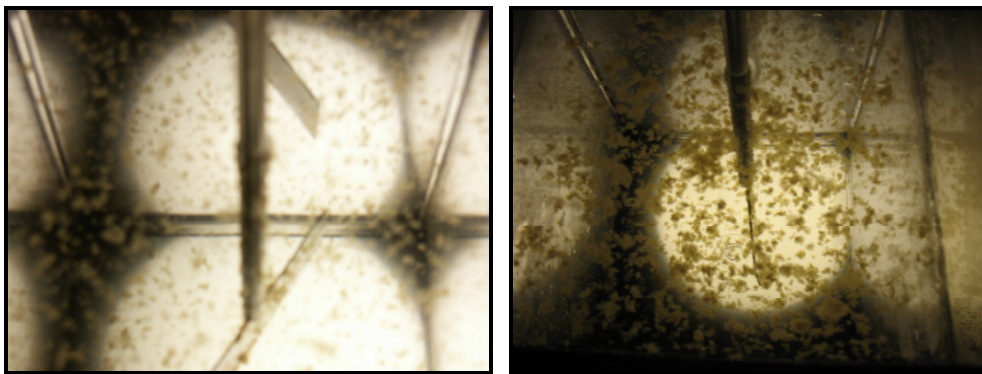


Figure 4.5: Alum flocs (left) and PACl flocs (right) produced during the jar tests.

At many treatment plants, it is typically considered that the information presented in Figures 4.1 through 4.4 and the visual observations concerning floc size and settleability are sufficient for the selection of an operating dose and if necessary, a preferred coagulant. In the case of the MWTP, the available data suggest that under the conditions investigated, either alum or PACl coagulation at a dose of ~ 30 mg/L in conjunction with 0.2 mg/L of cationic polyelectrolyte can achieve the highest levels of UV₂₅₄ and turbidity reduction (i.e., 0.02 to 0.05 AU and 0.3 to 1.0 NTU, respectively). Comparable or slightly higher levels of UV₂₅₄ and turbidity reduction could possibly be achieved at doses of 60 or 70 mg/L of either alum or PACl in conjunction with 0.2 mg/L of cationic polyelectrolyte; however, the marginal gains in treated water UV₂₅₄ and turbidity would not likely justify the additional costs associated with chemical consumption and sludge production.

To better quantify the errors associated with sampling and/or equipment use, two (2) additional jar tests were performed at 15 °C using the jar testing protocol that was utilized during the settling and floc characterization experiments; PACl was the primary coagulant during one (1) of those tests and alum was the primary coagulant during the other. The raw water UV₂₅₄ and turbidity during these experiments were approximately 0.23 AU and 4 NTU, respectively. UV₂₅₄ and turbidity were evaluated in multiple supernatant samples to better quantify the error of interest. The results are presented in Figures 4.6 and 4.7. Detailed and additional raw water quality data obtained during these experiments are presented in Appendix C.

In this raw water matrix, alum and PACl coagulation in conjunction with 0.2 mg/L of cationic polyelectrolyte achieved generally similar decreases in both the residual UV₂₅₄ values and turbidities. An alum dose of 30 mg/L resulted in a residual turbidity of ~ 0.8 NTU, which was comparable to the level of turbidity reduction achieved when the dose was increased to between 50, 60 or 70 mg/L of alum. In contrast, the optimal PACl dose for achieving turbidity reduction was 60 mg/L; higher doses of either coagulant were necessary to concurrently achieve the highest UV₂₅₄ and turbidity reductions.

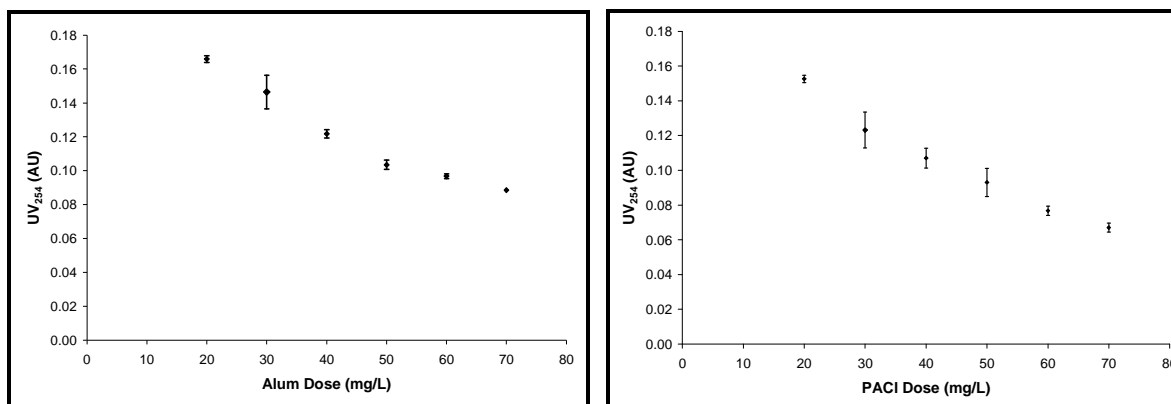


Figure 4.6: UV₂₅₄ values of supernatant obtained from additional alum and PACI jar tests (mean ± 1 standard deviation, n = 3).

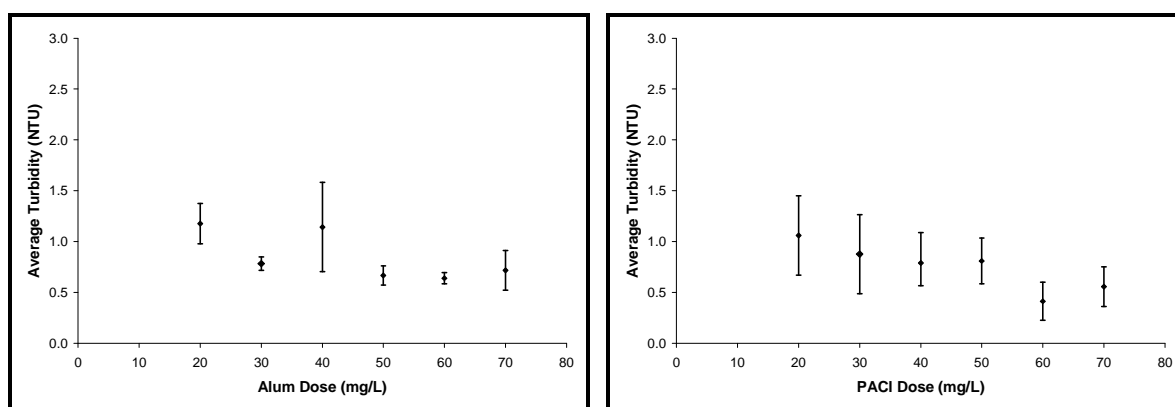


Figure 4.7: Turbidities of supernatant obtained from additional alum and PACI jar tests (mean ± 1 standard deviation, n = 3).

PACl refers to a class of soluble aluminum products in which aluminum chloride has been partly reacted with a base. The relative amount of OH⁻, compared to the amount of Al, determines the basicity of a particular PACl product. The PACl solution was not as acidic as alum (Table 3.2); consequently, it did not decrease pH as much as the equivalent amount of alum (e.g., a final pH value of 7.7 compared to 7.5 at dosages of 50 mg/L). The minimum solubility was reached and the dissolved hydrolysis products (i.e., Al(OH)²⁺) would have begun to precipitate out to form solids at an alum dose of 30 mg/L. At least 50 mg/L of

PACl were likely required for precipitation to occur because it was less acidic than alum, and because it has been found to have a higher pH of minimum solubility than alum (Pernitsky and Edzwald, 2003).

The results of the present investigation are generally consistent with those of the “Mannheim Water Treatment Plant Operating Strategy Review”, conducted in September of 2006 by Associated Engineering (AE) Ltd. (Edwards, 2006; Appendix D). However, it was determined by AE that only 30 mg/L of PACl resulted in the lowest residual UV_{254} and turbidity. The results of additional testing demonstrated that 30 mg/L of PACl, in combination with 0.1 mg/L of Magnafloc LT 22 S, described in detail in Section 3.3., was “optimal” for coagulation at the MWTP. An alum dose of 20 mg/L without polymer achieved the lowest residual UV_{254} and turbidity, but flocs were formed that were described as “light floaters” that settled “poorly”. Therefore, alum was not used for the remaining tests that introduced the use of a polymer. PACl, in conjunction with 0.2 mg/L of cationic polyelectrolyte was ultimately selected as the “preferred alternative”.

It should be noted that although no rationale was specified, AE utilized a jar test protocol that differed from the one that was utilized at the MWTP. It required between 160 and 300 rpm (i.e., $G \approx 120$ to 400 s^{-1}) for two (2) to three (3) minutes, followed by approximately 50 rpm (i.e., $G \approx 35$ to 45 s^{-1}) for fifteen (15) minutes and thirty (30) minutes of settling. Replicate samples of the supernatant were then collected and processed for standard water quality analysis (i.e., UV_{254} , turbidity, pH). In the “general comments” section of the report, it was noted that there was a gap of ten (10) to twenty (20) minutes between the two (2) turbidity readings, which might have allowed the later supernatant samples to have “extra settling time; thereby skewing the results”.

The selection of PACl as a primary coagulant at the MWTP is not surprising given that the plant is in Canada and treats cold water for a significant period of time annually. Many investigations have suggested that alum is less effective at lower temperatures because the

generated flocs have a lower densities (Hanson and Cleasby, 1990) and aggregate sizes (Morris and Knocke, 1984). Fitzpatrick *et al.* (2004) produced flocs using alum and PACl as the primary coagulants for a suspension of kaolin clay in tap water and qualitatively observed that PACl produced the largest flocs at various temperatures and alum generated the smallest. The use of PACl in the summer months, however, will not necessarily have any advantage over the use of alum.

Even though differences in residual UV_{254} and turbidity after a period of settling were observed during the jar test experiments described in the present investigation, it is noteworthy that there were no obvious visual differences in floc quantity and/or size as alum and PACl doses increased. This qualitative observation is contrary to the generally accepted notion that turbidity is directly proportional to solids concentration, which would suggest that more flocs should have been produced and settled in the jars containing 30, 60, and/or 70 mg/L of coagulant because the highest reductions in UV_{254} and turbidity were associated with those coagulant doses. As well, according to Stokes' law, those flocs should have been larger than flocs in the other jars because a floc that has an ESD_A of 25 μm should settle by gravity more readily than one that is 10 μm in diameter, assuming similar densities. Stokes' law, however, has been considered to be irrelevant for engineered flocs because aggregate porosity is not constant (Li and Ganczarczyk, 1989) and because flocculent settling (i.e., Type 2) likely occurs. The data from the settling tests were carefully examined to present a more quantitative assessment of the effect of aggregate settling on turbidity and UV_{254} reductions.

4.2 Settling Test Results

To quantitatively evaluate the differences in settling velocity of aggregates generated by various doses of alum and PACl coagulants, six (6) settling tests were performed. Three (3) jar tests were conducted at 5, 15 and 25 °C using alum as the primary coagulant and three (3) jar tests were conducted at 5, 15 and 25 °C using PACl as the primary coagulant. The

settling velocity results for flocs formed by alum and PACl coagulation at a raw water temperature of 5 °C are presented in Figures 4.8 and 4.9 respectively. Results of the tests performed at 15 and 25 °C are presented in Appendix E. Between 44 and 79 aggregates were collected from each jar (i.e., each coagulant dose) during each experiment. Samples were collected after a period of settling from the bottom of the jars so that it could be determined whether or not the settling rates and/or sizes of the aggregates that had settled would correspond to the UV_{254} and turbidity of the supernatant. These undisrupted flocs were then introduced into the settling columns so that settling velocity could be evaluated as a function of floc size by the commonly utilized approach discussed in Section 3.4.

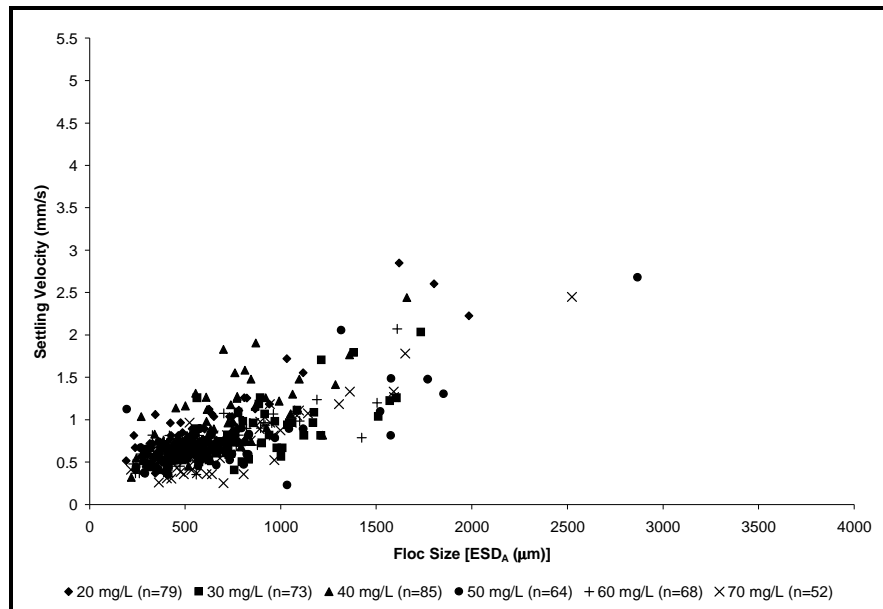


Figure 4.8: Settling velocity as a function of floc size for flocs produced by alum coagulation at a temperature of 5 °C.

In general, settling velocities of the aggregates ranged from 0.25 to 5 mm/s (i.e., 0.9 to 18 m/h). During all of the settling tests, $\geq 75\%$ of the aggregates ranged in ESD_A from 0 to 1000 μm with settling velocities ranging from 0.25 to 2.5 mm/s (i.e., 0.9 to 9 m/h). As might be expected based on Stokes' law, settling velocities generally increased with increasing floc

size. As discussed in Sections 2.3.1 (i.e., discussion of turbidity) and 4.1, the two (2) primary expectations of the settling test results with regard to coagulation were:

1. that flocs produced during PACl coagulation would settle more readily than those produced during alum coagulation, particularly at 5C; and
2. that larger and more settleable flocs would be produced by both coagulants at doses that achieved the highest UV_{254} and turbidity reductions. This is an assumption that is common to jar testing.

The observed settling velocities and sizes of the flocs generated by alum and PACl coagulation were relatively similar at 5 C (i.e., Figures 4.8 and 4.9), and at 15 and 25 C. Moreover, higher aggregate settling velocities (i.e., 4 to 5 mm/s, or 14.4 to 18 m/hr) were achieved as the temperature of the raw water increased. This result was expected because if floc size, shape and density are similar for a given dose, higher settling rates would be expected at higher temperatures because of a decrease in viscosity. Nonetheless, only a small number of aggregates attained velocities higher than 3.5 mm/s (i.e., 12.6 m/hr).

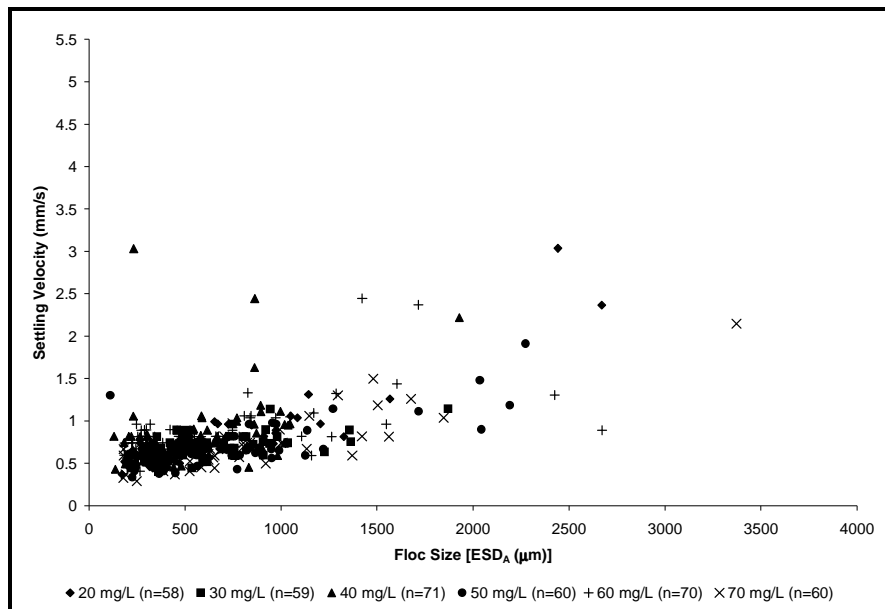


Figure 4.9: Settling velocity as a function of floc size for flocs produced by PACl coagulation at a temperature of 5 °C.

Although lower UV_{254} values and turbidities were measured from the jar test supernatant at coagulant doses of 30 mg/L and between 60 and 70 mg/L, there were no observable differences in settling velocities and/or floc size when compared to aggregates generated at doses of 20, 40 and 50 mg/L. Regardless of coagulant dose and floc size, the observed settling velocities were scattered between 0.25 to 5 mm/s, as is evidenced by the low coefficients of determination (R^2) obtained when least squares linear regression was utilized to examine settling velocity as a function of floc size for each coagulant dose (Appendix E); no trends were evident from these data. The only observable trend in the settling data was the settling test of aggregates generated by alum coagulation at 25C (Figure 4.10), in which there was a clear difference in size between the flocs produced by coagulant doses between 20 and 40 mg/L (ESD_A ranged from 89 to 1390 μm) and those that were generated by doses of 50, 60 and 70 mg/L (ESD_A ranged from 144 to 3835 μm). The higher doses of alum produced larger diameter flocs (i.e., ESD_A). Despite the differences in floc size; however, no differences in settling velocities were observed (i.e., smaller flocs settled as readily as the larger flocs).

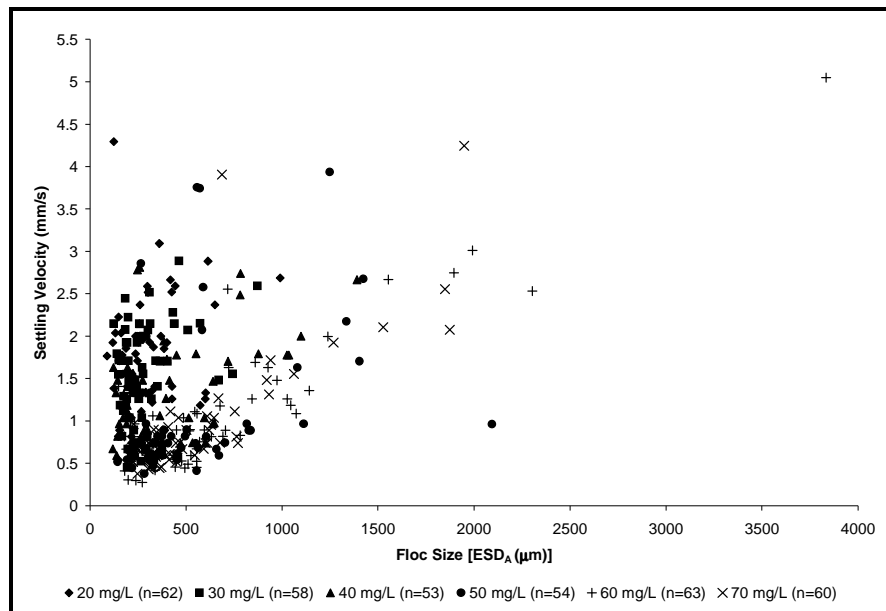


Figure 4.10: Settling velocity as a function of floc size for flocs produced by alum coagulation at a temperature of 25 °C.

It is important to recall that the sampling approach utilized herein evaluated the population of flocs that had settled, to address the assumption that larger and more settleable flocs would be produced by both coagulants at doses that achieved the highest UV_{254} and turbidity reductions. These results demonstrate that:

1. floc settling velocities were not directly proportional to floc size;
2. the production of larger and more settleable flocs could not be described by floc settling velocities; and
3. floc sizes and settling velocities were not directly related to either UV_{254} or turbidity reductions.

They also suggest that it is the population of particles and/or flocs that remain in suspension after the period of settling during the jar test protocol that dictates the measured degrees of UV_{254} and turbidity reductions. While this result seems obvious and logical in hindsight, it is critical to note that while it is logical to:

1. observe that at the same water temperature and mixing conditions the particles that settle at a certain depth (i.e. the bottom of a jar) have similar settling rates regardless of coagulant dose and/or type; and
2. assume that what remains in suspension after flocculation and settling drives the observed UV_{254} and turbidity reduction performance,

it is not logical to assume (as is often done) that the production of larger and more settleable flocs can be described by jar testing. Specifically, for a given raw water, if the settling rates, sizes, and size distributions of the settled flocs at a specified depth; for example, the bottom of a jar, are similar, what is it about the particles/flocs in the remaining supernatant that impacts observed differences in turbidity and UV_{254} ? While it is possible that the settling rates of those flocs/particles are different, it is also possible that other floc/particle characteristics contribute to the observed differences in UV_{254} and turbidity. Stokes' law was initially utilized to predict aggregate density because Sadar (2002) reported that floc density, and therefore porosity, would have a negative bias on turbidity measurement (i.e., dense

particles will cause the reported value will be slightly higher than the actual turbidity). Stokes' law is limited in applicability because it assumes that the particles are impermeable and spherical; however, it is known that engineered floc porosity is not constant (Li and Ganczarczyk, 1989). To rectify these inaccuracies, or potentially incorrect assumptions, settling velocity models (i.e., *Equations 2.21* and *2.22*) have been developed that directly account for the fractal nature of flocs but they could not be utilized during this investigation because accurate and/or precise three-dimensional information (i.e., D_3) could not be collected from the images captured by the stereoscopic microscope.

Therefore, according to Stokes' law, an engineered floc with a diameter (i.e., ESD_A) of 271.13 μm and a v of 0.737 mm/s, for example, would have a ρ_p of 0.0184 g/cm^3 , assuming a μ of 10^{-6} m^2/s . Figure 4.11 illustrates the calculated aggregate densities (i.e., based on *Equation 2.6*) for all of the aggregates collected from the jar test at 25C using alum as the primary coagulant; the remaining data are presented in Appendix E. Most of the engineered flocs that were sampled had a calculated density of less than 0.1 g/cm^3 ; a few of the smallest particles had a densities ≥ 0.2 g/cm^3 that did not correspond with higher settling velocities. Floc density estimates based on Stokes' law generally decreased with increasing floc size, regardless of coagulant type and dose. This result was expected because Stokes' law expresses density as being inversely proportional to the diameter squared. Unfortunately, the calculated density was not proportional to measured settling velocity, which therefore confirmed that these calculations were not applicable.

It is inappropriate, therefore, to use the settling velocity data herein to make conclusions about optimal coagulant dosages or to explain the differences in UV_{254} and turbidity reductions observed during the settling experiments. The settling results suggest that it is the population of particles and/or flocs that remain in suspension after the period of settling during the jar test protocol that dictates the measured values of UV_{254} and turbidity reductions. As well, the aggregate porosity was not constant as evidenced by the

photographs taken during testing Figure 4.12), which also confirms that Stokes' analysis did not apply.

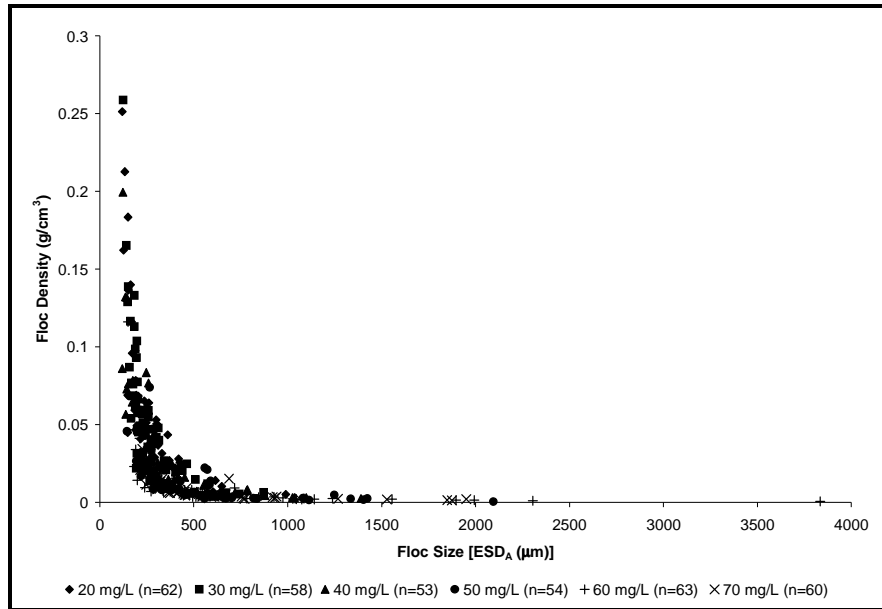


Figure 4.11: Particle densities for alum flocs produced and settled at a temperature of 25 °C.

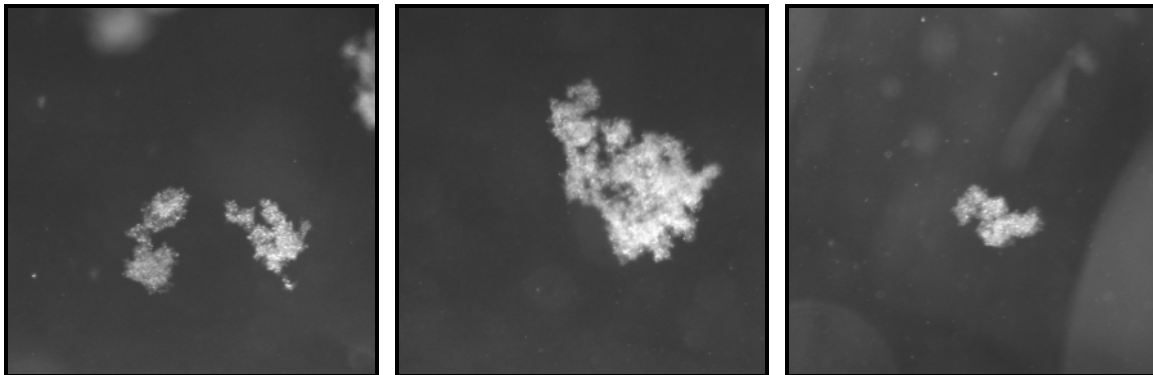


Figure 4.12: Photographs of flocs, taken during the settling column tests.

Fractal dimensions were utilized in the present analysis because they provide a more accurate description of objects where Euclidean geometry does not apply. Specifically, fractal dimensions D_1 and D_2 describe the complexity of the outlines of an object and how porous an

object is, respectively. Further details are provided in Section 2.4. More importantly, fractal dimensions can be directly utilized because they can be calculated based on easily measurable shape characteristics (i.e., floc area (A_c) and volume (V)). Water treatment investigations involving fractal dimensions have traditionally focused on describing floc structural characteristics in response to changes in coagulation regimes. In the present investigation, fractal approaches to floc characterization were utilized in conjunction with jar testing to investigate their potential use as indicators of UV_{254} and turbidity reduction during sedimentation.

4.3 Floc Characterization Results

The characterization of floc structure involves vacuum filtration of the sampled aggregates onto 0.45 μm Millipore HA filter membranes, digital image collection using light microscopy, and quantification and sizing using image analysis software. During this study, a total of 117 membranes were evaluated (i.e., one (1) filter per sample); 108 samples of engineered aggregates and nine (9) samples of raw water particles. Figure 4.11 is a visual representation of the experimental design. Between 1,500 and 20,000 aggregates/particles were characterized on each filter. The membranes were evaluated by a random selection approach, as discussed in Section 3.5.5.

Various geometric properties of the flocs and particles were quantified or calculated (e.g., A_c , p , L_D , ESD_A and v), and fractal properties were subsequently computed. The D_{50} for each sample was determined from particle size distributions that were plotted using the results of grain size analyses obtained by sample filtration, microscopy, and image analysis. All of the detailed particle size distributions and a summary of D_{50} values are presented in Appendix F.

D_{50} values of aggregates produced by alum and PACl coagulation ranged from 15.82 to 22.92 μm and 13.24 to 23.99 μm , respectively, but were generally between 16.5 and 19.5 μm . There were very few variations in D_{50} values as coagulant doses increased. As well,

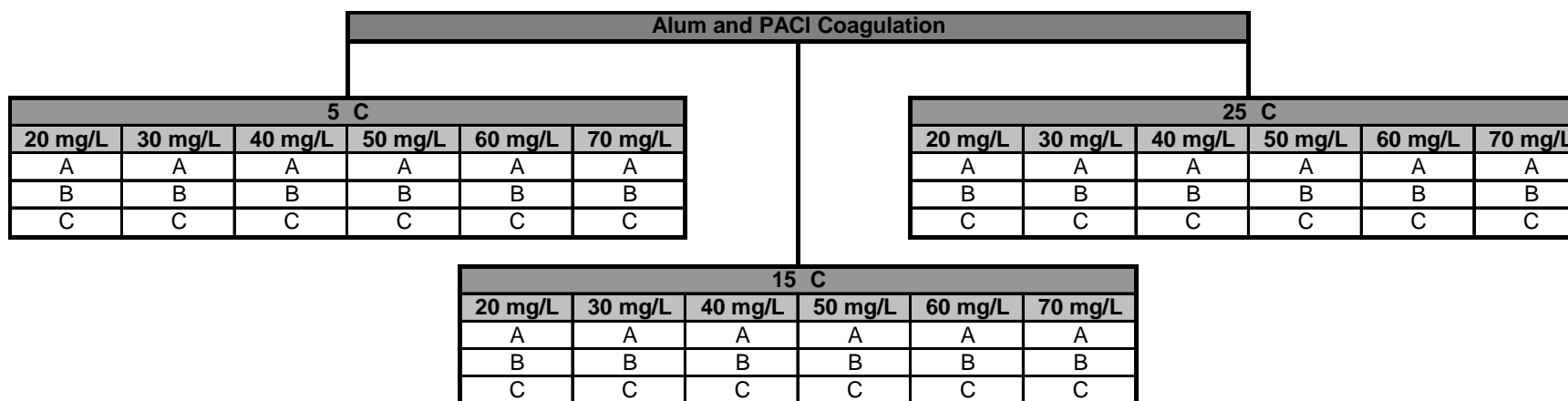


Figure 4.13: Visual representation of the floc characterization experimental design.

there were no differences in D_{50} values as the temperature of the raw water was increased. What is particularly notable about these analyses, however, is that at least 50%, and often 90% to 95%, of the aggregates/particles characterized from the sub-samples were smaller than those that were evaluated during the settling experiments. This observation may be attributable to the different sampling procedures used during the settling and floc characterization experiments. Flocs/particles collected for the settling experiments were removed directly from the bottom of the jars following the settling period, whereas flocs/particles that were collected to characterize fractal structure were collected from the flocculated suspension (i.e., without a period of settling). The different sampling procedures corresponded to different experimental objectives. The settling tests were performed to assess the impact of floc settling rates and sizes on the UV_{254} and turbidity of the supernatant after a period of settling, whereas the floc characterization experiments were completed to assess the implications of floc structure prior to settling on UV_{254} and turbidity of the supernatant after a period of settling.

As described in Section 4.2, flocs during the settling tests were collected following a period of settling, which resulted in the measurement of only a small number of aggregates that attained velocities that were higher than 3.5 mm/s (i.e., 12.6 m/h). Aggregates were collected for floc characterization to capture particle size distributions and structural characteristics of a population of aggregates that has changed as a result of flocculent settling. To reiterate, Type 2 or flocculent settling behavior is the coalescence of particles whereby particle mass increases and particles settle more rapidly (i.e., Figure 4.14), and likely influenced size distribution and structure of aggregates/particles that were collected for evaluation during the settling experiments. Typical nephelometric turbidity methods, as described by Ziegler (2002), with a detector orientation measurement angle at 90° are optimized for small particles.

Traditional jar test procedures qualitatively focus primarily on the size and/or settling rate of the aggregates that settle and attempt to link these observations to measured UV_{254} and turbidity reductions, as well as sedimentation performance (e.g., larger flocs will settle more

readily and result in low supernatant turbidities). However, consideration of the size, shape and perhaps structure of the flocs that remain in suspension (i.e., flocs that may be too small for the human eye to observe) is necessary to accurately describe all parameters that contribute to UV_{254} and turbidity reduction. To properly optimize full-scale pre-treatment and/or process performance, greater emphasis should be placed on determining the reason that these small, unsettled aggregates remain in suspension following chemical pre-treatment and sedimentation and perhaps their effect on subsequent treatment processes (i.e., filtration). It is for this reason that the floc characterization experiments were designed to sample all of the aggregates generated.

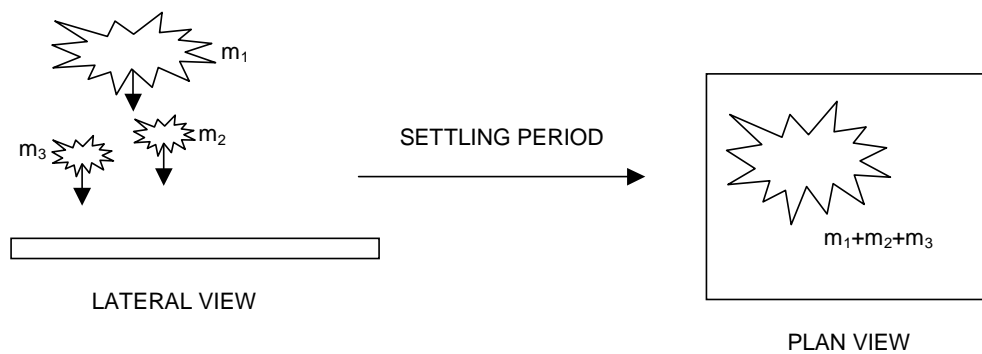


Figure 4.14: Depiction of flocculent settling of aggregates during jar testing.

To assess the potential rationale for the differences in supernatant UV_{254} and turbidity values measured during each of the six (6) tests, particle size distributions of the samples over the range of coagulant doses were compared. For example, Figure 4.15 is a particle size distribution of aggregates produced by alum coagulation at 25 °C. There were obvious differences in the upper particle size ranges of the flocs generated when various doses of both alum and PACl were utilized at all three (3) temperatures. In other words, the D_{70} , D_{80} , D_{90} and D_{95} values, for example, were considerably different, and the aggregates typically ranged in size from 100 to 250 μm . This result is not surprising given that the samples were collected at various times throughout the year. There were, however, discrepancies involving replicate samples. That is, it would have been expected that if the sub-samples of flocs were

truly replicates, then the particle size distributions would have been similar. They were not always similar; however, indicating that sampling was not reproducible. Regardless of the issue of replication, all of the aggregates from the three sub-samples were combined; a particle-size distribution was prepared and a D_{50} value (Appendix F) was calculated for each jar rather than for each replicate sample. This approach to data handling was acceptable and appropriate because the flocs were all collected from the same population and the size distribution of the combined data provided a more complete description of the overall floc population.

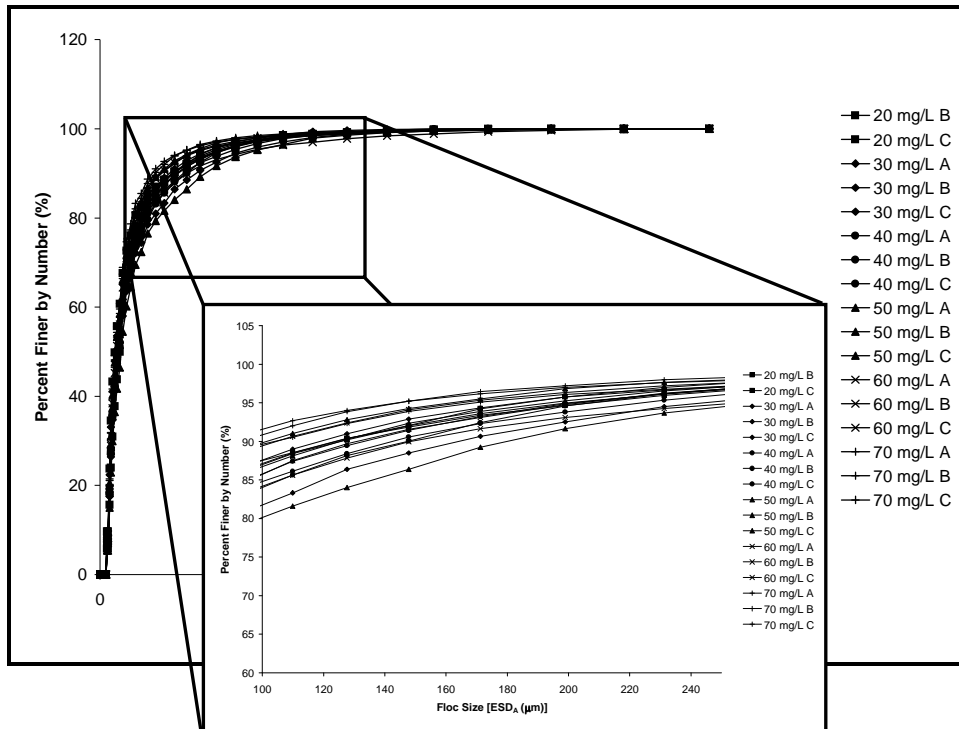


Figure 4.15: Particle size distribution of flocs produced by alum coagulation at 25 °C.

The D_{50} values of aggregates produced by alum and PACl coagulation were very similar, ranging only from 13.2 to 20.9 μm . As well, there were very few variations in D_{50} values as doses of both coagulants were increased and there were no differences in D_{50} values as the temperature of the raw water was increased. While raw water temperature did not appear to

have an effect on the D_{50} of the coagulated floc size distribution, the D_{70} , D_{80} , D_{90} and D_{95} , values, for example, were considerably different, where the aggregates typically ranged in size from 50 to 100 μm . D_{90} values (i.e., the size such that 90% of the particles are smaller than that size) were calculated and summarized (Appendix F), and ranged from 43.9 to 72.8 μm and 26.0 to 102.8 μm for flocs generated by alum and PACl coagulation, respectively. There were substantial variations in D_{90} values as doses of both coagulants were increased; as the PACl dose increased from 20 mg/L to 70 mg/L during jar test conducted at 25 C, for example, the D_{90} value increased as well from 30.8 μm to 65.0 μm .

As depicted in Figures 4.16 and 4.17 and those presented in Appendix F that compare aggregate D_{90} to residual UV_{254} and turbidity, measured values of UV_{254} and turbidity of the supernatant were generally inversely proportional to aggregate D_{90} ; that is, the residual UV_{254} and/or turbidity decreased as the value of D_{90} increased. Least-squares linear regression analyses of UV_{254} and turbidity, regressed on D_{90} are presented in Appendix F and generally indicated that this relationship was not linear. This result is not unexpected because turbidity, in particular, is only an indicator of particle concentration. It has been found that no linear relationship exists between particle concentration and turbidity for both raw and filtered water (Doyle, 1998; Bridgeman *et al.*, 2002). As well, it is possible that other floc/particle characteristics contribute to the observed differences in UV_{254} and turbidity.

It is important, however, to reiterate that D_{90} values were calculated from samples of aggregates that were collected prior to settling; UV_{254} and turbidity measurements were measured following a period of settling. This was done in order to predict particle removal performance (i.e., based on UV_{254} and turbidity reduction) by using the floc structural information of the aggregates generated during coagulation and flocculation. That said, the general trends depicted in Figures 4.16 and 4.17 may have been indicative of Type 2 (i.e., flocculent) settling. Specifically, the presence of larger flocs enabled the removal of higher quantities of smaller flocs/particles from suspension by flocculent settling, depicted in Figure 4.14. As a consequence, the UV_{254} and turbidity values of the remaining supernatant may

have decreased because some of the smaller aggregates/particles that are known to have the greatest impact on these measurements were removed. Examination of the aggregates in suspension (i.e., supernatant) after the period of settling would have enabled a more thorough evaluation of this hypothesis because it would allow a direct comparison of the particle size distributions before and after settling. It is critical to note; however, that turbidity and particle size distribution are not necessarily directed related, even when only smaller sizes of flocs/particles are evaluated (Sadar, 1998). Therefore, the absence of a clear difference in floc particle size distribution before and after settling, particularly in the smaller size ranges, would not necessarily imply the lack of an impact on turbidity. Accordingly, the relationship between D_{90} values calculated from samples of flocculated water prior to settling and UV_{254} and turbidity values of that water after a period of settling may be a simple tool that can be utilized to describe and potentially better predict flocculent settling performance. At present, this appears to be the first such tool of its kind that has been reported.

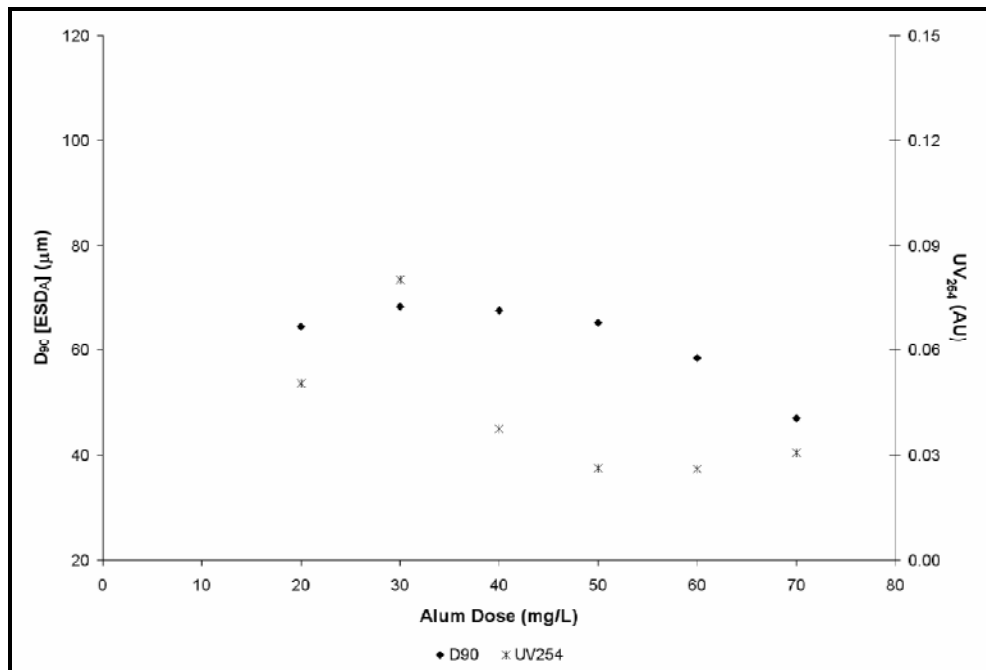


Figure 4.16: Comparing aggregate D_{90} to residual UV_{254} for alum coagulation at 15 °C.

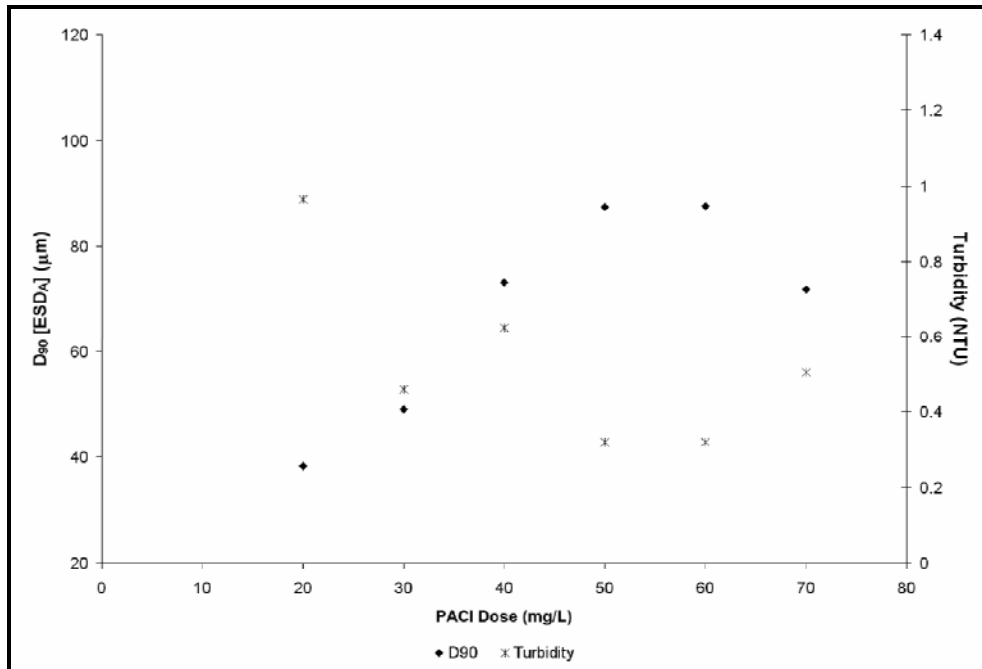


Figure 4.17: Comparing aggregate D_{90} to residual turbidity for PACl coagulation at 5 °C.

Floc size, however, as mentioned above, is not the only aggregate parameter that might impact the measurement of both UV_{254} and turbidity. Sadar (2002) reported that floc shape and density, and therefore porosity, would have a negative bias on turbidity measurement (i.e., dense, non-irregular particles will cause the reported value will be slightly higher than the actual turbidity). The question that has yet to be answered is “would an operator conducting bench-scale tests to optimize conventional chemical pre-treatment during full-scale drinking water treatment simply want choose an “optimal” coagulant dose based on jars which appear to have the largest flocs?”

Fractal dimensions, D_1 and D_2 , of engineered aggregates have the potential to be a useful and practical means of addressing several of the existing concerns associated with bench-scale testing and/or pre-treatment. Specifically, they can be utilized to indicate the complexity of the outlines of flocs and/or how well flocs fill two or three-dimensional space (Kenkel and Walker, 1996). They can be readily calculated by regression of geometric properties

following characterization of the flocs by one of the three (3) methods outlined in Section 2.5. Light microscopy and digital image analysis were employed throughout the present investigation; D_1 and D_2 were evaluated for each sample of aggregates collected during each test following to the methods presented in Section 3.5.3.

To quantify the variability in the fractal data, significant difference tests between each of the sub-samples were performed and for every test it was concluded that there were significant differences. For each sub-sample, 95% confidence intervals were then calculated on both the slope and the intercept of the regressions that determined both D_1 and D_2 and are summarized in Appendix G. The confidence intervals of sub-samples A, B and C were compared to one another to determine whether or not they were statistically similar. Significant differences between the sub-samples were still evident; there were only eight (8) instances in which all three (3) sub-samples could be combined. These results verified, as was thought during analysis of the particle-size distributions, that the aggregate sampling was not reproducible.

The statistical tests that were conducted in this investigation for comparing sub-samples are commonly utilized methods that have not been reported in floc characterization literature. Studies that have involved the collection of multiple samples of aggregates from one (1) population merely have not considered the reproducibility and representativeness of their sub-samples. The approach herein was a simple and effective method to quantify the variability in the characterization data

All of the aggregates from the three (3) sub-samples were combined and fractal dimensions D_1 and D_2 were calculated for each jar rather than for each replicate sample. As discussed above, this approach to data handling was acceptable and appropriate because the flocs were all collected from the same population and the size distribution of the combined data provided a more complete description of the overall floc population. Values of D_1 for aggregates generated by alum coagulation ranged from 1.107 to 1.128. Values of D_1 for aggregates generated by PACl coagulation ranged from 1.107 to 1.172. No direct

relationship could be discerned between D_f values and doses of both coagulants. During the PACl tests, D_f values decreased as the temperature of the raw water decreased; this did not occur during the alum tests. No direct relationship could be discerned between D_f and the UV_{254} and turbidity of the supernatant, as seen in Figure 4.18, for example; a direct comparison of D_f of aggregates produced by PACl coagulation at 15 °C and residual UV_{254} (i.e., following flocculation and a period of settling). The remaining figures are presented in Appendix H. The values with the associated error bars (i.e., the 95% confidence intervals) are the fractal values.

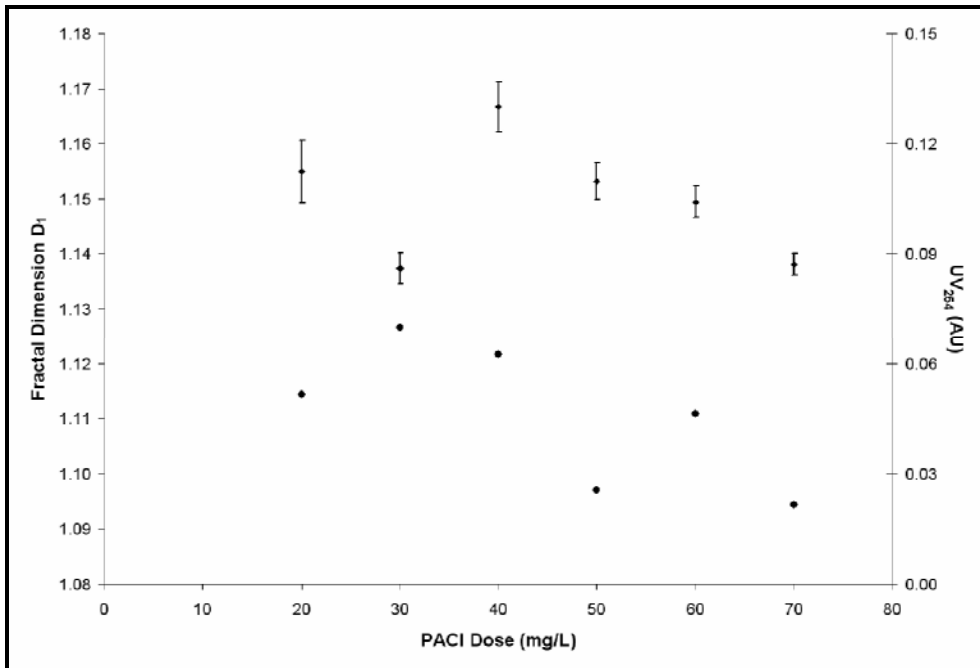


Figure 4.18: Comparing aggregate D_f to residual UV_{254} for PACl coagulation at 15 °C.

Prior to these tests, it was hypothesized that lower values of D_f would result in lower values of UV_{254} and turbidity in the supernatant (i.e., due to more settleable floc being generated) because higher values of D_f signify more complex particle outlines (deBoer and Stone, 1999). It might have been concluded, then, based on the results of this investigation, that aggregate shape possibly had less influence on UV_{254} and turbidity measurement than size

and/or density (i.e., porosity). Although Sadar (2002) reported that floc shape would have a negative bias on turbidity measurement, that relationship was not observed in the present investigation. However, difficulties associated with the floc characterization sampling and measurement methods may have impacted that result. Although they are discussed in greater detail in Section 4.3.1, an example of such an instance occurred when the sampling columns were placed in the jars to collect aggregates and caused flocs to fragment. While every effort was made to avoid such occurrences, some break-up was inevitable due to the fragile structure of the flocs.

Values of D_2 for aggregates generated by alum coagulation ranged from 1.799 to 1.864. Values of D_2 for aggregates generated by PACl coagulation ranged from 1.763 to 1.879. No direct relationship could be discerned between D_2 values and the temperature of the raw water. Figure 4.19 is a direct comparison of D_2 for aggregates produced by PACl coagulation at 5 °C and residual turbidity (i.e, following flocculation and a period of settling); the remaining figures are presented in Appendix H.

It was hypothesized that higher values of D_2 would result in better performance (i.e., due to more settleable floc being generated) because densely packed aggregates have a high D_2 , while lower values of D_2 result from large, highly branched and loosely bound structures (Chakraborti *et al.*, 2000). Chang et al. (2005) concluded that a good relationship between the two-dimensional fractal dimension of aggregates and the turbidity of settled water exists; namely, the more closed the structure of aggregates, the lower the settled effluent turbidity. As seen in Figure 4.19, the residual turbidity appeared to be inversely proportional to D_2 in most instances throughout this investigation. While this result appears to concur with theoretical concepts and studies that have validated these models. Further work is necessary to determine whether or not it is valuable and/or feasible to utilize fractal dimensions, such as D_2 , as a characteristic parameter in bench-scale testing for coagulant and/or dosage selection.

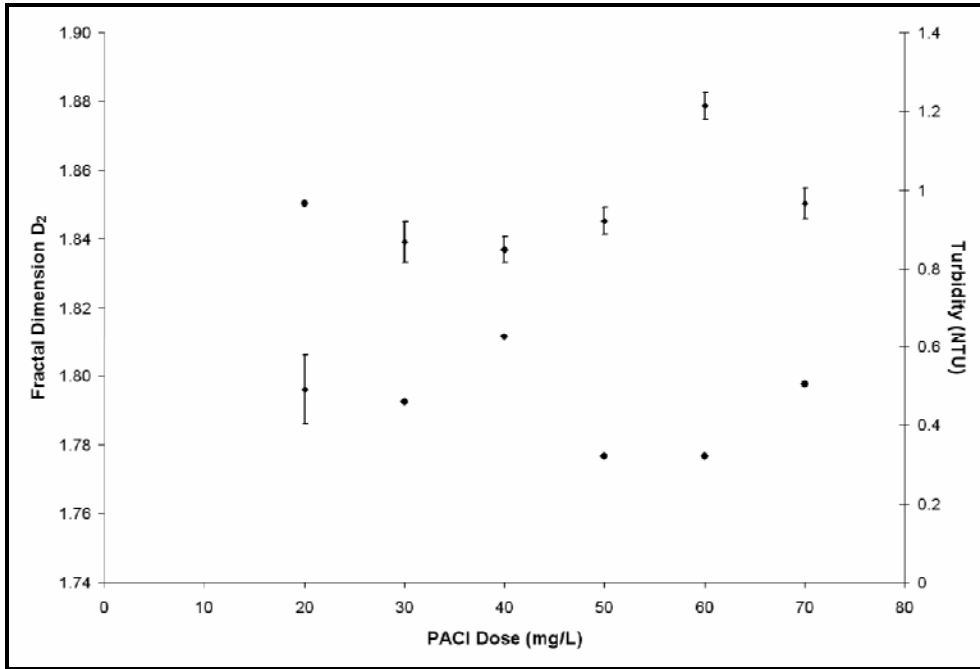


Figure 4.19: Comparing aggregate D_2 to residual turbidity for PACI coagulation at 5 °C.

4.3.1 Difficulties in Collecting Reliable Floc Characterization Data

Sampling of engineered aggregates for reliable characterization from the 2 L square acrylic jars was difficult. Firstly, the sampling columns easily and visibly caused the flocs to break-up if they were placed into and/or removed from the suspension too rapidly. Secondly, settling was beginning to occur towards the end of the ten (10) minute flocculation period (i.e., $G \approx 23$ to 28 s^{-1}); aggregates that had already settled out could not be sampled for characterization. Preferential settling onto the $0.45 \text{ }\mu\text{m}$ Millipore HA filter membranes posed another limitation associated with the sampling methods utilized throughout this investigation, and is depicted in Figure 4.20. In brief, the two-dimensional characteristics of the three-dimensional flocs depended on their orientation immediately prior to settling on the filter. Particles have a tendency to orient themselves such that they present their maximum area (Allen, 1997). Floc characteristics would have been altered if the flocs had settled in a different manner because the projected 2D image would be different.

Light microscopy with 2D image analysis works best for large, open aggregates because examination of single flocs allows detailed information on variation in floc structure (Jarvis *et al.*, 2005). However, it was often difficult to distinguish individual aggregates because they would frequently settle on top of one another. This complexity is depicted in Figure 4.21; a field of view with easily distinguishable flocs appears on the left, one that appears to have multiple aggregates settled on top of each other appears on the right. Incorrect measurement of floc size parameters (e.g., A_c , p and L_D) could have contributed considerable unquantifiable uncertainty to the results of the overall investigation, specifically the size distribution and fractal analysis.

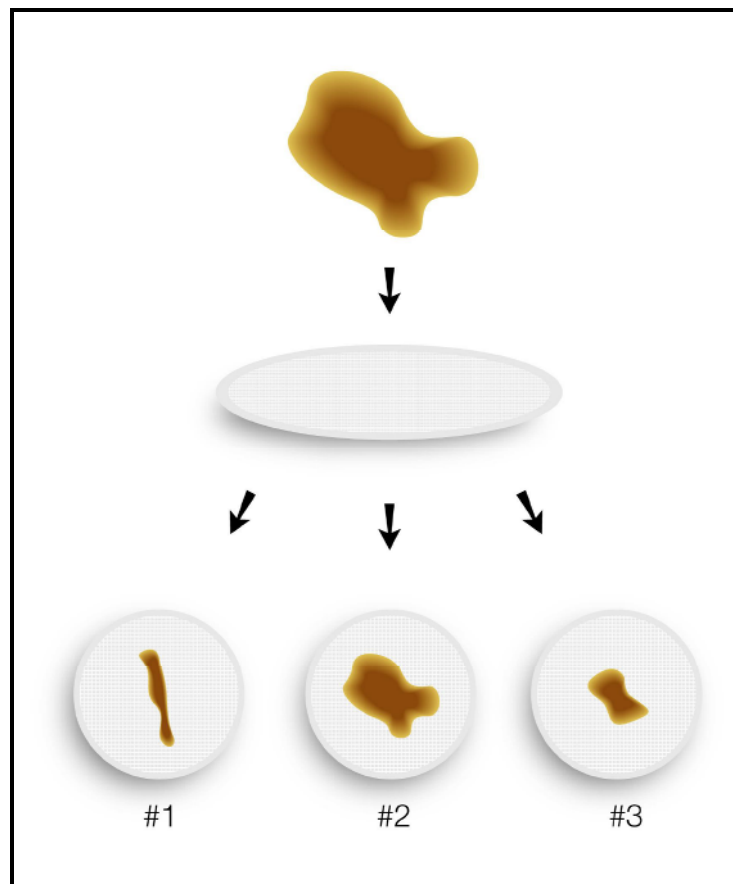


Figure 4.20: Visual depiction of preferential settling on the 0.45 μm Millipore HA filters.

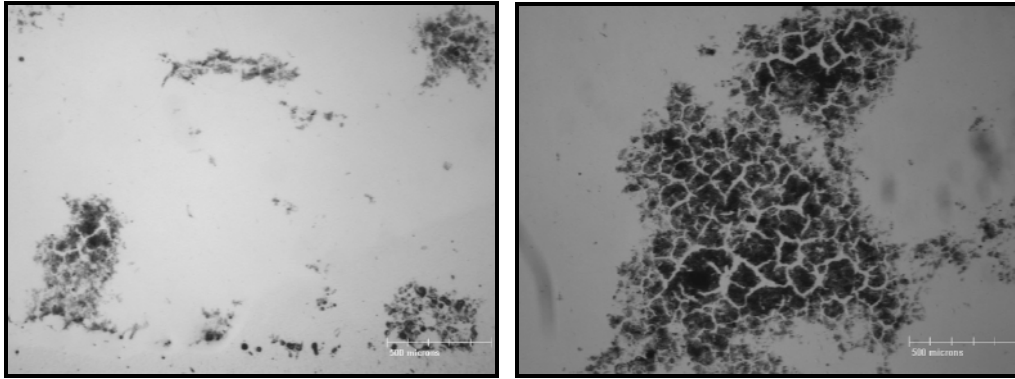


Figure 4.21: Images of engineered aggregates captured by a Sony XC75 CCD camera.

The algorithms that the image analysis program, Northern Eclipse™, utilized, were limited in their ability to calculate the perimeter for aggregates that had an area of ten (10) pixels or less. Therefore, flocs with an area less than $32 \mu\text{m}^2$ were manually removed from the data set when the 2.5x objective was utilized (i.e., for characterization of engineered aggregates). Flocs with an area less than $8 \mu\text{m}^2$ were removed when the 10x objective was utilized (i.e., for characterization of raw water particles). Figure 4.22 depicts a least squares linear regression in which flocs with an area of less than $32 \mu\text{m}^2$ were removed and the associated calculated value of D_I .

The difficulties associated with pixelation, or resolution, however, were particularly evident for the smallest flocs. Each pixel is known to have certain dimensions. The program calculates a value (e.g., area, length, etc.) based on how many pixels that the floc occupies rather than through direct measurement. Therefore, the parameters of many aggregates have been calculated as having the exact same value. When another size range of particles was removed, as is depicted in Figure 4.23, the intercept of the regression changed and D_I increased from 1.12 to 1.33. Significance difference tests ($\alpha = 0.05$) were performed on the intercept and slope of the regressions (i.e., *Equations 3.1 and 3.2*) and it was concluded that there were significance differences in the regressions. This analysis demonstrates the considerable effect that problems associated with common image analysis techniques can have on the experimental results (Jarvis *et al.*, 2005).

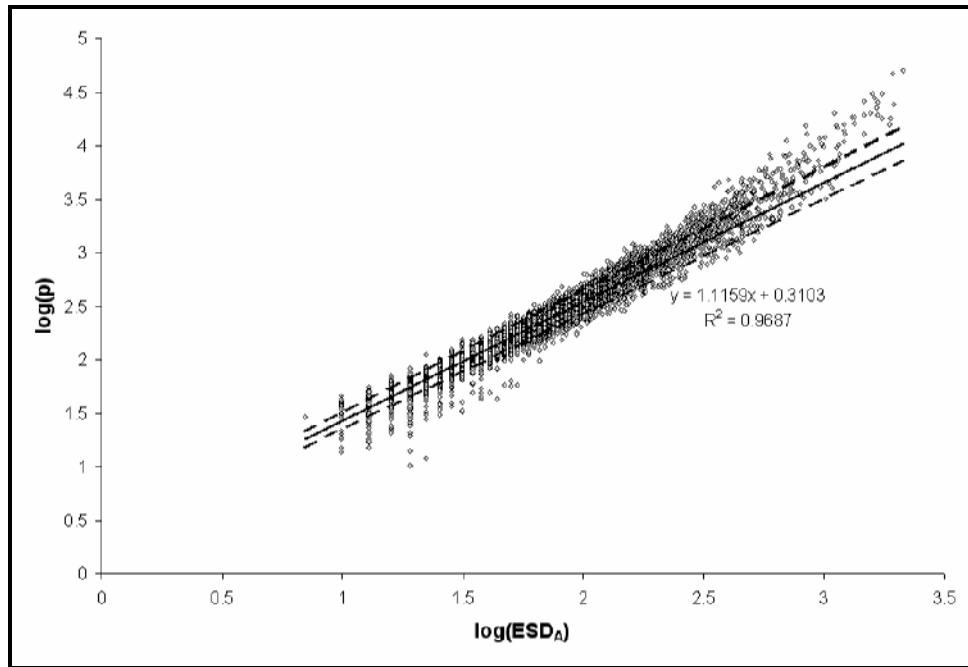


Figure 4.22: Linear regression to calculate D_1 value of flocs produced by alum coagulation at 5 °C.

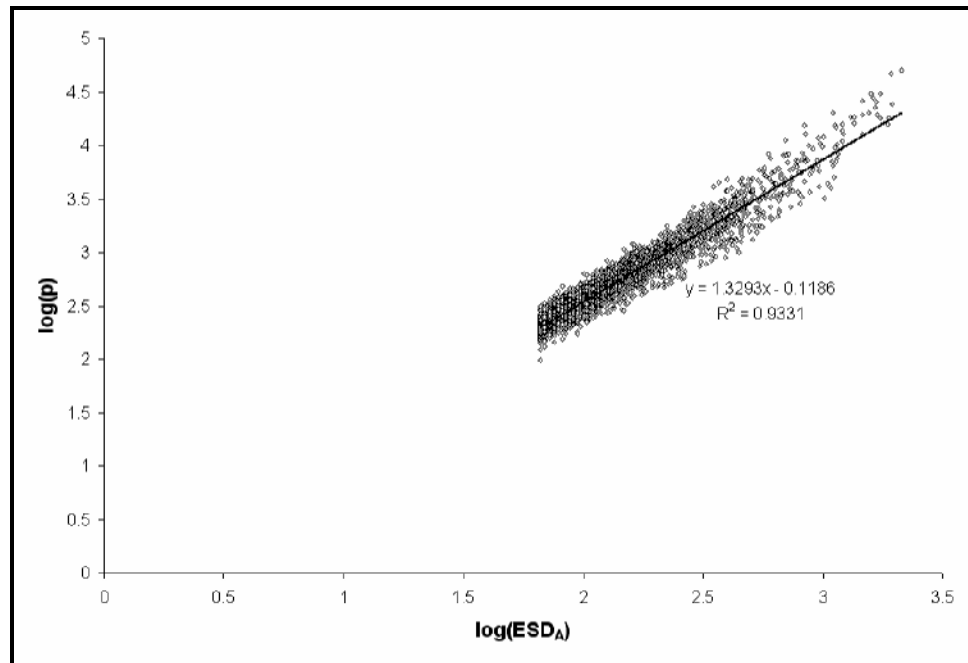


Figure 4.23: Linear regression to re-calculate D_1 value of flocs produced by alum coagulation at 5 °C.

The total number of engineered flocs and/or particles measured can also contribute significant uncertainty to floc characterization data, but this error can be readily quantified. One objective of this study was to evaluate the minimum number of flocs measured that were necessary to obtain a precise size and/or shape. Precision was quantified by the relative standard deviation (*RSD*). Figures 4.24 and 4.25 depict the *RSD* (%) calculated as a function of the cumulative number of engineered aggregates (n=9) and raw water particles characterized (n=9), respectively.

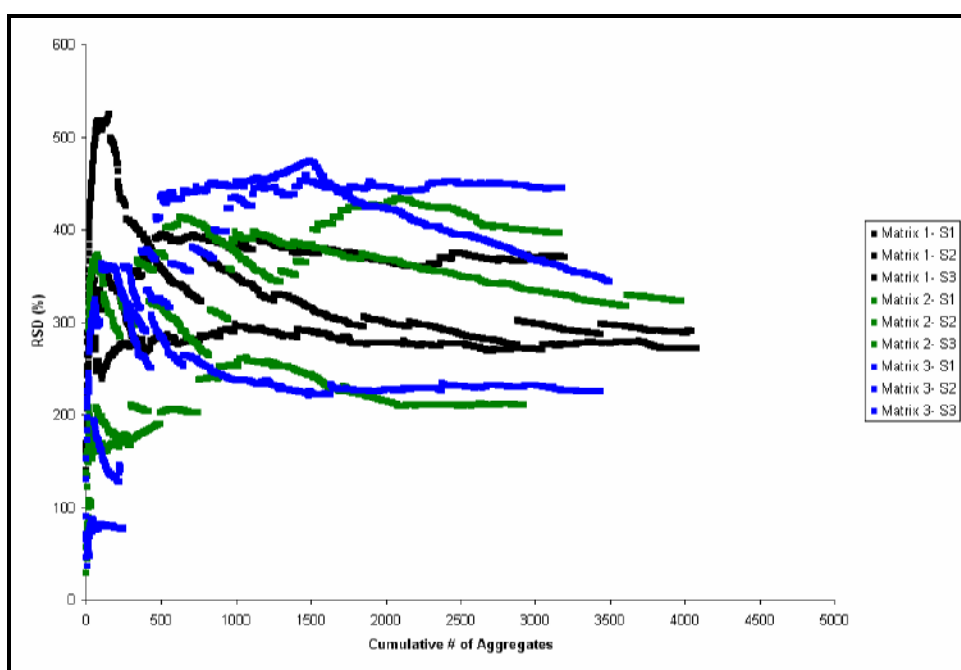


Figure 4.24: *RSD* as a function of the cumulative number of aggregates characterized (n=9).

The analysis depicted in Figure 4.24 suggested that counting at least 3000 engineered flocs at 2.5x magnification significantly improved methodological precision. The analysis depicted in Figure 4.25 suggested that counting at least 3000 raw water particles at 10x magnification significantly improved methodological precision. The oscillations in the *RSD* as the cumulative number of flocs/particles characterized increased were likely caused by random chance. That is, there were likely sections of the filters that were homogeneous and other

that were heterogeneous. Sections that were captured that had many small flocs/particles that were similar in size, for example, would have caused the RSD to decrease. If a section were captured that contained one (1) or two (2) large flocs, the RSD would have increased dramatically.

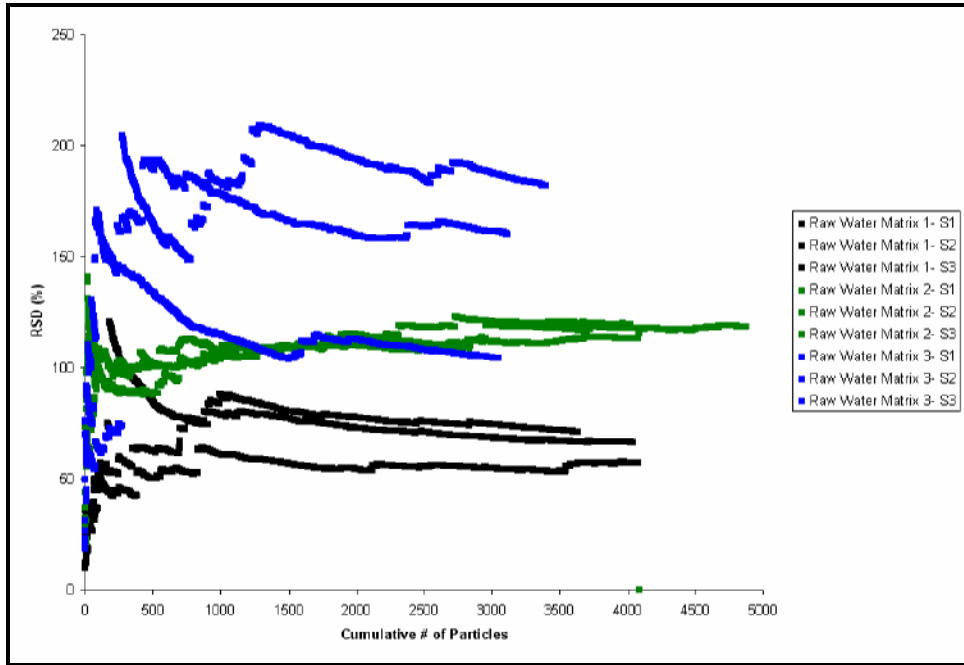


Figure 4.25: RSD as a function of the cumulative number of particles characterized (n=9).

Q-Q plots, examples of which are presented in Appendix I, indicated that the ESD_{AS} of the populations of engineered aggregates and raw water particles were approximately log-normally distributed, which justified the ANOVA analysis to evaluate the data once the data were transformed. The results of the ANOVA (Appendix I) determined that there were significant differences between the two magnifications and between the counts (e.g., between 2000 and 2900 flocs/particles counted). As well, the variances of the counts were not equivalent across the water matrices. Multiple comparison tests indicated that most of the aggregates samples were similar to one another and that most of the raw water particle samples were similar to one another. Aggregate samples were significantly different from

raw water particle samples. Further experimentation is required in which more than 2900 flocs/particles are characterized to determine the exact number that need to be captured so that a significant difference between the counts does not exist. Until then, however, at least 3000 raw water particles/engineered flocs by microscopy and digital image analysis will significantly improved methodological precision.

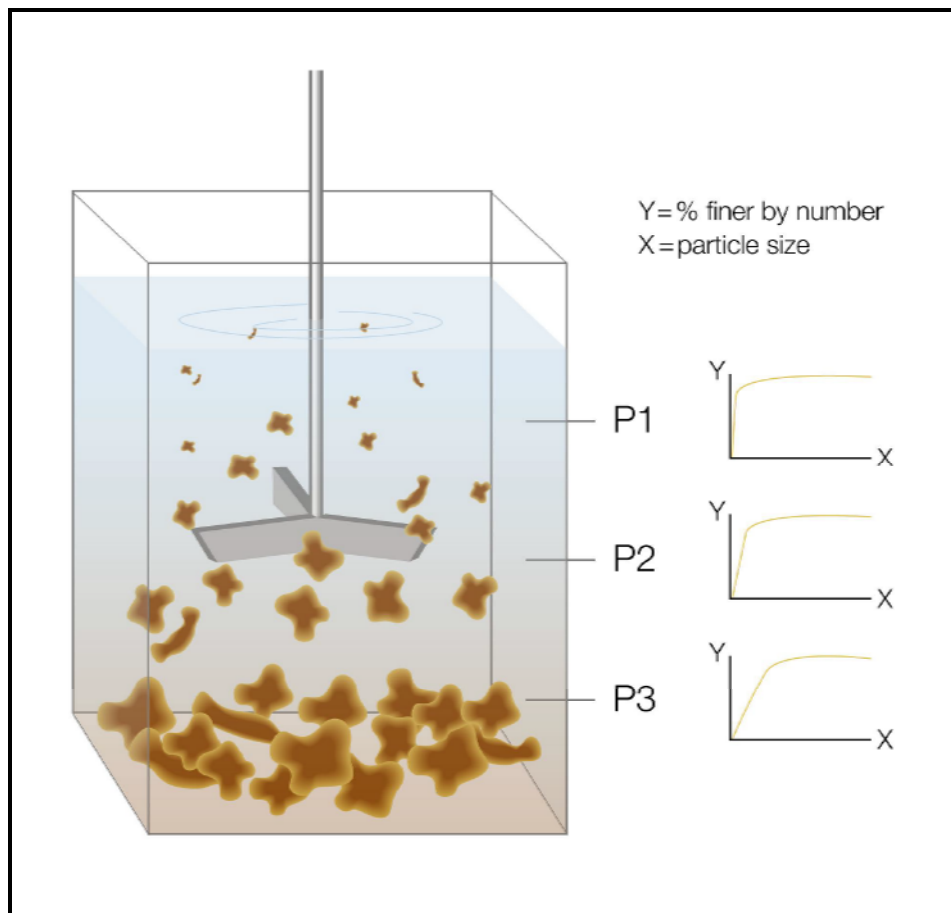


Figure 4.26: Possible variation of particle size distribution with depth in standard 2 L jars after fifteen (15) minutes of settling.

The floc characterization data, however, were not the only information collected throughout the present investigation that may have contained errors. Aside from the errors associated with the actual measurement methods (e.g., ASTM Method 5310), UV_{254} and turbidity

reductions are dictated by the concentration of particles and/or flocs that remain in suspension after the period of settling. While it seems logical to observe the same water temperature and mixing conditions at all depths in the jars, particles with different characteristics (i.e., size, density, etc.) will settle at different rates. As illustrated in Figure 4.26 (above), this will cause stratification of particles in the jar after the settling period. UV₂₅₄ and turbidity measurements would have depended on how deep the 40 ml EPA vile was placed into the jar. Sampling approach, therefore, will impact the variability in the data because the sampling population changes with different methodologies. One has to make sure that the questions that are being asked are addresses with the appropriate sampling approach.

4.4 Full-Scale Floc Sampling Results

Full-scale sampling at the MWTP occurred on three (3) separate occasions during which triplicate samples of PACl induced aggregates were collected from both the full-scale flocculation basin and at the outlet of the inclined plate settlers. They were then characterized according to the methods outlined in Section 3.5. Particle size distributions were plotted based on the results of grain size analyses and evaluated for D_{50} and D_{90} . Fractal dimensions D_1 and D_2 were calculated from regressions for each sample. The particle size distributions and a summary of D_{50} , D_{90} , D_1 and D_2 values are presented in Figure 4.27 and Table 4.2, respectively.

Table 4.2: Structural characterization data of flocs in the flocculation basin, and at the outlet of the inclined plate settlers at the MWTP.

	Pre-Sedimentation				Post-Sedimentation			
	D_{50} (μm)	D_{90} (μm)	D_1	D_2	D_{50} (μm)	D_{90} (μm)	D_1	D_2
Apr 14/08	5.44	18.74	1.305	1.781	4.76	10.30	1.103	1.509
April 22/08	4.93	12.89	1.324	1.719	4.85	10.84	1.108	1.360
May 6/08	10.22	27.30	1.261	1.807	4.76	9.78	1.103	1.526

There were obvious differences in particle size distributions prior to and subsequent to settling. Generally, there were larger aggregates in the flocculation basin than those that were collected at the outlet of the inclined plate settlers, as D_{90} was reduced from between ~ 13 and 27 μm to an average of 10 μm . Average D_{50} did not vary which meant that the smaller flocs were likely not settling and/or the larger flocs were being broken-up during transport from one process to the next. The aggregates from every sample, however, rarely had an ESD_A that was greater than 60 μm .

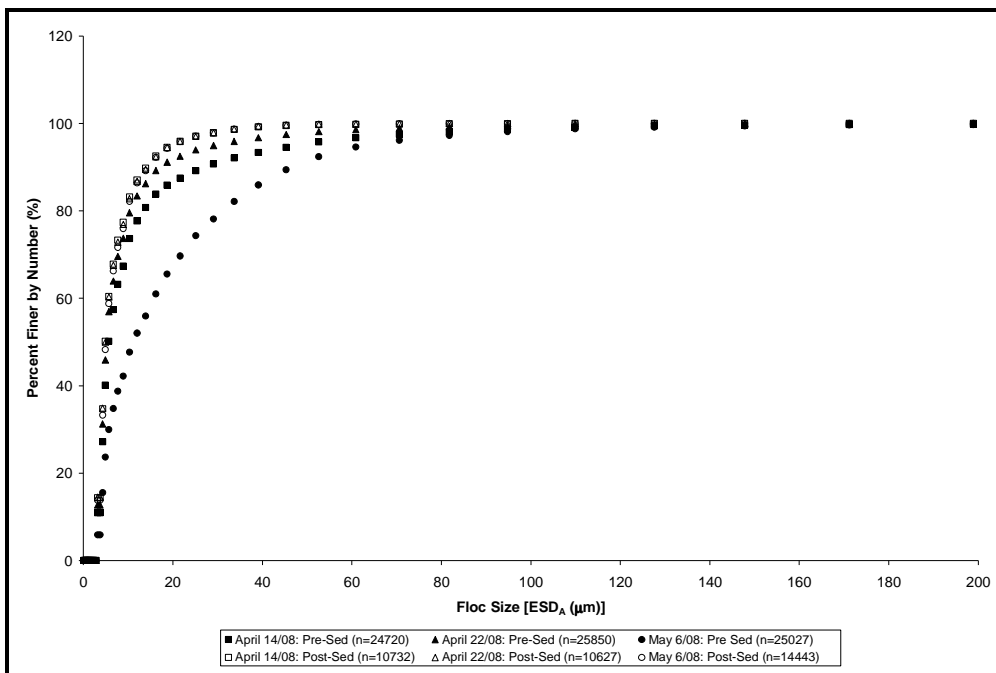


Figure 4.27: Particle size distribution of flocs in the flocculation basin, and at the outlet of the inclined plate settlers at the MWTP.

From the flocculation basin to the outlet of the inclined plate settlers, D_1 values were lowered from ~ 1.3 to 1.1 and D_2 values were lowered from ~ 1.75 to between ~ 1.37 and 1.53. What this may signify is that small, loosely bound aggregates with less complicated particle outlines (i.e., almost spherical) are not settling and are subsequently causing a build-up on the surface of and within the filters. Although the doses of coagulant (i.e., between 22.2 and

25.4 mg/L at the time that the sampling was conducted) allowed the MWTP to achieve a reasonable level of turbidity reduction (i.e., a settled water turbidity of ≈ 0.5 NTU) without removing so many particles that filtration performance would be negatively affected (Al-Ani et al., 1986), the aggregates that remained in suspension were potentially preventing the MWTP from reaching its operational capacity. In other words, pre-treatment may not be optimized to ensure that downstream processes are achieving the most effective treatment.

The most important conclusion that can be drawn from this investigation regarding operations at the MWTP is that the size and structure of aggregates generated at bench-scale at the MWTP were clearly not indicative of the size and structure of those produced at full-scale. As seen in Figure 4.28, and upon comparing the values in Table 4.2 to the results of presented in Section 4.3 (i.e., PACl aggregates with $D_{50} \approx 10$ to $25 \mu\text{m}$, $D_{90} \approx 25$ to $105 \mu\text{m}$, $D_1 \approx 1.105$ to 1.175 , and $D_2 \approx 1.76$ to 1.88), the aggregates that were generated at full-scale were much smaller and denser than those that were produced in any of the PACl jar tests (i.e., under all conditions considered). The full-scale results were only compared to the PACl jar tests because the MWTP currently uses this coagulant throughout the entire year. Ensuring that the bench-scale tests are representative is not only essential for optimization purposes, but for more effectively responding to frequent changes in raw water quality.

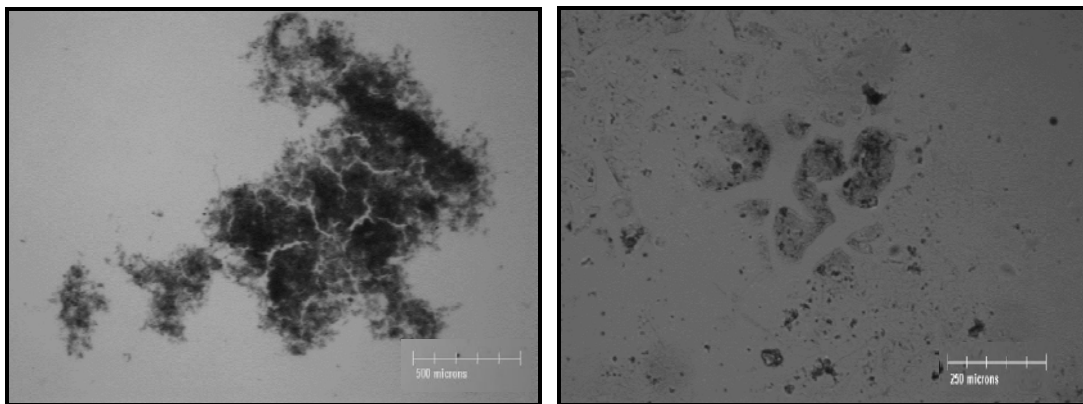


Figure 4.28: PACl flocs generated at the MWTP at bench-scale (left) and full-scale (right).

Possible explanations for the misrepresentation of full-scale performance by the jar tests might include:

- Differing velocity gradients during rapid mix (i.e., at full-scale, a G of 1000 s^{-1} is maintained; the jar test apparatus can only induce a maximum G of 400 s^{-1}); and/or
- differing methods for coagulant addition (i.e., at full-scale, coagulant is added to the raw water through pipes that are inserted into the center of the basin so that the coagulant is fully dispersed into the system. At bench-scale, coagulant is added to the water surface); and/or
- differing geometry (i.e., the flocculation basin at the MWTP is large and rectangular but if it were scaled down, it would not have the same dimensions as the standard 2 L Phipps & Bird jar); and/or
- differing mixing regimes, which is a function of the basin geometry and the paddles. The paddles at full-scale do not have the same shape as those that are a part of the standard Phipps & Bird jar testing apparatus.

4.4.1 The Importance of Full-Scale Performance Prediction

The provision of safe drinking water requires adequate disinfection of pathogenic organisms. Common drinking water disinfection technologies become decreasingly effective as levels of additional particulate matter in waters to be treated increase. Therefore, for many source waters and all surface waters, solids removal processes must precede drinking water disinfection. Chemical pre-treatment methods are designed and operated based upon information derived from jar tests that are used to simulate full-scale treatment performance.

A global assessment of data since 1970 has shown it is likely that anthropogenic warming has and will continue to have a discernable influence on many physical and biological systems. The effects on water resources may include increased run-off and earlier spring peak discharge in rivers and warming of lakes and rivers in many regions (Cromwell *et al.*, 2007). Because of this, global warming has the potential to cause simultaneous adverse

changes in both the quantity and quality of available water. These compounded effects could greatly weaken the foundation of some existing drinking water treatment strategies.

The bottom line in drinking water treatment planning has always been a matter of coping with variability. A treatment plant must be robust or resilient to challenge. With the coming changes in climate, there will be a heightened need to respond to increased variability (Cromwell *et al.*, 2007). Jar tests are crucial for managing this concern in that operators at drinking water treatment plants can attempt alternative treatment doses and strategies without altering the performance of the full-scale treatment plant. Being able to readily conduct these tests at bench-scale to achieve accurate and prompt information is especially valuable if there are rapid changes in both water quality and quantity. At the MWTP and likely many full-scale water treatment plants, however, the only reliable indicator of full-scale performance is full-scale data because jar tests are not indicative of full-scale performance (i.e., floc formation). The bench-scale tests utilized by the MWTP should be optimized to improve full-scale performance predictability. This may involve the inclusion of the particle characterization techniques discussed herein to measure parameters (e.g., D_{50} and D_2) that may be indicators of UV_{254} and turbidity reduction after a period of settling. Further work is necessary to develop the relationships uncovered during the investigations presented in this study.

5 CONCLUSIONS

The solids removal processes of coagulation, flocculation, and clarification remain a critical component of the drinking water treatment process for utilities that treat surface water. These processes are typically designed, operated and optimized based on information derived from bench-scale protocols (e.g., jar tests) that are used to simulate full-scale treatment performance. By regularly performing such tests, water treatment operators can assess alternative treatment strategies without altering plant performance. The primary goal of this thesis research was to improve the predictive capacity of bench-scale protocols commonly used for optimizing conventional chemical pre-treatment in full-scale drinking water treatment plants.

Twelve (12) jar tests using the MWTP protocol were performed throughout this investigation. The UV_{254} and turbidity of the supernatant was evaluated during each jar test to investigate potential relationships between these parameters and floc settling rates and structure. Results of this evaluation indicated that:

1. at the conditions investigated, either alum or PACl coagulation at a dose of ~ 30 mg/L in conjunction with 0.2 mg/L of cationic polyelectrolyte can achieve the lowest levels of UV_{254} and turbidity (i.e., 0.02 to 0.05 AU and 0.3 to 1.0 NTU, respectively) after flocculation and a period of settling. Comparable or slightly lower levels of UV_{254} and turbidity can possibly be achieved at doses of 60 or 70 mg/L of either alum or PACl in conjunction with 0.2 mg/L of cationic polyelectrolyte; however, the marginal gains in treated water UV_{254} and turbidity would not likely justify the additional costs associated with chemical consumption and sludge production.

Six (6) of the twelve (12) jar tests were conducted to generate aggregates for settling tests. Results from these tests indicated that:

2. floc settling velocities were not directly proportional to floc size;

3. the production of larger and more settleable flocs could not be described by floc settling velocities; and
4. floc sizes and settling velocities were not directly related to either UV_{254} or turbidity reductions.

Accordingly, the six (6) jar tests were repeated to characterize the fractal structure of the flocs by digital image analysis with microscopy. Results from these tests indicated that:

5. measured values of UV_{254} and turbidity of the supernatant were generally inversely proportional to aggregate D_{90} ; that is, the residual UV_{254} and/or turbidity decreased as the value of D_{90} increased. This may have been indicative of flocculent settling. As a consequence, the UV_{254} and turbidity values of the remaining supernatant may have decreased because some of the smaller aggregates/particles that are known to have the greatest impact on these measurements were removed by flocculant settling. Floc size was not the only aggregate parameter that might have impacted both UV_{254} and turbidity of the supernatant, however
6. no direct relationship could be discerned between D_1 and the UV_{254} and turbidity of the supernatant. It might have been concluded, then, based on the results of this investigation, that aggregate shape possibly had less influence on UV_{254} and turbidity measurement than size and/or density (i.e., porosity), as indicated by D_2 . Calculations of this D_2 indicated that
7. the turbidity after flocculation and a period of settling appeared to be inversely proportional to D_2 in most instances throughout this investigation.

Quantification of the variability in the characterization data, evaluated by significant difference tests and 95% confidence intervals, determined that:

8. significant differences between the sub-samples were evident. These results indicated that the aggregate sampling was not reproducible. A statistical assessment of light microscopy and digital image analysis specified that

9. counting at least 3000 engineered flocs at 2.5x magnification significantly improved methodological precision; at least 2000 raw water particles at 10x magnification significantly improved methodological precision.

Full-scale sampling at the MWTP indicated that:

10. the size and structure of aggregates generated at bench-scale at the MWTP were clearly not indicative of the size and structure of those produced at full-scale. The aggregates that were generated at full-scale were much smaller and denser than those that were produced in any of the PACl jar tests (i.e., under all conditions considered). At the MWTP, it is likely that at present
11. the only reliable indicator of full-scale performance is full-scale data because jar tests are not indicative of full-scale performance (i.e., floc formation).

6 RECOMMENDATIONS

The secondary goal of this research was to provide recommendations and strategies for further optimizing conventional chemical pre-treatment at the MWTP. It is inappropriate to use the data herein to make such recommendations until additional experimentation at the MWTP is conducted that focuses primarily on:

1. optimizing the bench-scale tests utilized by the MWTP to improve full-scale performance predictability. Once this issue has been sufficiently addressed, studies can be developed to focus on
2. collecting raw water samples over a range of raw water turbidities to speculate about the performance of one coagulant relative to one another through jar testing.

Further research is also required to develop the general understanding of aggregate settling so as to improve the prediction capacity of aggregate settling velocities. Additional experimentation may include investigating:

1. methods to accurately and precisely quantify three-dimensional floc characteristics (i.e., D_3) so that more appropriate variations of Stokes' law can be validated and developed. These models will likely still be unable to account for flocculent settling behavior and studies should, therefore, continue to investigate
2. the relationship between D_{90} values of aggregates prior to settling and UV_{254} and turbidity measurements after a period of settling as a simple tool that can be utilized to describe and potentially better predict flocculent settling performance (i.e., during bench-scale testing).

The results of the floc characterization experiments have demonstrated that fractal dimensions, namely D_2 , might also be used to assess and/or predict pre-treatment and/or particle removal performance. Performing additional investigations to further develop the validity of this concept may be hindered by the difficulties associated with the floc

characterization method. Ongoing research may benefit from further development of existing methods including:

1. testing new aggregate sampling methods so as to minimize break-up of the flocs and/or avoid preferential settling on the membranes filters;
2. improving the algorithms that the image analysis program, Northern Eclipse™, utilized, so that aggregates that have an area of 10 pixels or less can be quantified; and
3. further developing essential guidance for determining how to characterize floc populations in a statistically significant manner.

Jar test sampling approaches to sample either the supernatant or flocs will impact the variability in the data because the sampling population changes with different methodologies. One has to always make sure that the questions that are being asked are addresses with the appropriate sampling approach. For example, although it has previously been demonstrated that DOC consistently comprises 90% of the TOC in the raw water, the measurement of DOC rather than TOC throughout the current study would have permitted verification of the UV₂₅₄ data, and ensured more accurate interpretation of the results (i.e., UV₂₅₄ is only an indicator of DOC). DOC analysis would have reduced the confounding, and unquantified portion of the NOM associated with particulate matter. Variability in both water quality and floc characterization data, however, should always be quantified using either the methods described herein, or other well-established approaches.

References

- Aguilar, M. I., J. Saez, M. Llorens, A. Soler, and J.F. Ortuno (2003). "Microscopic observation of particle reduction in slaughterhouse wastewater by coagulation–flocculation using ferric sulphate as coagulant and different coagulant aids." *Water Research* 37(9): 2233-2241
- Al-Ani, M. Y., D. W. Hendricks, G.S. Logsdon, and C.P. Hibler (1986). "Removing Giardia Cysts from Low Turbidity Waters by Rapid Rate Filtration." *Journal of the American Water Works Association* 78(5): 66-73.
- Allen, T. (1997). Data presentation and interpretation. *Powder Size Measurement, Powder Sampling and Particle Size Measurement*. T. Allen. London, Chapman and Hall: 44-111.
- American Water Works Association, Coagulation and Filtration Committee (1982). "Survey of polyelectrolyte use in the United States." *Journal of the American Water Works Association* 74: 600-607.
- Amirtharajah, A., and K.M. Mills (1982). "Rapid Mix Design for Mechanisms of Alum Coagulation." *Journal of the American Water Works Association* 74(4): 210-216.
- Argaman, Y. A. (1971). "Pilot-Plant Studies of Flocculation." *Journal of the American Water Works Association* 63(12): 775-777.
- ASTM International (1996). Method 5310B- High Temperature Combustion Method.
- ASTM International (1996). Method 5910B- Ultraviolet Absorption Method.
- Barham, W. L., J. L. Matherne, and A.G. Keller (1956). Clarification, Sedimentation, and Thickening Equipment- A Patent Review. Bulletin No. 54, Engrg. Expt. Station. Baton Rouge, LA, Louisiana State University.
- Boardman, G. D. and O. J. Sproul (1977). Adsorption as a Protective Mechanism for Poliovirus. American Water Works Association Annual Conference and Exposition, Anaheim, California.
- Bratby, J. (2006). *Coagulation and Flocculation in water and wastewater treatment*. London, UK, IWA Publishing.
- Bushell, G. C., Y. D. Yan, D. Woodfield, J. Raper, and R. Amal (2002). "On techniques for the measurement of the mass fractal dimension of aggregates." *Advances in Colloid and Interface Science* 95(1): 1-50.

- Camp, T. R. and P. C. Stein (1943). "Velocity gradients and internal work in fluid motion." *Journal of the Boston Society of Civil Engineers* 85: 219-237.
- Chae, G.-T., J. Stimson, M.B. Emelko, D.W. Blowes, C.J. Ptacek, and M. Mesquita (2008). "Statistical assessment of the accuracy and precision of bacteria- and virus-sized microsphere enumerations by epifluorescence microscopy." *Water Research* 42(6-7): 1431-1440.
- Chakraborti, R. K., J. F. Atkinson, and J.E. Van Benschoten (2000). "Characterization of Alum Flocculation by Image Analysis." *Environmental Science and Technology* 34(18): 3969-3976.
- Chakraborti, R. K., K. H. Gardner, J.F. Atkinson, and J.E. Van Benschoten (2003). "Changes in fractal dimension during aggregation." *Water Research* 37(4): 873-883.
- Chang, Y., Q.-j. Liu, and J.S. Zhang (2005). "Flocculation control based on fractal theory." *Journal of Zhejiang University SCIENCE* 6B(10): 1038-1044.
- Clark, M. M. (1985). "A Critique of Camp and Stein's RMS Velocity Gradient." *Journal of Environmental Engineering* 111(6): 741-754.
- Clarke, P. (2007). Regional Municipality of Waterloo 2007 Annual Water Quality Report. Kitchener, ON, The Ontario Ministry of the Environment (MOE) Drinking Water Systems Regulation O. Reg. 170/03.
- Cleasby, J. L. (1984). "Is Velocity Gradient a Valid Turbulent Flocculation Parameter?" *Journal of Environmental Engineering* 110(5): 875-897.
- Cleasby, J. L. and G. S. Logsdon (1999). Chapter 8: Granular Bed and Precoat Filtration. *Water Quality and Treatment: A Handbook of Community Water Supplies*. R. D. Letterman. New York, NY, McGraw Hill.
- Cohn, P. D., M. Cox, and P.S. Berger (1999). Chapter 2: Health and Aesthetic Aspects of Water Quality. *Water Quality and Treatment: A Handbook of Community Water Supplies*. R. D. Letterman. New York, NY, McGraw Hill.
- Craig, R. F. (1997). *Soil Mechanics*. New York, NY, Chapman and Hall.
- Cromwell, J. E., J. B. Smith, and R.S. Raucher (2007). "No Doubt About Climate Change and Its Implications for Water Suppliers." *Journal of the American Water Works Association* 99(9): 112-117.

- Crook, J. (1998). Chapter 7: Water Reclamation and Reuse Criteria. Wastewater Reclamation and Reuse. T. Asano. Lancaster, PA, Technomic Publishing Co.
- deBoer, D. H. and M. Stone (1999). "Fractal dimensions of suspended solids in streams: comparison of sampling and analysis techniques." *Hydrological Processes* 13: 239-254.
- Deryagin, B. V. and L. D. Landau (1941). "Theory of Stability of Strongly Charged Lyophobic Soles and Coalescence of Strongly Charged Particles in Solutions of Electolytes." *Acta Physico-Chimica Sinica* 14.
- Droppo, I. G., D. T. Flannigan, G.G. Leppard, and S.N. Liss (1996). "Microbial floc stabilization and preparation for structural analysis by correlative microscopy " *Water Science and Technology* 34(5): 155-162.
- Droppo, I. G., G. G. Leppard, D.T. Flannigan, and S.N. Liss (1997). "The freshwater floc: a functional relationship of water and organic and inorganic floc constituents affecting suspended sediment properties." *Water, Air and Soil Pollution* 99(1): 43-53.
- Droppo, I. G. (2001). "Rethinking what constitutes suspended sediment." *Hydrological Processes* 15(9): 1551-1564.
- Droppo, I. G., G. G. Leppard, S.N. Liss, and T.G. Milligan (2005). *Flocculation in Natural and Engineered Systems*. Boca Raton, FL, CRC Press.
- Edwards, E. (2006). *The Regional Municipality of Waterloo Mannheim Water Treatment Plant Operating Strategy Review*. Toronto, ON, Associated Engineering.
- Ellms, J. W. (1928). *Water Purification*. New York, NY, McGraw Hill.
- Emelko, M. B., P. M. Huck, B.M. Coffey, and E.F. Smith (2006). "Effects of media, backwash, and temperature on full-scale biological filtration." *Journal of the American Water Works Association* 98(12): 61-73.
- Farrow, J. and L. Warren (1993). *Measurement of the size of aggregates in suspension. Dewatering Technology and Practice*. D. M. Moudgil and B. J. Scheiner. New York, NY, Engineering Foundation: 61-64.
- Feachem, R. G., D. J. Bradley, H. Garelick, and D.D. Mara (1983). *Sanitation and Disease: Health Aspects of Excreta and Wastewater Management*. John Wiley and Sons. New York, NY, The World Bank.
- Fitzpatrick, C. S. B., E. Fradin, J. Gregory (2004). "Temperature effects on flocculation, using different coagulants." *Water Science and Technology* 50(12): 171-175.

- Flynn, C. M. (1984). "Hydrolysis of inorganic iron (III) salts." *Chemical Reviews* 84(1): 31-41.
- Gehr, R., M. Wagner, P. Veerasubramanian, and P. Payment (2003). "Disinfection efficiency of peracetic acid, UV and ozone after enhanced primary treatment of municipal wastewater." *Water Research* 37(19): 4573-4586.
- Gorczyca, B. and J. Ganczarczyk (2001). "Fractal Analysis of Pore Distributions in Alum Coagulation and Activated Sludge Flocs." *Water Quality Research Journal of Canada* 36(4): 687-700.
- Goyer, R. A. (1993). "Lead Toxicity: current concerns." *Environmental Health Perspectives* 100: 177.
- Grammer, J. (2007). "Phipps and Bird Inc." Retrieved December, 2007, from www.phippsbird.com.
- Gregory, J. (1998). "The Role of Floc Density in Solid-Liquid Separation." *Advances in Filtration and Separation Technology* 12: 405-414.
- Gregory, R. and T. F. Zabel (1999). Chapter 7: Sedimentation and Flotation. *Water Quality and Treatment: A Handbook of Community Water Supplies*. R. D. Letterman. New York, NY, McGraw Hill.
- Gregory, J. and J. Duan (2001). "Hydrolyzing metal salts as coagulants." *Pure and Applied Chemistry* 73(12): 2017-2026
- Gregory, J. (2006). *Particles in Water: Properties and Processes*. Boca Raton, FL, CRC Press.
- Guan, J., T. D. Waite, and R. Amal (1998). "Rapid Structure Characterization of Bacterial Aggregates." *Environmental Science and Technology* 32(23): 3735-3742.
- Hahn, H. H. and W. Stumm (1968). "Kinetics of coagulation with hydrolyzed Al(III). The rate-determining step." *Journal of Colloid and Interface Science* 28: 134-144.
- Han, M. and D. F. Lawler (1992). "The (Relative) Insignificance of G in Flocculation." *Journal of the American Water Works Association* 84(10): 79-91.
- Hanson, A. T. and J. L. Cleasby (1990). "The Effects of Temperature on Turbulent Flocculation: Fluid Dynamics and Chemistry." *Journal of the American Water Works Association* 82(11): 56-73.

- Hejkal, T. W., F. M. Wellings, P.A. LaRock, and A.L. Lewis (1979). "Survival of poliovirus within organic solids during chlorination." *Applied and Environmental Microbiology* 38(1): 114-118.
- Hroncich, J. A. (1999). Chapter 4: Surface Water. *Water Quality and Treatment: A Handbook of Community Water Supplies*. R. D. Letterman. New York, NY, McGraw Hill.
- Hrudey, S. E., P. M. Huck, P. Payment, R.W. Gillham, and E.J. Hrudey (2002). "Walkerton: Lessons learned in comparison with waterborne outbreaks in the developed world." *Journal of Environmental Engineering Science* 1: 397-407.
- Hudson, H. E. (1965). "Physical Aspects of Flocculation." *Journal of the American Water Works Association* 57(7): 885-892.
- Jarvis, P., B. Jefferson, and S.A. Parsons (2005). "Measuring floc structural characteristics." *Reviews in Environmental Science and Bio/Technology* 4: 1-18.
- Je, C. H. and S. Chang (2004). "Simple approach to estimate flocculent settling velocity in a dilute suspension." *Environmental Geology Berlin* 45(7): 1002-1009.
- Jefferson, B. and P. R. Jarvis (2006). *Practical application of fractal dimension. Interface Science in Drinking Water Treatment*. G. Newcombe and D. Dixon. St. Louis, MO, Elsevier Ltd.
- Jiang, Q. and B. E. Logan (1996). "Fractal dimensions of aggregates from shear devices." *Journal of the American Water Works Association* 88(2): 100-113.
- Johnson, C. P., X. Li, and B. Logan (1996). "Settling Velocities of Fractal Aggregates." *Environmental Science and Technology* 30(6): 1911-1918.
- Kapoor, B. and A. Acrivos (1995). "Sedimentation and sediment flow in settling tanks with inclined walls." *Journal of Fluid Mechanics* 290: 39.
- Kenkel, N. C. and D. J. Walker (1996). "Fractals in the biological sciences." *Coenoses* 11(2): 77-100.
- Kim, A. Y. and J. C. Berg (2000). "Fractal Heteroaggregation of Oppositely Charged Colloids." *Journal of Colloid and Interface Science* 229(2): 607-614.
- Kim, S. H., B. H. Moon, and H.I. Lee (2001). "Effects of pH and dosage on pollutant removal and floc structure during coagulation." *Microchemical Journal* 68(2-3): 197-203.

- Kirchman, D., J. Sigda, R. Kapuscinski, and R. Mitchell (1982). "Statistical analysis of the direct count method for enumerating bacteria." *Applied and Environmental Microbiology* 44(2): 376-382.
- Lee, S. A., A. G. Fane, R. Amal, and T.D. Waite (2003). "The Effect of Floc Size and Structure on Specific Cake Resistance and Compressibility in Dead-End Microfiltration." *Separation Science and Technology* 38(4): 869-888.
- Letterman, R. D., J. E. Quon, and R.S. Gemmill (1973). "Influence of Rapid-Mix Parameters on Flocculation." *Journal of the American Water Works Association* 65(11): 716-722.
- Letterman, R. D. and P. Sricharoenchaikit (1982). "Interaction of Hydrolyzed Al and Polyelectrolyte Coagulants." *Journal of Environmental Engineering* 108(5): 883-899.
- Letterman, R. D. (1999). Chapter 6: Coagulation and Flocculation. *Water Quality and Treatment: A Handbook of Community Water Supplies*. R. D. Letterman. New York, NY, McGraw Hill.
- Li, D. H. and J. Ganczarczyk (1989). "Fractal geometry of particle aggregates generated in water and wastewater treatment processes." *Environmental Science and Technology* 23(11): 1385-1389.
- Li, D. H. and J. J. Ganczarczyk (1986). "Physical Characteristics of Activated Sludge Flocs." *CRC Critical Reviews in Environmental Control* 17(1): 53-87.
- Licsko, I. (2004). "Coagulation processes-- nano- and microprocesses." *Water Science and Technology* 50(12): 193-200.
- Lisle, J. T. and J. B. Rose (1995). "Cryptosporidium contamination of water in the USA and UK: A mini review." *Journal of Water Supply: Research and Technology* 44(3): 103-117.
- Lyklema, J. (1978). *Surface chemistry of colloids in connection with stability. The Scientific Basis of Flocculation*. K. J. Ives. The Netherlands, Sijthoff and Noordhoff.
- Madigan, M. M., J. Martinko, and J. Parker (2000). *Brock Biology of Microorganisms*. Upper Saddle River, NJ, Prentice-Hall.
- Mandelbrot, B. (1982). *The Fractal Geometry of Nature*, W.H. Freeman and Co.
- Mawdsley, J. L., R. D. Bardgett, R.J. Merry, B.F. Pain, and M.K. Theodorou (1994). "Pathogens in livestock waste, their potential for movement through soil and environmental pollution." *Applied Soil Ecology* 2(1): 1-15.

- McConnachie, G. L. (1991). "Turbulence Intensity of Mixing in Relation to Flocculation." *Journal of Environmental Engineering* 117(6): 731-750.
- Metcalf, L. and H. Eddy (2003). *Wastewater Engineering: Treatment and Reuse*. New York, NY, McGraw-Hill, Inc.
- Michael, J. R. (1983). "The Stabilized Probability Plot." *Biometrika* 70(1): 11-17.
- Morris, J. K. and W. R. Knocke (1984). "Temperature Effects on the Use of Metal-Ion Coagulants for Water Treatment." *Journal of the American Water Works Association* 76(3): 74-79.
- O'Melia, C. R. (1995). "From Algae to Aquifers: Solid-Liquid Separation in Aquatic Systems." *Advances in Chemistry Series* 244.
- O'Melia, C. (2007). *A Discussion of "Sweep" Flocculation*. M. B. Emelko. Baltimore, Maryland.
- Ongley, E. D., B. G. Krishnappan, I.G. Droppo, S.S. Rao, and R.J. Marguire (1992). "Cohesive sediment transport: emerging issues for toxic chemical management." *Hydrobiologia* 235-236(1): 177-187.
- Ontario Ministry of the Environment (MOE) (2003). *O. Reg 170/03- Drinking Water Systems Regulation*.
- Pask, D. (1993). *Jar Testing: Getting Started on a Low Budget*, National Environmental Service Center.
- Pernitsky, D. J. and J. K. Edzwald (2003). "Solubility of polyaluminum coagulants." *Journal of Water Supply: Research and Technology* 52(6): 395-406.
- Pernitsky, D. J. and J. K. Edzwald (2006). "Selection of alum and polyaluminum coagulants: principles and applications." *Journal of Water Supply: Research and Technology* 55(2): 121-141.
- Prandtl, L. and O. G. Tietjens (1957). *Fundamentals of Hydro-and Aeromechanics*. Mineola, NY, Dover Publications.
- Ratcliffe, H. E., G. M. Swanson, and L.J. Fischer (1996). "Human Exposure to Mercury: A Critical Assessment of the Evidence of Adverse Health Effects." *Journal of Toxicology and Environmental Health* 49(3): 221-270.

- Sadar, M. (1998). Determining Correlation of Nephelometric Turbidity Measurement to Suspended Solids in Industrial Samples. Loveland, Colorado, HACH Company.
- Sadar, M. (2002). Turbidity Instrumentation- An overview of Today's Available Technology FISC Turbidity Workshop Sponsored by the U.S. Geological Survey, Reno, NV.
- Satterfield, Z. (2005). "Jar Testing." The National Environmental Services Center Tech Brief 5(1): 2-4.
- Sawyer, C.N, P.L. McCarty, and G.F. Parkin (2003). Chemistry for Environmental Engineering and Science. New York, NY, McGraw-Hill, Inc.
- Schwartzberg, H. G. and R. E. Treybal (1968). "Fluid and Particle Motion in Turbulent Stirred Tanks. Particle Motion." Industrial & Engineering Chemistry Fundamentals 7(1).
- Sproul, O. J. (1972). "Virus Inactivation by Water Treatment." Journal of the American Water Works Association 64(1): 31-35.
- Stagg, C. H., C. Wallis, C.H. Ward, and C.D. Gerba (1978). "Chlorination of Solids Associated Coliphages." Progress in Water Technology 10(12).
- Stone, M. (2007). A Discussion of the minimum number of particles to be counted to achieve statistically significant results. A. Arnold. Kitchener, ON.
- Stone, M. and B. G. Krishnappan (2003). "Floc morphology and size distributions of cohesive sediment in steady-state flow." Water Research 37: 2739-2747.
- Swamee, P. K. and A. Tyagi (1996). "Design of Class-I Sedimentation Tanks." Journal of Environmental Engineering 122(1): 71-73.
- Tang, P., J. Greenwood, and J.A. Raper (2002). "A Model to Describe the Settling Behavior of Fractal Aggregates." Journal of Colloid and Interface Science 247(1): 210-219.
- Valioulis, I. A. and E. List (1984). "Numerical simulation of a sedimentation basin." Environmental Science and Technology 18: 242-247.
- Van de Hulst, H. C. (1957). Light Scattering by Small Particles. New York, NY, John Wiley and Sons.
- Waite, T. D. (1999). "Measurement and implications of floc structure in water and wastewater treatment." Colloids and Surfaces A: Physicochemical and Engineering Aspects 152(1-2): 27-41.

- Wang, X. C., P. K. Jin, and J. Gregory (2002). "Structure of Al-humic flocs and their removal at slightly acidic and neutral pH." *Water Science and Technology* 2(2): 99-106.
- Wesolowski, D. J. and D. A. Palmer (1992). "Aluminum speciation and equilibria in aqueous solution: II. The solubility of gibbsite in acidic sodium chloride solutions from 30 to 70 °C." *Geochimica et Cosmochimica Acta* 56(3): 1093-1111.
- Wesolowski, D. J. and D. A. Palmer (1994). "Aluminum speciation and equilibria in aqueous solution: V. Gibbsite solubility at 50°C and pH 3-9 in 0.1 molal NaCl solutions (a general model for aluminum speciation; analytical methods)." *GEOCHIMICA ET COSMOCHIMICA ACTA* 58(14): 2947.
- Wu, R. M., D. J. Lee, T.D. Waite, and J. Guan (2002). "Multilevel Structure of Sludge Flocs." *Journal of Colloid and Interface Science* 252(2): 383-392.
- Yao, K. M. (1973). "Design of High-Rate Settlers." *Journal of the Environmental Engineering Division* 99(5): 621-637
- Zhao, Y. Q. (2004). "Settling behaviour of polymer flocculated water-treatment sludge I: analyses of settling curves." *Separation and Purification Technology* 35(1): 71-80.

Appendix A

Common Equivalent Spherical Diameters for Characterizing Floc

Floc Diameter	Description	Diagram	Equation for Calculation
<i>Perimeter diameter, d_c</i>	The diameter of a circle with the same perimeter (P) as the measured particle.		$d_c = \frac{P}{\pi}$
<i>Projected area diameter1, d_a</i>	The diameter of a circle with the same projected cross-sectional area (A) as the floc measured in a stable orientation.		$d = 2\sqrt{\frac{A}{\pi}}$
<i>Projected area diameter2, d_p</i>	The diameter of a circle with the same projected area as the floc measured in a random orientation.		
<i>Surface diameter, d_s</i>	The diameter of a sphere having the same surface area (S) as the floc.		$d_s = \sqrt{\frac{S}{\pi}}$
<i>Volumetric diameter, d_v</i> <i>(OR equivalent spherical diameter)</i>	The diameter of a circle with the same volume (V) as the floc measured.		$d_v = \sqrt[3]{\frac{6V}{\pi}}$
<i>Surface-volume diameter, d_{sv}</i>	The diameter of a sphere with the same surface area to volume ratio as the floc.		$d_{sv} = \frac{d_v^3}{d_s^2}$
<i>Free-falling diameter, d_r</i>	The diameter of a sphere having the same density and free-falling speed as the floc in the same fluid at the same density and viscosity.		
<i>Stoke's diameter, d_{st}</i>	The diameter of a free falling particle in the laminar flow range (where $Re < 0.2$).		$d_{st} = \frac{18\mu V}{\rho_f - \rho}$
<i>Feret's diameter, d_F</i>	The (mean) value between pairs of parallel tangents to the projected outline of the particle.		-
<i>Martin's diameter, d_M</i>	The length of the chord parallel to a fixed direction which splits the floc projected area into two equal parts.		-

Source: Dharmarajah and Cleasby, 1986; Allen, 1997.

Appendix B

MWTP Jar Test Protocol Sample Data Sheet

MWTP				JAR TESTING			
Stn#2 - RAW				Stn#2 - RAW		Sedimentation	
Date	Time			Date	Time	Side I	Side II
Sample data:	Units			Sample data:	Units		
pH				pH			
Conductivity	uS/cm			Conductivity	uS/cm		
Temp	oC			Temp	oC		
Turbidity	NTU			Turbidity	NTU		
UV at 254 nm	abs			UV at 254 nm	abs		
UV at 254 nm	%T			UV at 254 nm	%T		
Mixing:	RPM	sec	min				
Coagulation:	300	30					
Flocculation:	100		2				
	55		3				
	25		10				
Settling:	0		20				
JAR TEST I							
Jar #		1	2	3	4	5	6
Coagulant, mg/l	Sternpac						
Polymer, mg/l	LT 22S						
Floc formation							
Floc size							
Floc quantity							
Settling speed							
Filterability							
Supernatant:	Units						
Turbidity	NTU						
UV at 254 nm	abs						
UV at 254 nm	%T						
JAR TEST II							
Jar #		1	2	3	4	5	6
Coagulant, mg/l	Sternpac						
Polymer, mg/l	LT 22S						
Floc formation							
Floc size							
Floc quantity							
Settling speed							
filterability							
Supernatant:	Units						
Turbidity	NTU						
UV at 254 nm	abs						
UV at 254 nm	%T						

Appendix C

Jar Test Results: Water Quality Analyses Data

Table C.1: Water quality of the supernatant collected during the alum settling test experiments.

		Settling Tests				
		Alum Jar Tests				
		TOC (mg/L)	Conductivity (µS)	pH	UV Absorbance (AU)	Turbidity (NTU)
T1 (5 °C)	20 mg/L	5.46	401	8.0	0.14	0.57
	30 mg/L	6.28	392	7.7	0.12	0.36
	40 mg/L	5.13	509	8.0	0.07	0.37
	50 mg/L	5.07	320	7.8	0.08	0.63
	60 mg/L	5.32	505	7.6	0.05	0.38
	70 mg/L	4.87	420	8.1	0.08	0.32
T2 (15 °C)	20 mg/L	5.96	462	7.6	0.12	0.42
	30 mg/L	5.68	450	7.5	0.08	0.48
	40 mg/L	5.21	422	7.6	0.09	0.72
	50 mg/L	4.58	415	7.9	0.26	0.87
	60 mg/L	5.56	390	7.4	0.08	0.96
	70 mg/L	5.13	390	7.8	0.12	0.71
T3 (25 °C)	20 mg/L	6.29	479	8.0	0.13	0.65
	30 mg/L	5.88	489	8.2	0.13	0.4
	40 mg/L	5.42	363	8.0	0.08	0.37
	50 mg/L	4.78	490	8.0	0.07	0.75
	60 mg/L	4.94	510	8.0	0.07	0.79
	70 mg/L	5.46	472	8.1	0.08	0.62

Table C.2: Water quality of the supernatant collected during the PACl settling test experiments.

		Settling Tests				
		PACl Jar Tests				
		TOC (mg/L)	Conductivity (µS)	pH	UV Absorbance (AU)	Turbidity (NTU)
T1 (5 °C)	20 mg/L	5.41	503	7.2	0.12	0.33
	30 mg/L	5.49	522	7.6	0.07	0.37
	40 mg/L	4.61	500	7.8	0.08	0.62
	50 mg/L	4.74	510	8.3	0.07	0.56
	60 mg/L	4.36	459	7.7	0.08	0.57
	70 mg/L	4.39	449	8.1	0.07	0.59
T2 (15 °C)	20 mg/L	4.91	470	8.0	0.10	0.45
	30 mg/L	5.86	487	7.9	0.14	0.47
	40 mg/L	4.60	403	7.7	0.08	0.49
	50 mg/L	4.85	386	8.0	0.06	0.64
	60 mg/L	4.30	507	7.4	0.10	0.44
	70 mg/L	5.14	507	7.6	0.08	0.32
T3 (25 °C)	20 mg/L	7.08	507	8.6	0.13	0.65
	30 mg/L	5.54	292	7.8	0.08	0.36
	40 mg/L	6.04	516	8.2	0.11	0.45
	50 mg/L	5.50	514	8.2	0.09	0.82
	60 mg/L	4.69	516	8.2	0.06	0.61
	70 mg/L	4.56	453	7.7	0.07	0.4

Table C.3: Water quality of the supernatant collected during the alum characterization experiments.

Floc Characterization						
Alum Jar Tests						
		TOC (mg/L)	Conductivity (µS)	pH	UV Absorbance (AU)	Turbidity (NTU)
T1 (5 °C)	20 mg/L	5.75	538	8.6	0.06	0.61
	30 mg/L	5.50	551	8.4	0.08	0.46
	40 mg/L	4.69	522	8.2	0.07	0.49
	50 mg/L	5.44	383	8.5	0.06	0.4
	60 mg/L	5.04	545	8.2	0.03	0.51
	70 mg/L	3.86	534	8.0	0.05	0.27
T2 (15 °C)	20 mg/L	4.85	543	8.1	0.05	0.38
	30 mg/L	5.65	557	8.5	0.08	0.32
	40 mg/L	5.10	530	8.2	0.04	0.39
	50 mg/L	4.54	550	7.7	0.03	0.43
	60 mg/L	4.43	528	8.1	0.03	0.26
	70 mg/L	4.53	554	8.1	0.03	0.31
T3 (25 °C)	20 mg/L	5.03	553	8.2	0.05	0.52
	30 mg/L	5.40	519	8.6	0.09	0.33
	40 mg/L	5.09	559	8.5	0.08	0.9
	50 mg/L	4.86	552	8.5	0.03	0.47
	60 mg/L	4.89	556	8.6	0.06	0.3
	70 mg/L	4.63	558	8.4	0.06	0.6

Table C.4: Water quality of the supernatant collected during the PACl characterization experiments.

Floc Characterization						
PACl Jar Tests						
		TOC (mg/L)	Conductivity (µS)	pH	UV Absorbance (AU)	Turbidity (NTU)
T1 (5 °C)	20 mg/L	6.11	530	8.3	0.05	0.965
	30 mg/L	5.61	503	8.3	0.04	0.46
	40 mg/L	4.16	518	8.2	0.08	0.625
	50 mg/L	11.70	551	7.9	0.07	0.32
	60 mg/L	5.29	545	8.5	0.05	0.32
	70 mg/L	5.06	524	8.2	0.07	0.505
T2 (15 °C)	20 mg/L	4.58	523	8.4	0.05	1.195
	30 mg/L	5.18	535	8.3	0.07	0.845
	40 mg/L	3.79	543	8.6	0.06	1.02
	50 mg/L	3.47	521	8.0	0.03	0.775
	60 mg/L	4.40	550	8.4	0.05	0.85
	70 mg/L	4.16	552	8.5	0.02	0.83
T3 (25 °C)	20 mg/L	4.90	531	8.5	0.09	1.145
	30 mg/L	4.49	536	8.8	0.07	0.705
	40 mg/L	3.93	538	8.1	0.06	0.965
	50 mg/L	4.09	543	8.9	0.03	0.845
	60 mg/L	4.39	536	8.2	0.05	0.75
	70 mg/L	4.28	550	8.0	0.02	0.79

Table C.5: Raw water quality data for the additional alum and PACl jar test experiments.

		Additional Jar Tests @ 15 C Raw Water Quality				
		TOC (mg/L)	Conductivity (µS)	pH	UV Absorbance (AU)	Turbidity (NTU)
<i>Raw Water</i>	<i>A</i>	6.61	511	8.0	0.22	3.75
	<i>B</i>	7.16	513	8.0	0.23	4.51
	<i>C</i>	5.99	391	8.0	0.22	3.61

Table C.6: Water quality of the supernatant collected during the additional PACl jar test experiment.

		Additional Alum Jar Test @ 15C				
		TOC (mg/L)	Conductivity (µS)	pH	UV Absorbance (AU)	Turbidity (NTU)
<i>20 mg/L</i>	<i>A</i>	5.83	537	7.7	0.17	1.39
	<i>B</i>	4.90	543	7.7	0.16	1.14
	<i>C</i>	3.88	546	7.7	0.17	1.00
<i>30 mg/L</i>	<i>A</i>	3.85	545	7.7	0.14	0.75
	<i>B</i>	4.26	550	7.6	0.14	0.86
	<i>C</i>	3.75	550	7.6	0.14	0.74
<i>40 mg/L</i>	<i>A</i>	3.81	550	7.6	0.12	1.65
	<i>B</i>	4.08	539	7.7	0.12	0.90
	<i>C</i>	3.80	549	7.6	0.12	0.88
<i>50 mg/L</i>	<i>A</i>	5.16	543	7.5	0.11	0.76
	<i>B</i>	5.21	551	7.4	0.10	0.67
	<i>C</i>	3.32	551	7.5	0.10	0.57
<i>60 mg/L</i>	<i>A</i>	3.60	542	7.4	0.10	0.69
	<i>B</i>	3.61	553	7.4	0.10	0.65
	<i>C</i>	3.22	554	7.4	0.10	0.58
<i>70 mg/L</i>	<i>A</i>	5.27	548	7.3	0.09	0.78
	<i>B</i>	3.49	554	7.3	0.09	0.67
	<i>C</i>	4.04	555	7.3	0.09	0.70

Table C.7: Water quality of the supernatant collected during the additional alum jar test experiment.

		Additional PACl Jar Test @ 15C				
		TOC (mg/L)	Conductivity (µS)	pH	UV Absorbance (AU)	Turbidity (NTU)
<i>20 mg/L</i>	<i>A</i>	7.03	520	7.9	0.15	0.80
	<i>B</i>	7.10	505	7.8	0.15	0.78
	<i>C</i>	7.52	526	7.8	0.15	1.51
<i>30 mg/L</i>	<i>A</i>	5.46	545	7.8	0.11	0.54
	<i>B</i>	5.58	511	7.8	0.12	0.79
	<i>C</i>	9.52	545	7.7	0.13	1.30
<i>40 mg/L</i>	<i>A</i>	5.46	551	7.7	0.11	1.01
	<i>B</i>	5.06	554	7.7	0.11	0.91
	<i>C</i>	5.34	552	7.8	0.10	0.45
<i>50 mg/L</i>	<i>A</i>	4.97	552	7.7	0.10	1.06
	<i>B</i>	4.36	551	7.6	0.09	0.74
	<i>C</i>	4.84	524	7.7	0.09	0.63
<i>60 mg/L</i>	<i>A</i>	2.81	553	7.5	0.08	0.36
	<i>B</i>	3.41	558	7.5	0.07	0.26
	<i>C</i>	4.16	558	7.5	0.08	0.62
<i>70 mg/L</i>	<i>A</i>	3.77	557	7.5	0.07	0.78
	<i>B</i>	3.88	568	7.5	0.07	0.42
	<i>C</i>	3.48	562	7.5	0.07	0.47

Appendix D

Mannheim Water Treatment Plant Operating Strategy Review: Jar Test Results

045052 - RMOW Mannheim Water Treatment Plant Operating Strategy Review
Coagulation Study

7/16/00
Compiled by Vincent Laplanche

NOTE: All quantities of coagulant are reported as Al₂O₃.

Jar Testing Data Log Alum - Acidified 10 % H₂SO₄ Test No. 1

Raw Water Quality		
Parameter	Test 1	Test 2
Temperature (°C)	14	
pH	7.90	
TOC (UV absorbance)	0.147	0.149
Turbidity (NTU)	2.95	
Mean UV absorbance (cm ⁻¹)	0.148	
Mean Turbidity (NTU)	2.95	

Other Data
Cell length 1 cm

Jar test conditions		
	Time (mins)	Speed (rpm)
Rapid Mixing:	2	300
Flocculation:	15	51
Settling:	30	0

Parameter	Jar Numbers					
	1	2	3	4	5	6
<i>Coagulant</i>						
Concentration (mg/L)	5	10	20	30	40	60
Volume added (uL)	179	357	714	1071	1429	2143
<i>After Rapid Mix</i>						
Temperature (°C)	15	15	15	15	15	15
Relative floc size	A	E	B	B	B	B
<i>Settled Water</i>						
Sludge thickness (mm)	1	6	9	9	9	5
Turbidity (1) (NTU)	6.48	1.31	4.68	6.99	13.00	21.50
Turbidity (2) (NTU)	6.46	1.29	4.70	6.95	13.00	21.80
pH	7.06	7.15	6.88	6.27	5.02	4.60
Temperature (°C)	15.4	16.1	15.8	15.6	15.7	16.2
UV absorbance 1	0.095	0.060	0.041	0.037	0.036	0.053
UV absorbance 2	0.096	0.058	0.043	0.035	0.036	0.052
Mean UV absorbance (cm ⁻¹)	0.096	0.059	0.042	0.036	0.036	0.053
Mean Turbidity (NTU)	6.47	1.30	4.69	6.97	13.00	21.65

Comments:

Jar 2 showed more floc during flocculation
After 25 minutes of settling, jar 1 had no visible settling

NOTE: All quantities of coagulant are reported as Al₂O₃.

Jar Testing Data Log - PACl

Test No. 1

Raw Water Quality		
Parameter	Test 1	Test 2
Temperature (°C)	17.3	
pH	8.38	
TOC (UV absorbance)	0.196	
Turbidity (NTU)	9.67	9.21
Mean UV absorbance (cm ⁻¹)	0.196	
Mean Turbidity (NTU)	9.4	

Other Data

Cell length 1 cm

Jar test conditions		
	Time (mins)	Speed (rpm)
Rapid Mixing:	2	230/250
Flocculation:	15	53
Settling:	30	0

Parameter	Jar Numbers					
	1	2	3	4	5	6
<i>Coagulant</i>						
	PACl	PACl	PACl	PACl	PACl	PACl
Concentration (mg/L)	10	20	30	40	60	100
Volume added (uL)	194	388	583	777	1165	1942
<i>Polymer</i>						
Concentration (mg/L)						
Volume added (uL)						
<i>Ballast</i>						
Concentration (mg/L)						
Weight (mg)						
<i>After Rapid Mix</i>						
Temperature (°C)	19	19	19	19	19	19
Relative floc size	A+	A+	A	A	A	A
<i>Settled Water</i>						
Sludge thickness (mm)	11	12	14	15	16	25
Turbidity (1) (NTU)	0.880	0.540	0.485	0.330	0.266	0.165
Turbidity (2) (NTU)	0.845	0.509	0.475	0.350	0.255	0.182
pH	7.77	7.57	7.40	7.23	7.00	6.60
Temperature (°C)	21.1	20.1	20.3	20.3	20.8	21.2
UV absorbance 1	0.078	0.070	0.061	0.056	0.047	0.036
UV absorbance 2						
Mean UV absorbance (cm ⁻¹)	0.078	0.070	0.061	0.056	0.047	0.036
Mean Turbidity (NTU)	0.86	0.52	0.48	0.34	0.26	0.17
Removal of Turbidity efficiency %	90.9	94.4	94.9	96.4	97.2	98.2
Removal of UV efficiency %	60.2	64.3	68.9	71.4	76.0	81.6

Comments:

Looking at the curves produced for the Mean Turbidity & UV absorbance, we fix 30 mg/L PACl as the best dose, and 40 mg/L PACl as the high dose.

Jar Testing Data Log - PACI + LT27A + PAC

Test No. 3

Raw Water Quality		
Parameter	Test 1	Test 2
Temperature (°C)	17.4	
pH	8.33	
TOC (UV absorbance)	0.175	0.179
Turbidity (NTU)	6.15	5.90
Mean UV absorbance (cm ⁻¹)	0.177	
Mean Turbidity (NTU)	6.0	

Other Data

Cell length 1 cm

Comments:

- Could not test jar 6 since the stirrer is broken.
- Jar 4&5 – delay in NTU measurement

Jar test conditions		
	Time (mins)	Speed (rpm)
Rapid Mixing:	3	160/180/200
Flocculation:	15	50
Settling:	30	0

Parameter	Jar Numbers					
	1	2	3	4	5	6
<i>Coagulant</i>						
	PACI	PACI	PACI	PACI-HIGH	PACI-HIGH	
Concentration (mg/L)	30	30	30	40	40	
Volume added (uL)	583	583	583	777	777	
<i>Polymer</i>						
	LT27A	LT22S	LT27A	LT27A	LT27A	
Concentration (mg/L)	0.05	0.1	0.2	0.1	0.1	
Volume added (uL)	100	200	400	200	200	
<i>Ballast</i>						
	PAC	PAC	PAC	PAC	PAC	
Concentration (mg/L)	20	20	20	10	20	
Weight (mg)	40.0	40.1	41.3	20.1	40.0	
<i>After Rapid Mix</i>						
Temperature (°C)						
Relative floc size	A	A	A	A	A	
<i>Settled Water</i>						
Sludge thickness (mm)	18	19	20	21	21	
Turbidity (1) (NTU)	0.940	0.370	0.403	0.293	0.320	
Turbidity (2) (NTU)	0.870	0.330	0.397	0.310	0.330	
pH	7.37	7.36	7.40	7.29	7.23	
Temperature (°C)	20.3	19.9	21.1	20.9	20.9	
UV absorbance 1	0.049	0.048	0.050	0.044	0.040	
UV absorbance 2	0.049	0.047	0.052	0.041	0.039	
Mean UV absorbance (cm ⁻¹)	0.052	0.048	0.051	0.043	0.040	
Mean Turbidity (NTU)	0.91	0.35	0.40	0.30	0.33	
Removal of Turbidity efficiency %	90.4	96.3	95.8	96.8	96.6	

Turbidity @ 5 mins 2.5 0.61 0.54 0.61 0.67

Appendix E

Settling Column Test Results

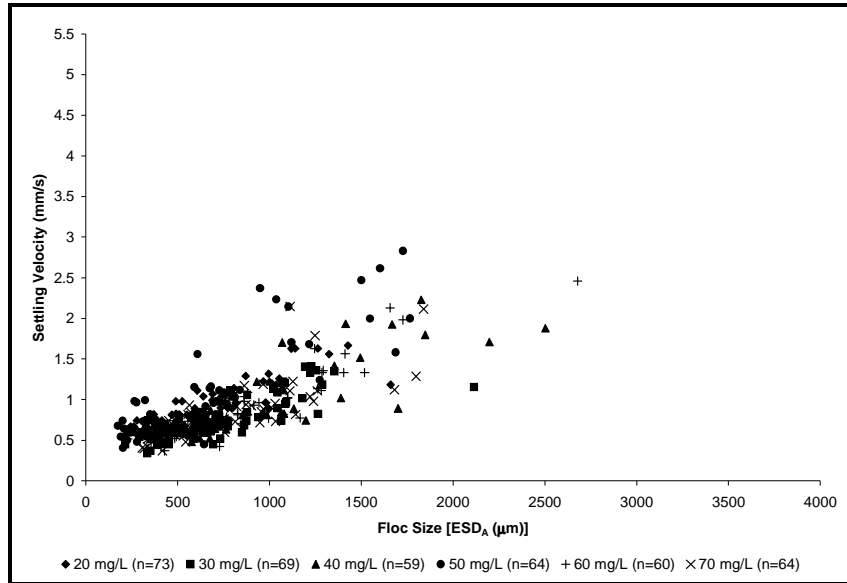


Figure E.1: Settling velocity as a function of floc size for flocs produced by alum coagulation at a temperature of 15 °C.

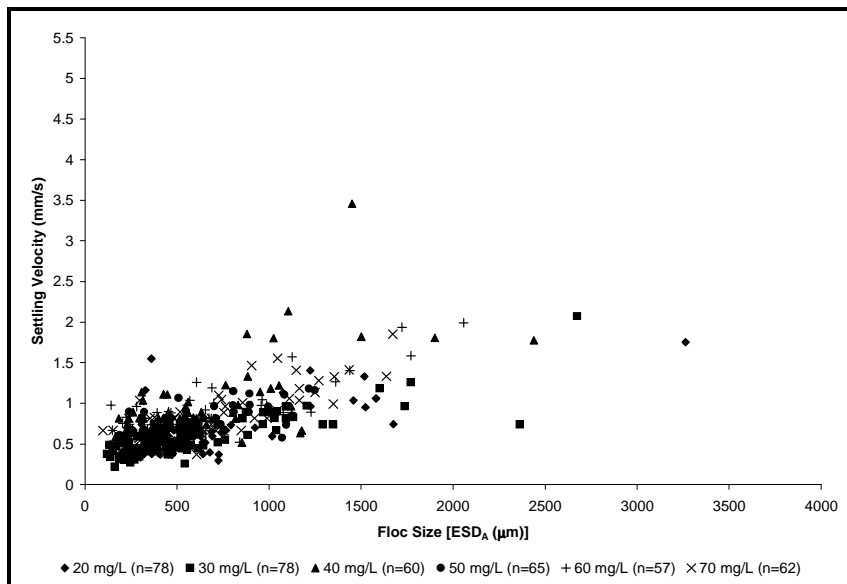


Figure E.2: Settling velocity as a function of floc size for flocs produced by PACl coagulation at a temperature of 15 °C.

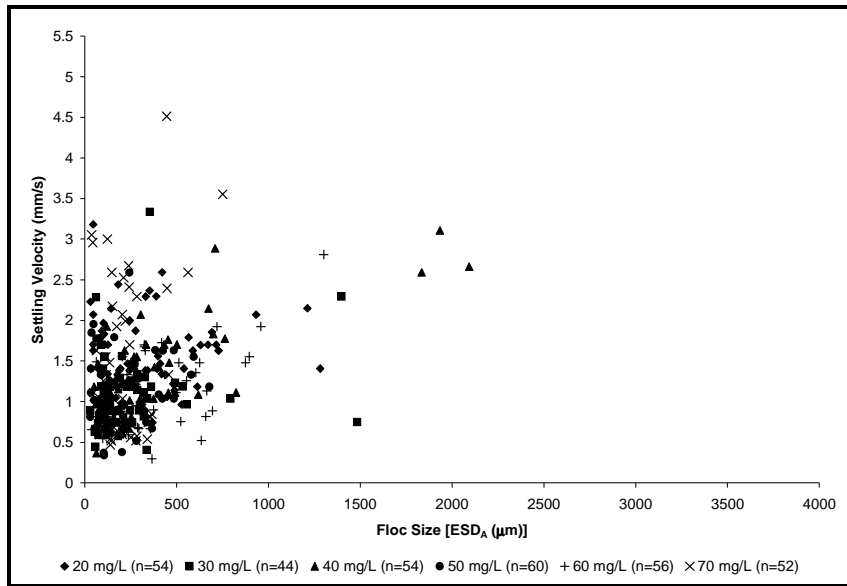


Figure E.3: Settling velocity as a function of floc size for flocs produced by PACI coagulation at a temperature of 25 °C.

Table E.1: Summary of r^2 values of settling velocity vs. floc size for each coagulant dose.

	r^2					
	20 mg/L	30 mg/L	40 mg/L	50 mg/L	60 mg/L	70 mg/L
Coagulant = PACI						
<i>T</i> = 5 °C	0.8502	0.5602	0.5084	0.6301	0.6376	0.8093
<i>T</i> = 15 °C	0.6933	0.6354	0.7323	0.7205	0.8449	0.6195
<i>T</i> = 25 °C	0.0606	0.1044	0.2002	0.1341	0.8103	0.6097
Coagulant = Alum						
<i>T</i> = 5 °C	0.8043	0.4091	0.1341	0.5041	0.3487	0.7102
<i>T</i> = 15 °C	0.4680	0.7216	0.3917	0.4559	0.6444	0.6269
<i>T</i> = 25 °C	0.0012	0.0302	0.5628	0.0169	0.3985	0.0818

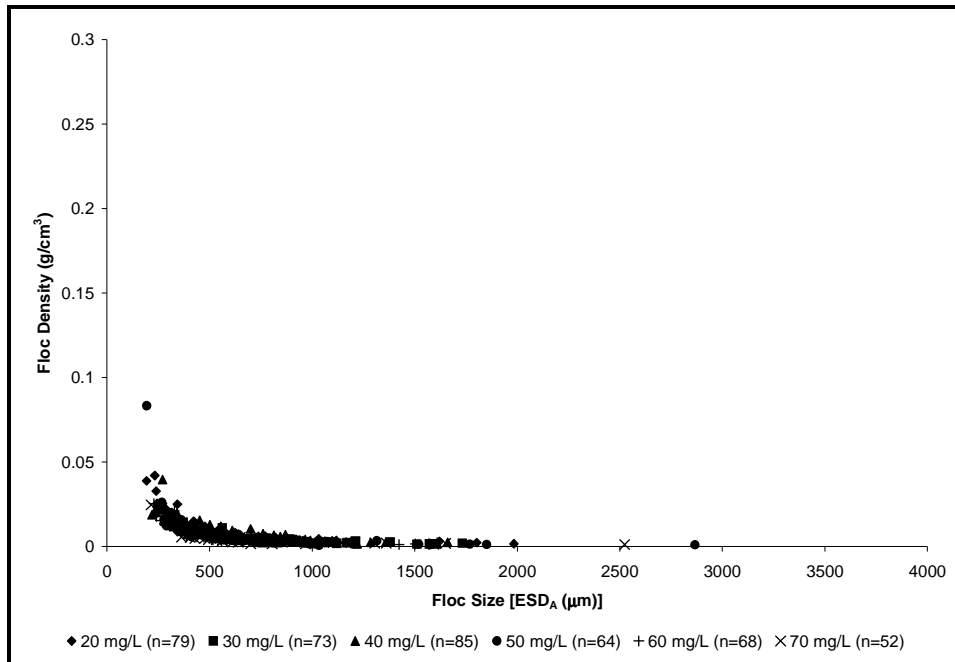


Figure E.4: Particle densities for alum flocs produced and settled at a temperature of 5 °C.

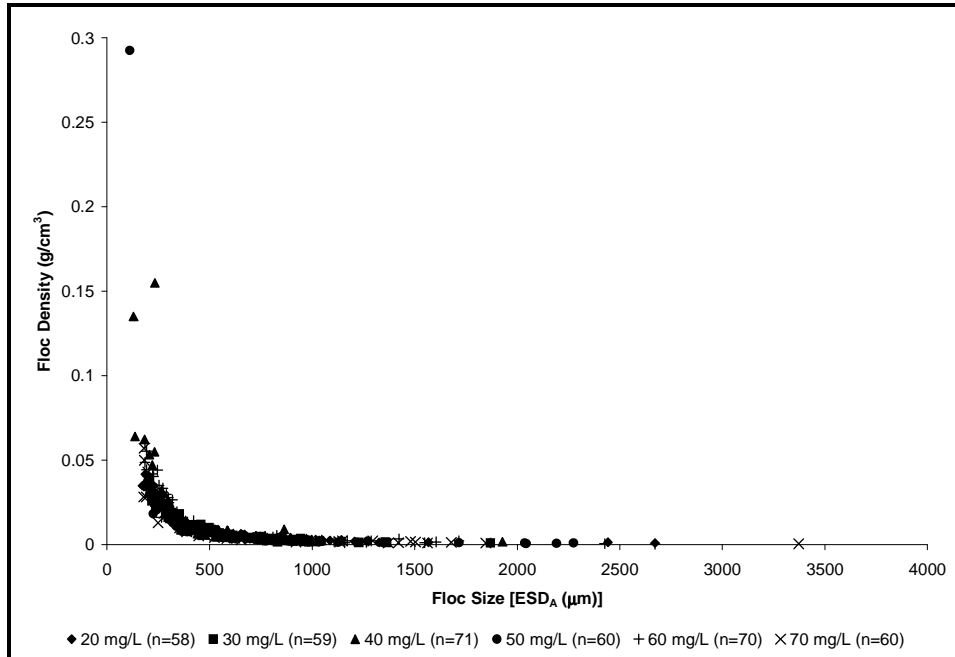


Figure E.5: Particle densities for PACl flocs produced and settled at a temperature of 5 °C.

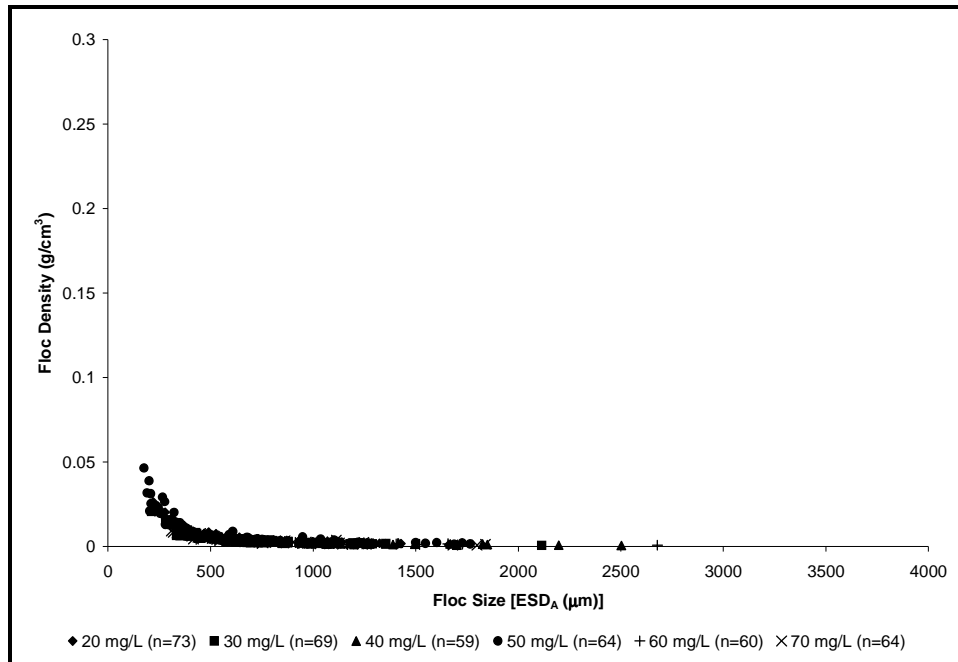


Figure E.6: Particle densities for alum flocs produced and settled at a temperature of 15 °C.

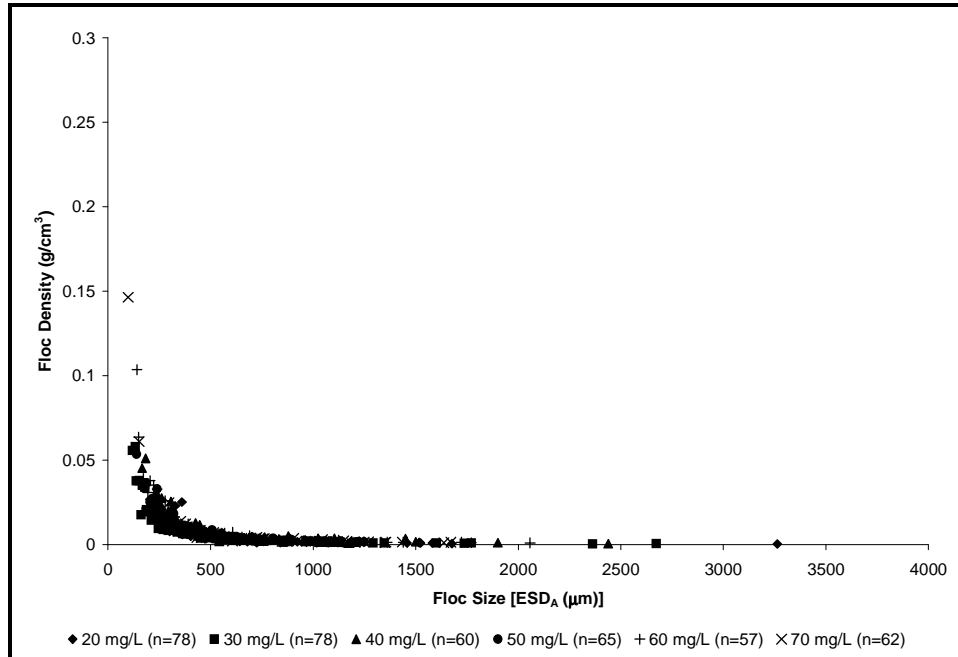


Figure E.7: Particle densities for PACl flocs produced and settled at a temperature of 15 °C.

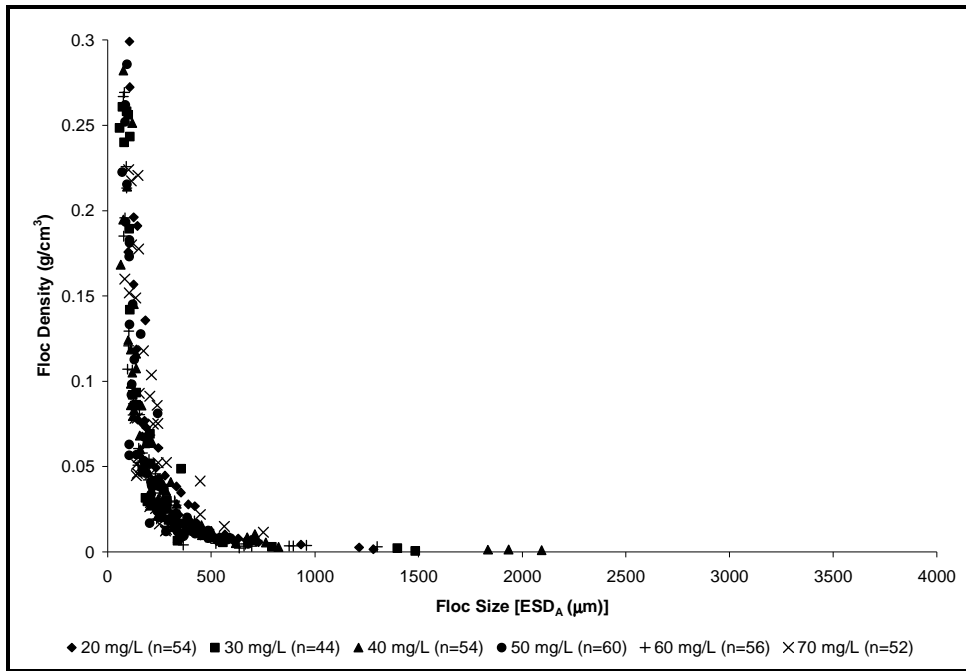


Figure E.8: Particle densities for PACI flocs produced and settled at a temperature of 25 °C.

Appendix F

Particle Size Distribution Data

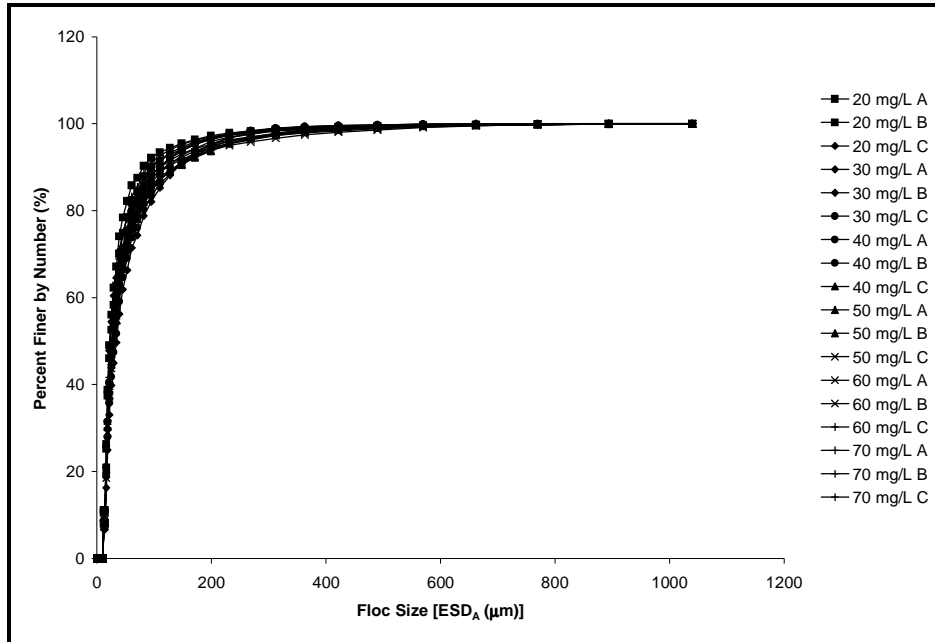


Figure F.1: Particle size distribution of flocs produced by alum coagulation at 5 °C.

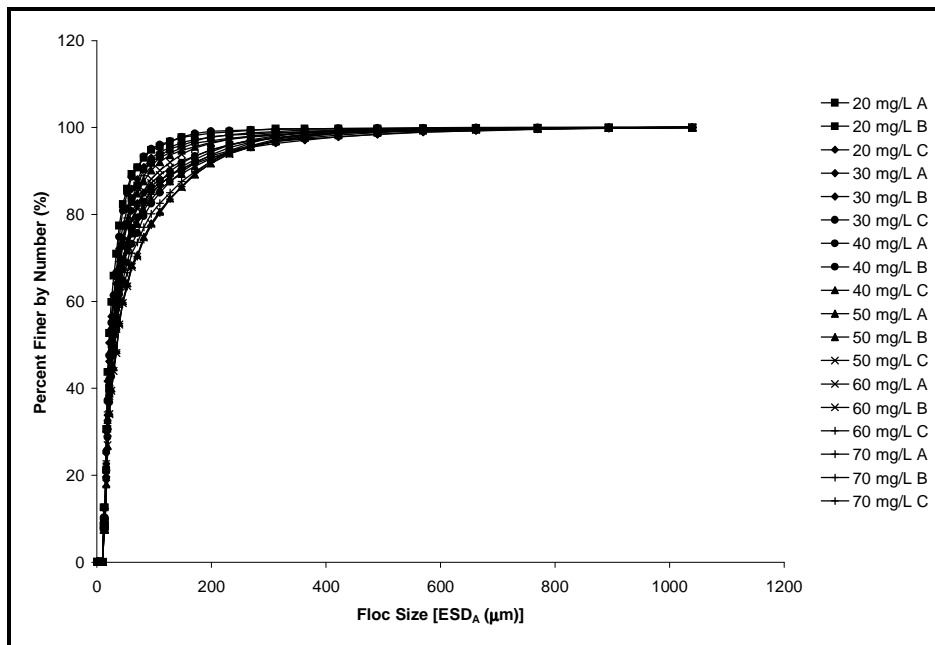


Figure F.2: Particle size distribution of flocs produced by PACl coagulation at 5 °C.

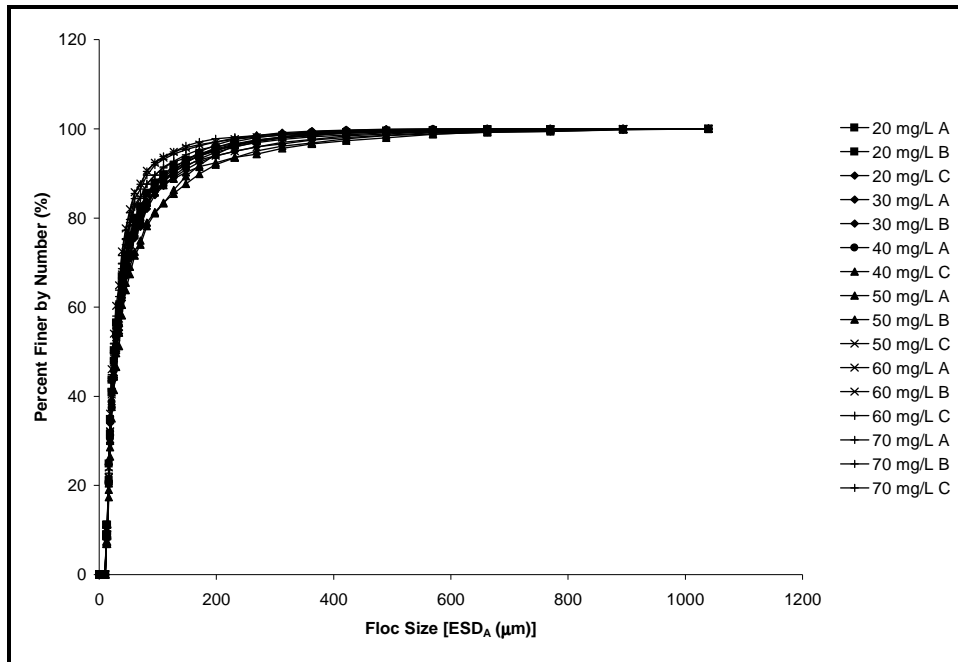


Figure F.3: Particle size distribution of flocs produced by alum coagulation at 15 °C.

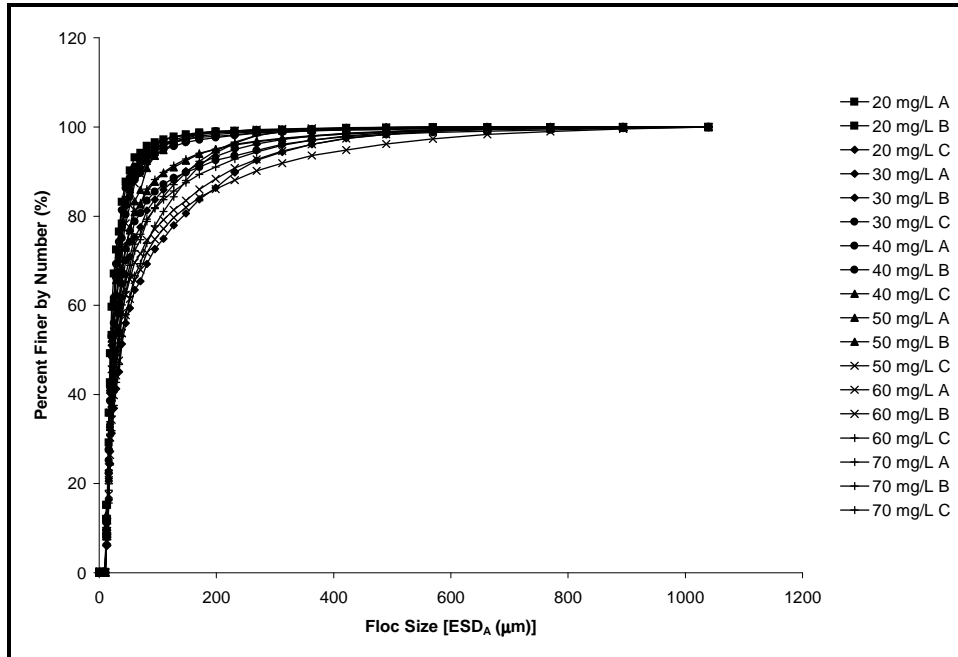


Figure F.4: Particle size distribution of flocs produced by PACl coagulation at 15 °C.

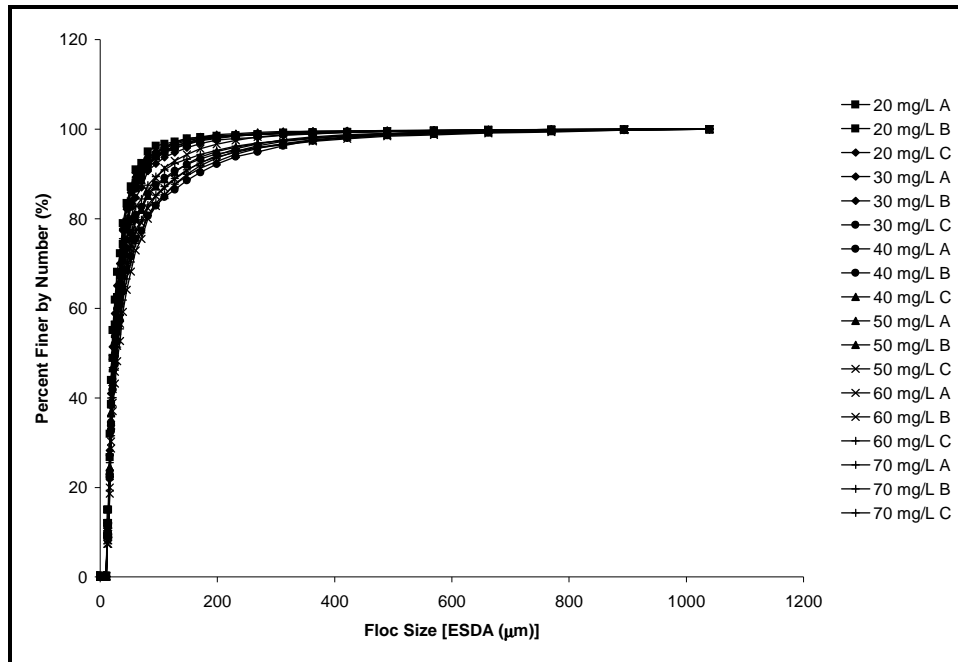


Figure F.5: Particle size distribution of flocs produced by PACl coagulation at 25 °C.

Table F.1: Summary of D_{50} values of flocs produced by alum coagulation.

	Alum Coagulation					
	T = 5 °C		T = 15 °C		T =25 °C	
	D_{50}	n	D_{50}	n	D_{50}	n
20 mg/L A	15.82	5420	18.04	4256	N/A	N/A
20 mg/L B	16.59	3082	17.33	2579	22.65	2124
20 mg/L C	15.82	2099	17.33	2258	17.33	2811
30 mg/L A	22.09	6100	19.37	4041	20.01	10957
30 mg/L B	18.38	27797	19.69	11562	18.04	3008
30 mg/L C	18.72	4885	N/A	N/A	20.93	4921
40 mg/L A	20.63	8061	18.72	5194	20.93	8688
40 mg/L B	18.04	8965	N/A	N/A	20.63	5921
40 mg/L C	19.05	4059	20.63	2817	20.63	2964
50 mg/L A	18.72	7605	19.05	7304	18.38	8558
50 mg/L B	19.05	4768	19.37	4587	19.69	9209
50 mg/L C	18.38	3120	15.82	6167	22.92	5102
60 mg/L A	19.37	7341	18.04	6106	20.63	4641
60 mg/L B	19.37	5235	18.04	5286	19.05	6583
60 mg/L C	19.69	3958	17.33	7013	19.69	4080
70 mg/L A	18.38	7351	17.69	5607	18.04	12425
70 mg/L B	18.72	7580	16.96	6270	18.38	11987
70 mg/L C	17.69	8508	16.96	5753	18.04	9033

Table F.2: Summary of D_{50} values of flocs produced by PACl coagulation.

	PACl Coagulation					
	T = 5 °C		T = 15 °C		T =25 °C	
	D_{50}	n	D_{50}	n	D_{50}	n
20 mg/L A	18.04	1656	14.58	1454	14.58	2577
20 mg/L B	14.15	1656	13.24	3548	15.01	5263
20 mg/L C	16.21	2301	15.01	1687	15.01	3298
30 mg/L A	17.69	2655	19.69	10093	16.96	3311
30 mg/L B	14.58	4868	23.99	4733	14.15	6602
30 mg/L C	16.21	1676	17.69	4206	16.96	4299
40 mg/L A	20.01	7360	15.42	6623	16.96	3980
40 mg/L B	19.05	13459	14.58	2260	17.69	3603
40 mg/L C	17.33	7075	18.38	2190	16.21	3162
50 mg/L A	18.38	8438	14.58	3334	16.21	4013
50 mg/L B	21.81	8301	16.96	5530	16.96	4098
50 mg/L C	19.05	8339	22.65	5718	17.33	4785
60 mg/L A	22.65	8048	16.21	5006	19.05	8006
60 mg/L B	19.37	5745	19.69	7208	19.69	6017
60 mg/L C	21.81	13748	17.33	8959	15.01	3951
70 mg/L A	18.04	4772	20.01	14208	16.96	8534
70 mg/L B	19.69	9456	21.81	11373	15.82	11240
70 mg/L C	16.96	7223	20.63	6155	18.38	18185

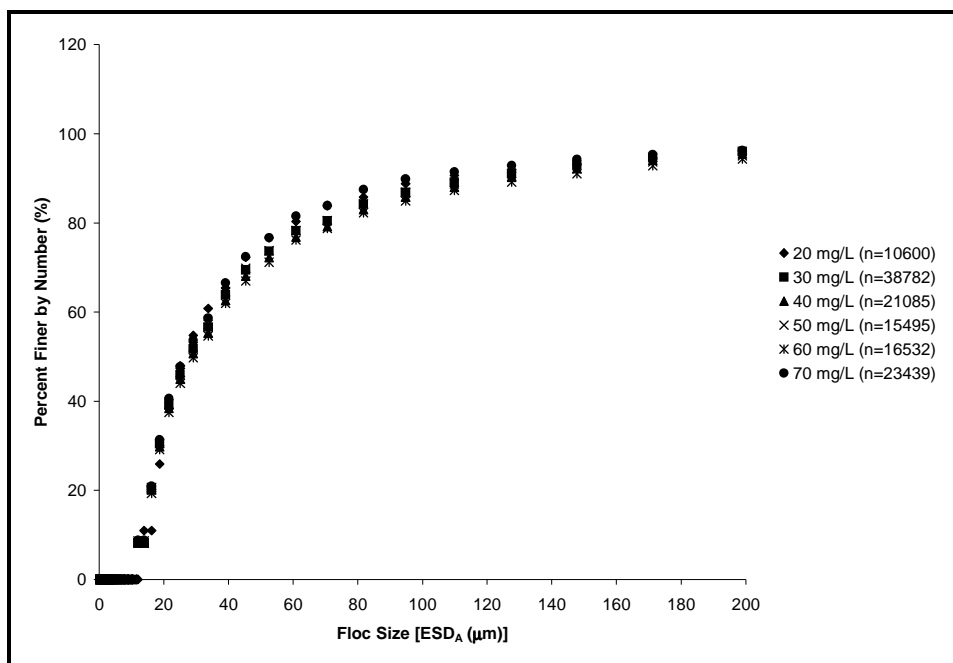


Figure F.6: Re-calculated particle size distribution of flocs produced by alum coagulation at 5 °C.

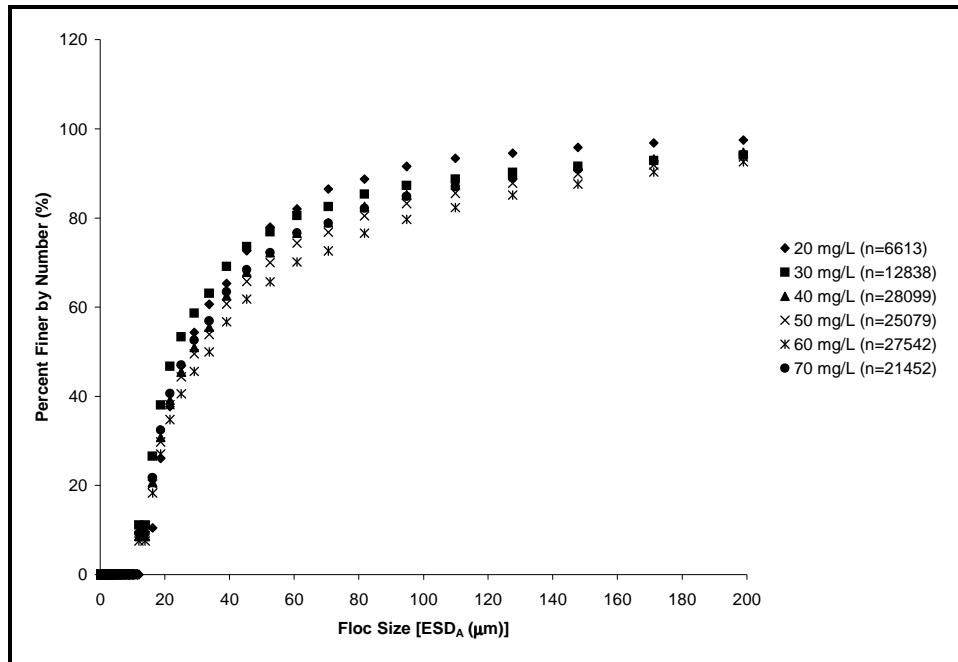


Figure F.7: Re-calculated particle size distribution of flocs produced by PACl coagulation at 5 °C.

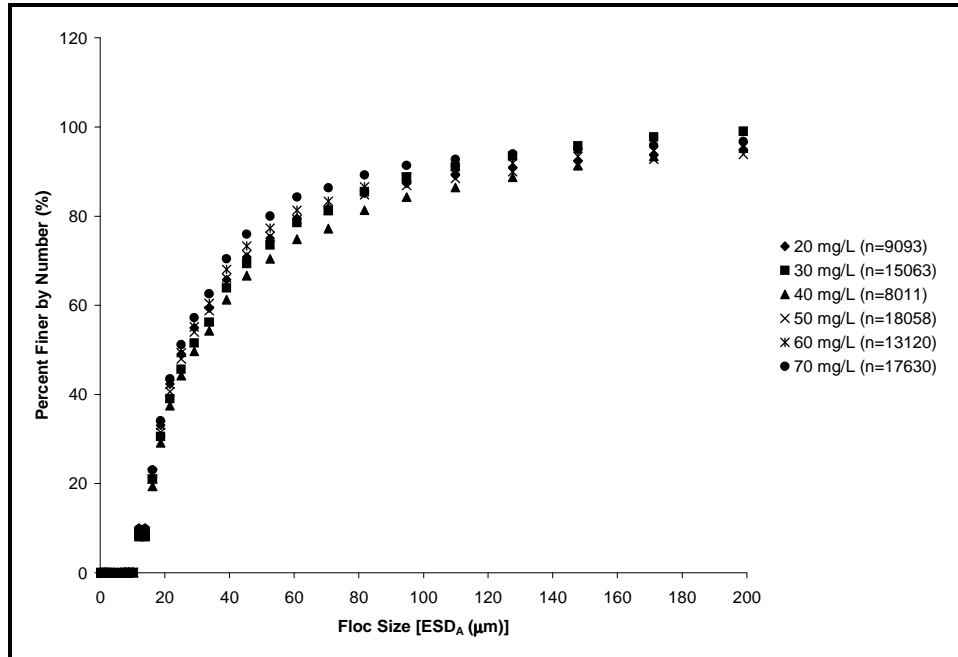


Figure F.8: Re-calculated particle size distribution of flocs produced by alum coagulation at 15 °C.

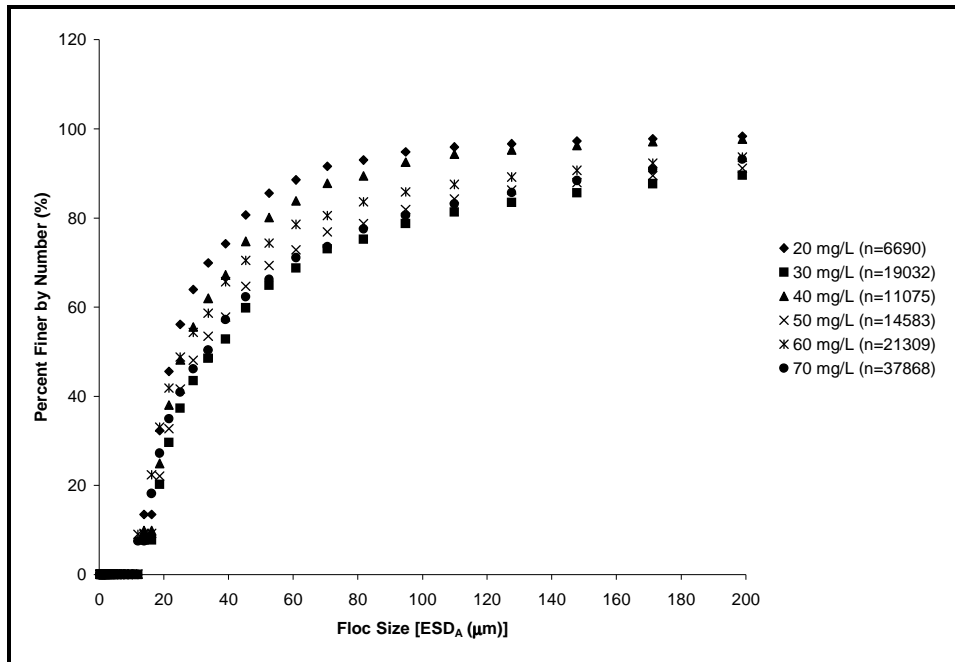


Figure F.9: Re-calculated particle size distribution of flocs produced by PACI coagulation at 15 °C.

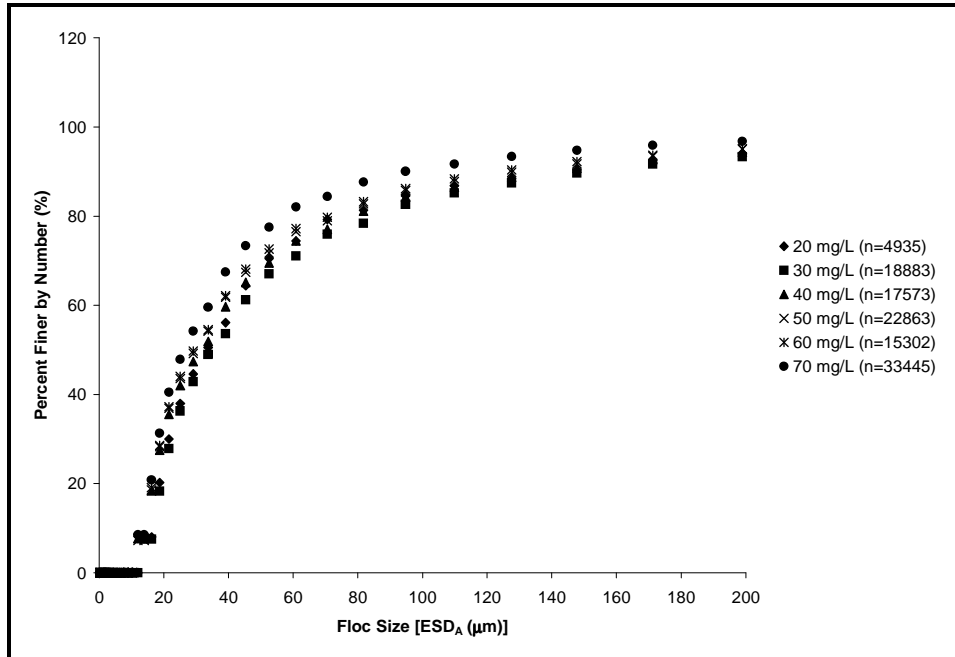


Figure F.10: Re-calculated particle size distribution of flocs produced by alum coagulation at 25 °C.

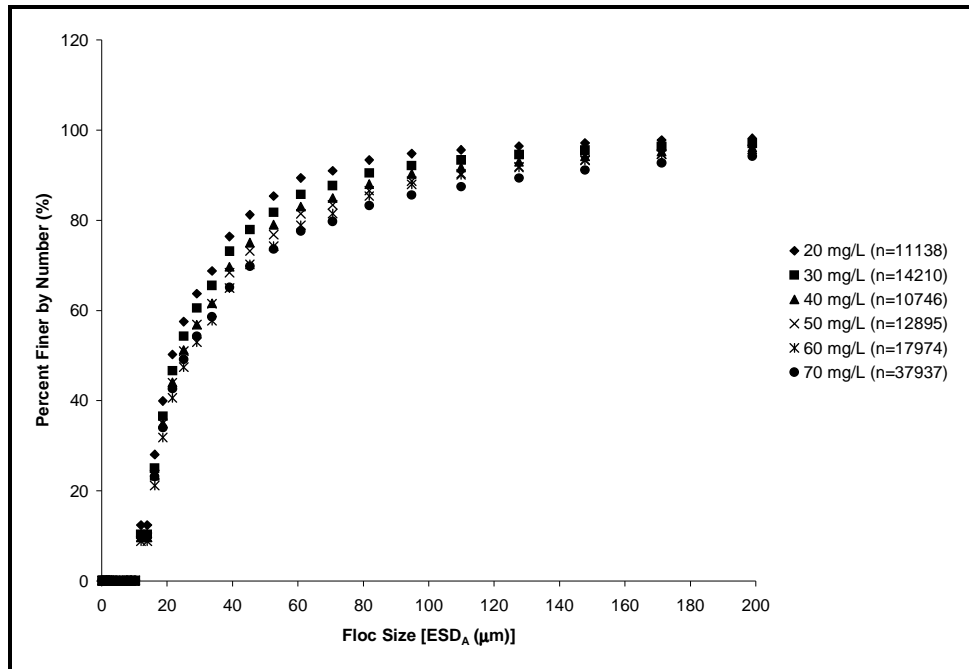


Figure F.11: Re-calculated particle size distribution of flocs produced by PACl coagulation at 25 °C.

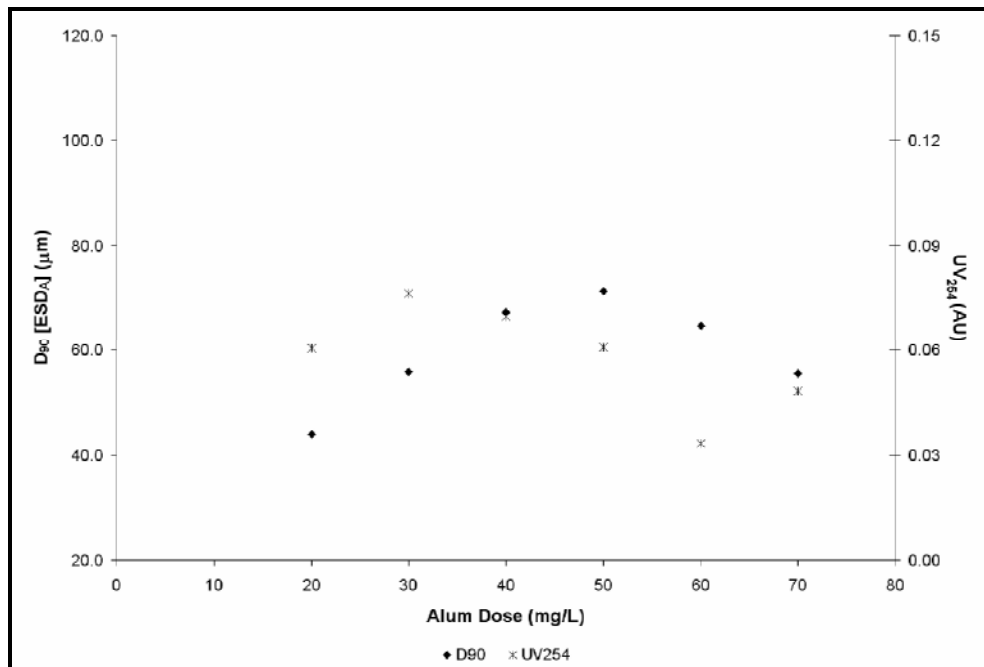


Figure F.12: Comparing aggregate D_{90} to residual UV_{254} for alum coagulation at 5 °C.

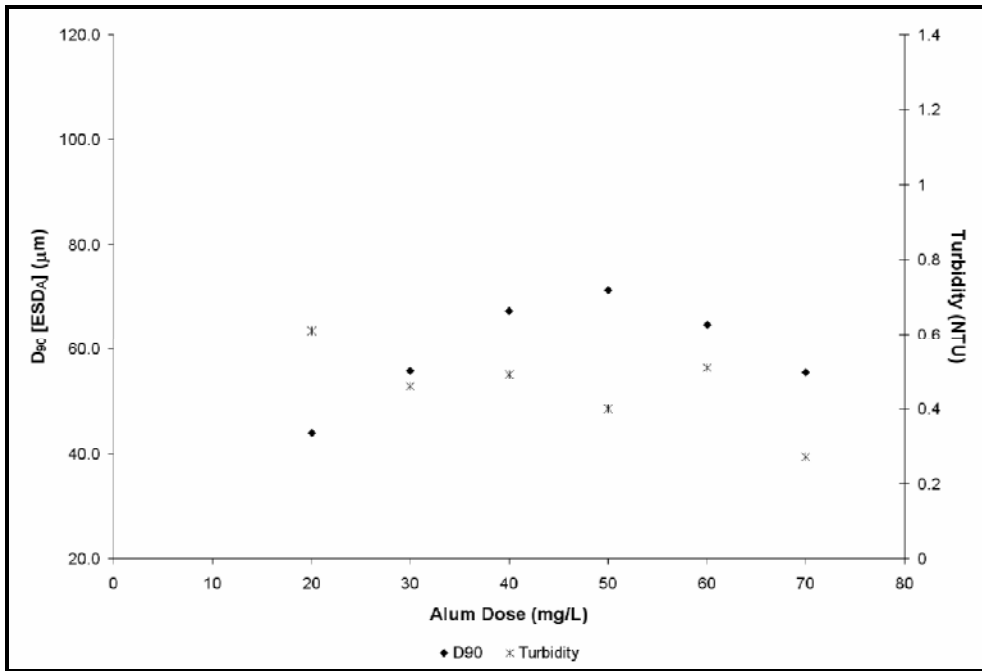


Figure F.13: Comparing aggregate D_{90} to residual turbidity for alum coagulation at 5 °C.

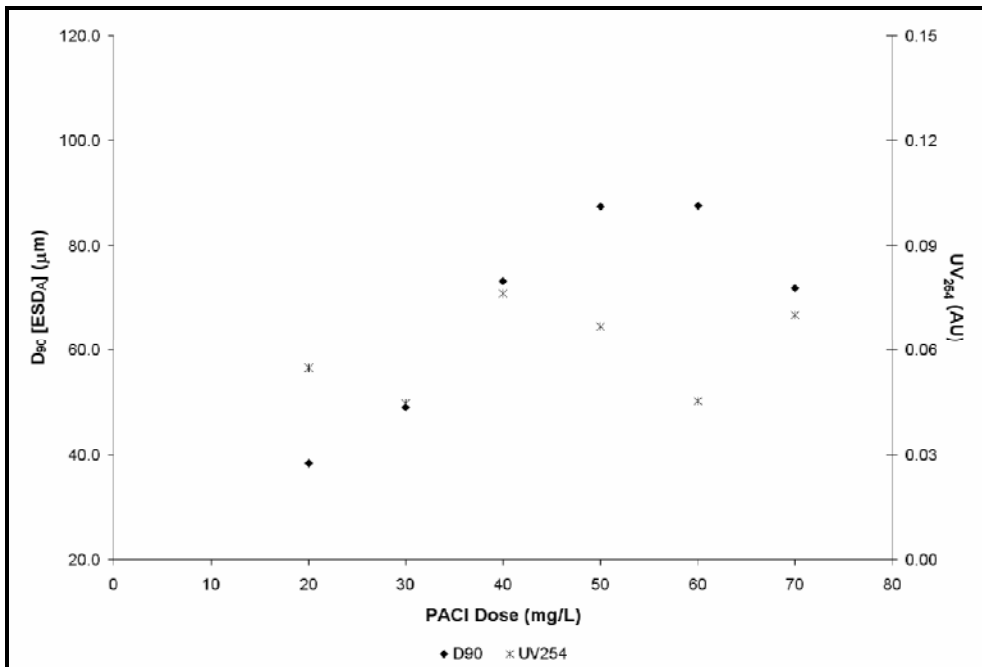


Figure F.14: Comparing aggregate D_{90} to residual UV₂₅₄ for PACI coagulation at 5 °C.

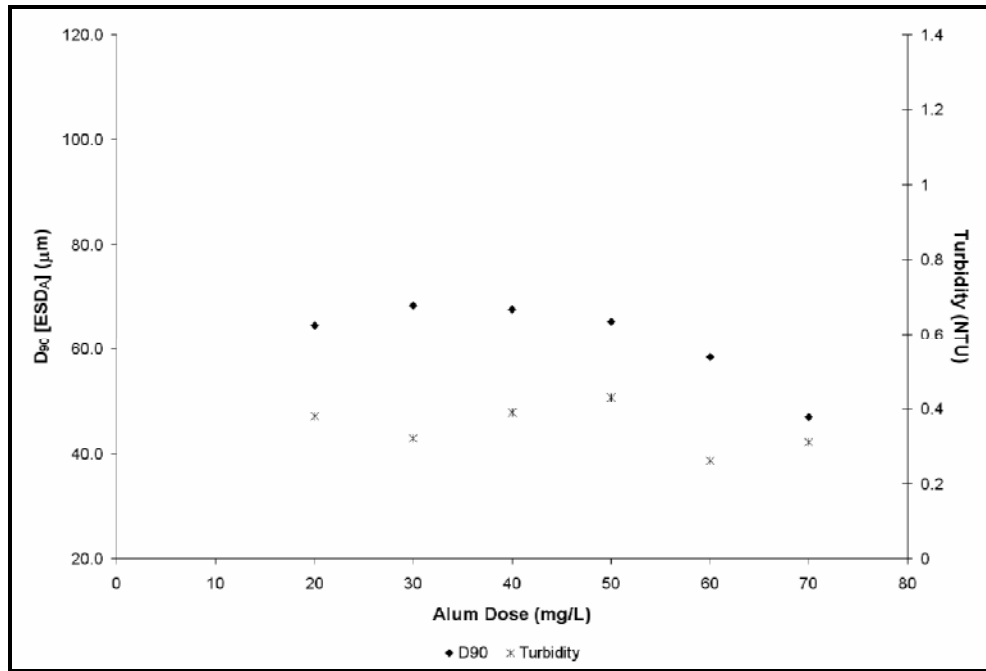


Figure F.15: Comparing aggregate D_{90} to residual turbidity for alum coagulation at 15 °C.

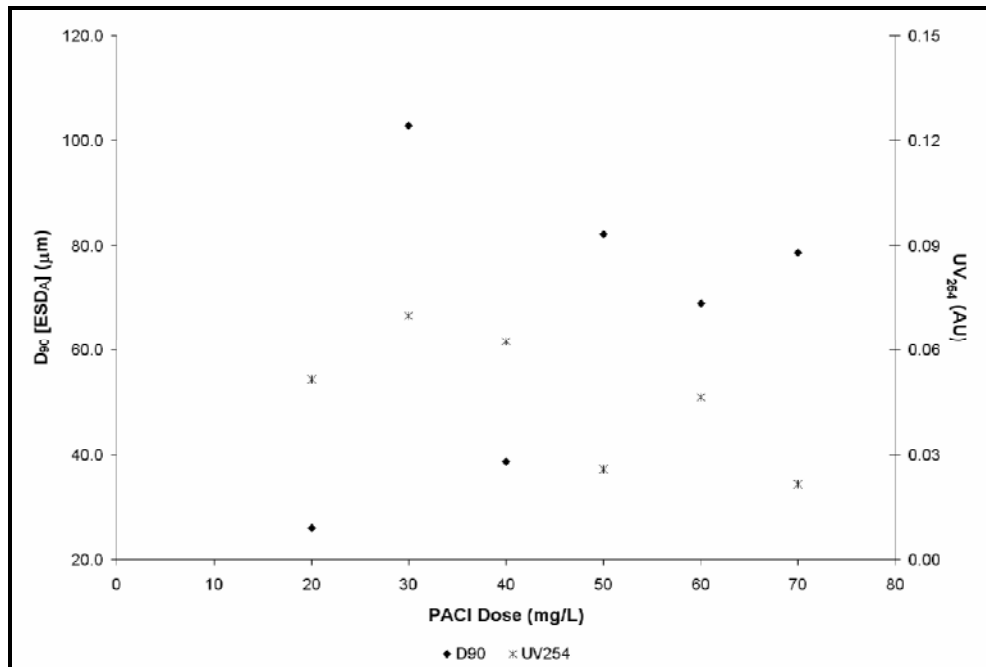


Figure F.16: Comparing aggregate D_{90} to residual UV₂₅₄ for PACI coagulation at 15 °C.

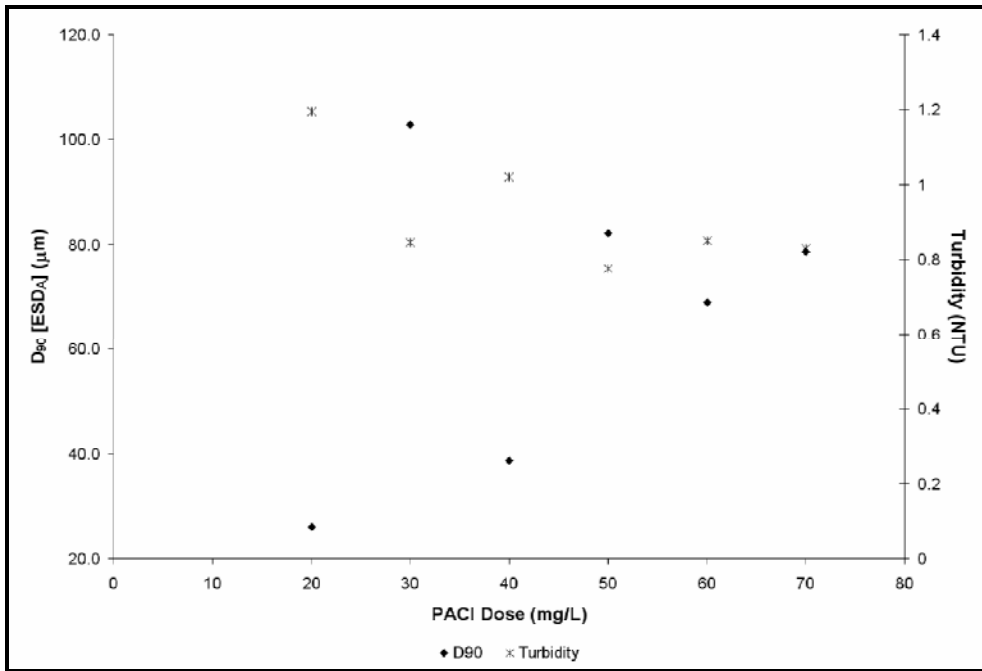


Figure F.17: Comparing aggregate D_{90} to residual turbidity for PACI coagulation at 15 °C.

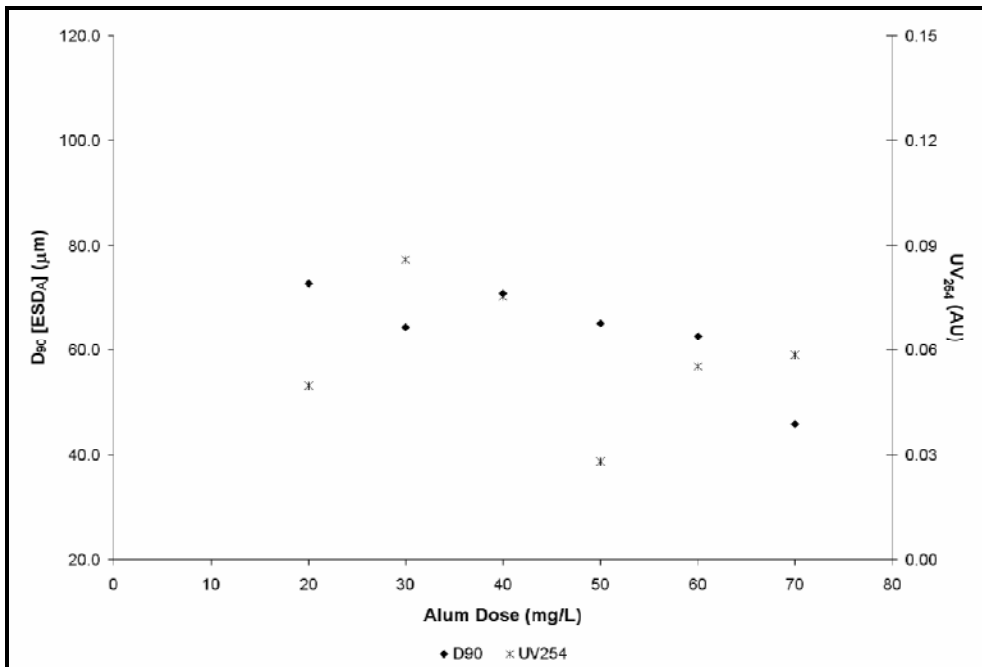


Figure F.18: Comparing aggregate D_{90} to residual UV₂₅₄ for alum coagulation at 25 °C.

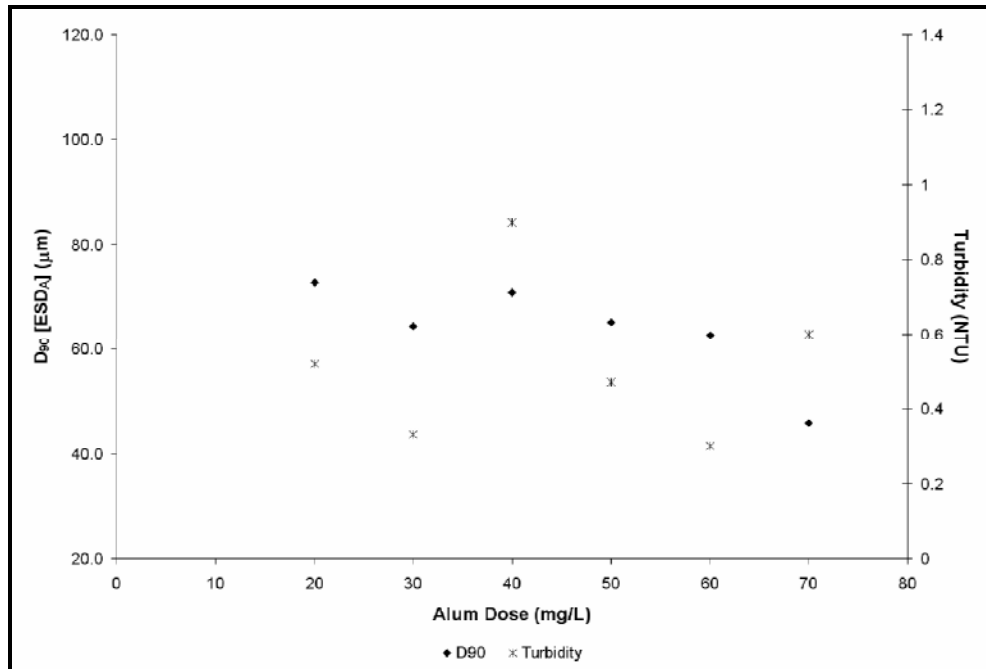


Figure F.19: Comparing aggregate D_{90} to residual turbidity for alum coagulation at 25 °C.

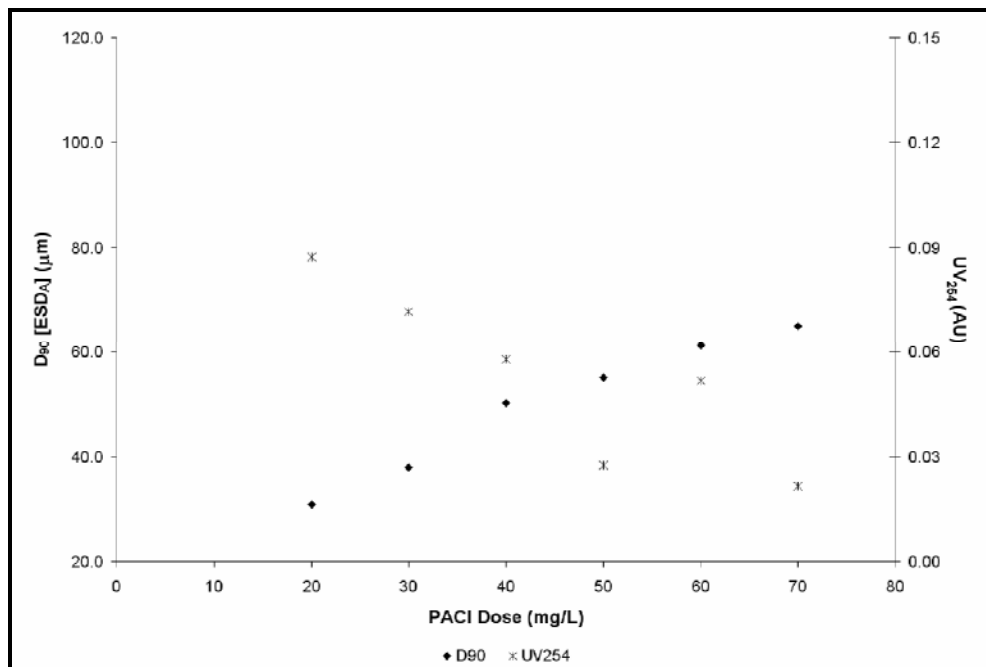


Figure F.20: Comparing aggregate D_{90} to residual UV₂₅₄ for PACl coagulation at 25 °C.

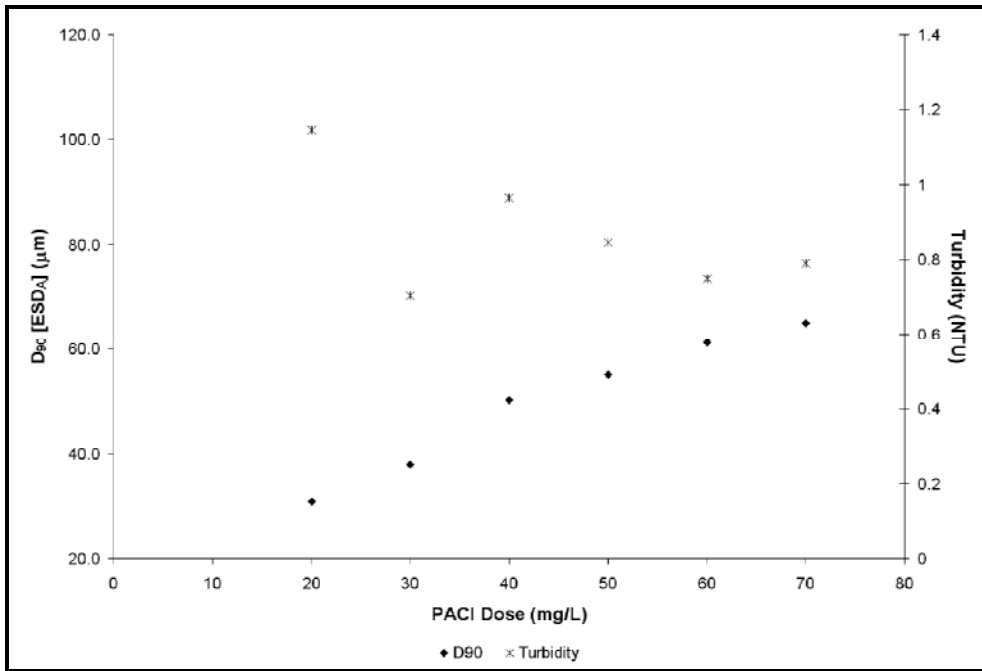


Figure F.21: Comparing aggregate D_{90} to residual turbidity for PACI coagulation at 25 °C.

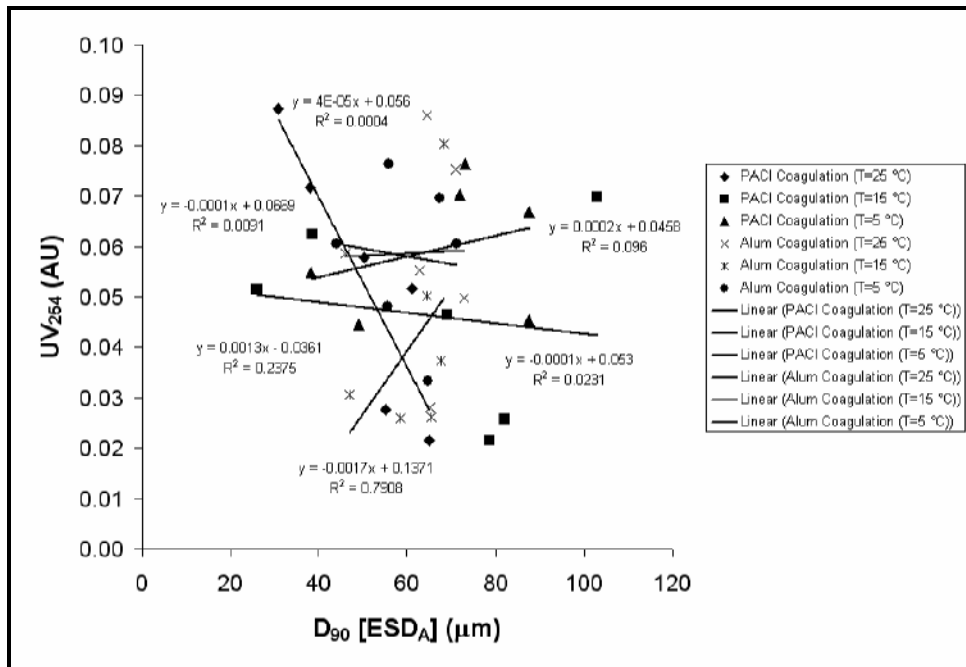


Figure F.22: Linear regression of UV₂₅₄ and D_{90} values.

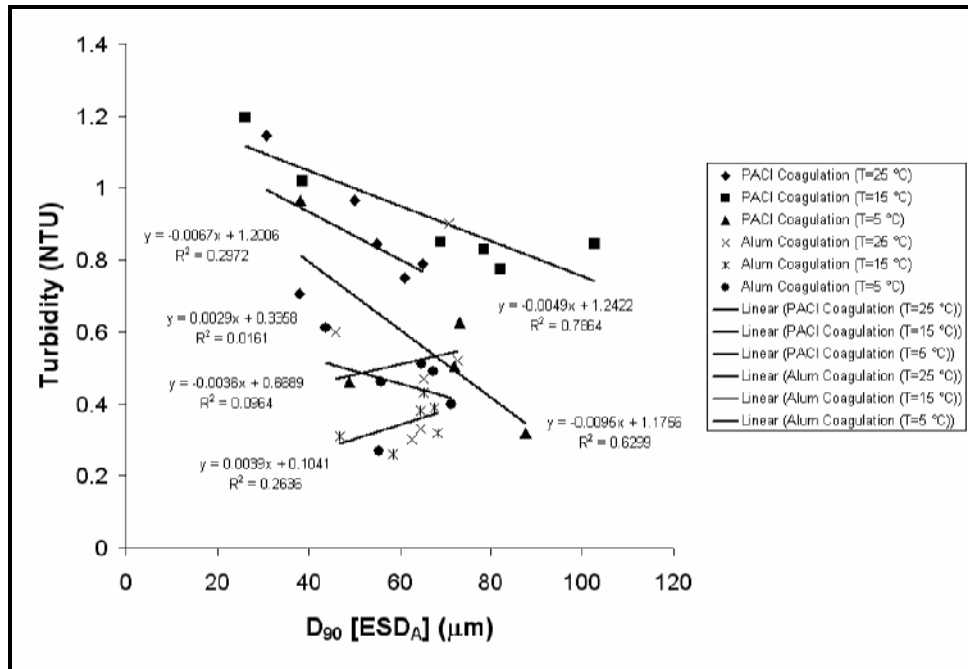


Figure F.23: Linear regression of turbidity and D_{90} values.

Appendix G

Fractal Regression Confidence Intervals

Table G.1: 95% confidence intervals on both the slope and the intercept of each alum regression of aggregates generated by alum coagulation.

Alum Coagulation								
	D1 Intercept		D1 Slope		D2 Intercept		D2 Slope	
	Lower 95%	Upper 95%	Lower 95%	Upper 95%	Lower 95%	Upper 95%	Lower 95%	Upper 95%
J4-1A	N/A	N/A	N/A	N/A	N/A	N/A	N/A	N/A
J4-1B	0.28152	0.30653	1.11883	1.13470	-0.14276	-0.09057	1.80900	1.84212
J4-1C	0.31385	0.33383	1.10033	1.11346	-0.17669	-0.13778	1.82354	1.84912
J4-2A	0.32427	0.33489	1.09677	1.10361	-0.17117	-0.15066	1.83389	1.84710
J4-2B	0.35769	0.37668	1.06591	1.07831	-0.18131	-0.13921	1.82447	1.85194
J4-2C	0.32140	0.33627	1.09895	1.10818	-0.20601	-0.17737	1.85643	1.87423
J4-3A	0.34379	0.35492	1.08394	1.09097	-0.16782	-0.14615	1.84022	1.85391
J4-3B	0.32681	0.34092	1.09321	1.10218	-0.18446	-0.15722	1.84141	1.85873
J4-3C	0.34165	0.36084	1.07971	1.09182	-0.21397	-0.17647	1.85344	1.87710
J4-4A	0.35173	0.36331	1.07650	1.08415	-0.15580	-0.13237	1.82341	1.83890
J4-4B	0.31856	0.33007	1.10266	1.11005	-0.17715	-0.15572	1.84396	1.85773
J4-4C	0.29731	0.31356	1.11031	1.12016	-0.26420	-0.23505	1.89187	1.90956
J4-5A	0.32168	0.33787	1.09605	1.10635	-0.17111	-0.14142	1.83547	1.85436
J4-5B	0.32711	0.34066	1.09349	1.10233	-0.14977	-0.12383	1.82081	1.83776
J4-5C	0.32378	0.34103	1.09342	1.10426	-0.20114	-0.16992	1.85289	1.87252
J4-6A	0.32747	0.33810	1.09568	1.10277	-0.13211	-0.11297	1.80975	1.82250
J4-6B	0.29246	0.30333	1.12097	1.12812	-0.12686	-0.10764	1.80265	1.81528
J4-6C	0.33487	0.34698	1.08963	1.09775	-0.10820	-0.08608	1.79407	1.80890
J5-1A	0.32495	0.34079	1.09478	1.10572	-0.14324	-0.11365	1.80200	1.82242
J5-1B	0.31845	0.33845	1.09853	1.11198	-0.14717	-0.10991	1.80683	1.83189
J5-1C	0.31973	0.34280	1.09586	1.11126	-0.20332	-0.16025	1.84333	1.87208
J5-2A	0.33489	0.34868	1.08691	1.09554	-0.21827	-0.19030	1.86430	1.88179
J5-2B	0.36453	0.37094	1.07092	1.07514	-0.16401	-0.15103	1.83639	1.84495
J5-2C	0.30104	0.31708	1.11197	1.12229	-0.22064	-0.19091	1.85628	1.87542
J5-3A	0.32653	0.33868	1.09530	1.10300	-0.20067	-0.17783	1.85690	1.87136
J5-3B	0.34449	0.35609	1.08334	1.09101	-0.18625	-0.16307	1.84133	1.85665
J5-3C	0.32096	0.33773	1.09731	1.10804	-0.20569	-0.17350	1.85030	1.87088
J5-4A	0.29535	0.30844	1.11909	1.12758	-0.16212	-0.13932	1.82684	1.84165
J5-4B	0.32012	0.33570	1.09867	1.10875	-0.19720	-0.16674	1.84398	1.86370
J5-4C	0.31214	0.33153	1.09873	1.11123	-0.19676	-0.15999	1.83892	1.86261
J5-5A	0.33467	0.34690	1.08895	1.09677	-0.20147	-0.17745	1.85702	1.87239
J5-5B	0.27872	0.29483	1.12582	1.13601	-0.15891	-0.13267	1.82698	1.84357
J5-5C	0.33091	0.34746	1.09193	1.10247	-0.18519	-0.15249	1.83738	1.85821
J5-6A	0.30968	0.32333	1.10602	1.11492	-0.12670	-0.10201	1.79543	1.81152
J5-6B	0.29783	0.31184	1.11503	1.12427	-0.11713	-0.09224	1.78917	1.80557
J5-6C	0.30172	0.31461	1.11413	1.12275	-0.11233	-0.08987	1.78951	1.80453
J6-1A	0.30351	0.32031	1.10990	1.12090	-0.15066	-0.11954	1.80987	1.83024
J6-1B	0.30937	0.33017	1.10713	1.12085	-0.14550	-0.10740	1.80915	1.83429
J6-1C	0.29986	0.32337	1.10791	1.12310	-0.19948	-0.15674	1.83571	1.86333
J6-2A	0.33255	0.34897	1.09004	1.10056	-0.19172	-0.16053	1.84630	1.86628
J6-2B	0.34635	0.35620	1.08238	1.08874	-0.19529	-0.17542	1.85309	1.86593
J6-2C	N/A	N/A	N/A	N/A	N/A	N/A	N/A	N/A
J6-3A	0.33593	0.35040	1.09058	1.09995	-0.18134	-0.15187	1.83636	1.85546
J6-3B	N/A	N/A	N/A	N/A	N/A	N/A	N/A	N/A
J6-3C	0.32584	0.34564	1.08991	1.10229	-0.25519	-0.21585	1.88135	1.90595
J6-4A	0.28222	0.29601	1.12278	1.13152	-0.19520	-0.17186	1.84242	1.85722
J6-4B	0.29942	0.31692	1.11311	1.12400	-0.22460	-0.19380	1.85952	1.87868
J6-4C	0.26994	0.28514	1.13938	1.14975	-0.16386	-0.13353	1.80520	1.82588
J6-5A	0.34527	0.35923	1.08029	1.08946	-0.17406	-0.14733	1.83658	1.85414
J6-5B	0.32255	0.33798	1.09657	1.10657	-0.17440	-0.14623	1.82772	1.84597
J6-5C	0.31341	0.32711	1.10520	1.11434	-0.12697	-0.10149	1.79662	1.81362
J6-6A	0.32800	0.34413	1.09036	1.10123	-0.11112	-0.08121	1.78654	1.80671
J6-6B	0.32525	0.34017	1.09727	1.10749	-0.09664	-0.06980	1.77747	1.79586
J6-6C	0.33493	0.34958	1.08777	1.09756	-0.13829	-0.11047	1.80158	1.82017

Table G.2: 95% confidence intervals on both the slope and the intercept of each regression of aggregates generated by PACI coagulation.

	PACI Coagulation							
	D ₁ Intercept		D ₁ Slope		D ₂ Intercept		D ₂ Slope	
	Lower 95%	Upper 95%	Lower 95%	Upper 95%	Lower 95%	Upper 95%	Lower 95%	Upper 95%
J1-1A	0.27567	0.30011	1.13113	1.14851	-0.11845	-0.07751	1.78729	1.81640
J1-1B	0.23173	0.25085	1.16653	1.17980	-0.08322	-0.05069	1.72944	1.75202
J1-1C	0.25258	0.27792	1.14294	1.16069	-0.13883	-0.09636	1.76140	1.79117
J1-2A	0.21346	0.23925	1.16339	1.18060	-0.14841	-0.11179	1.79184	1.81627
J1-2B	0.23076	0.24848	1.16871	1.18126	-0.08255	-0.05354	1.72127	1.74181
J1-2C	0.22745	0.24763	1.16655	1.17953	-0.24880	-0.21540	1.86778	1.88927
J1-3A	0.26295	0.28404	1.13553	1.14993	-0.13011	-0.09627	1.79186	1.81496
J1-3B	0.23502	0.25646	1.15790	1.17140	-0.24742	-0.21382	1.86233	1.88348
J1-3C	0.20894	0.23472	1.17200	1.18955	-0.17397	-0.13632	1.82133	1.84695
J1-4A	0.22613	0.24866	1.16114	1.17661	-0.17470	-0.13984	1.81860	1.84254
J1-4B	0.24172	0.26175	1.15364	1.16663	-0.21428	-0.18202	1.84444	1.86536
J1-4C	0.24092	0.26008	1.15293	1.16512	-0.20508	-0.17703	1.84406	1.86191
J1-5A	0.24987	0.26490	1.14648	1.15628	-0.13493	-0.11242	1.80400	1.81867
J1-5B	0.22874	0.24524	1.16218	1.17242	-0.21145	-0.18538	1.84074	1.85692
J1-5C	0.24732	0.26955	1.14900	1.16447	-0.13232	-0.09834	1.77854	1.80218
J1-6A	0.22762	0.24227	1.16650	1.17592	-0.21353	-0.19141	1.84431	1.85853
J1-6B	0.24530	0.25844	1.15340	1.16209	-0.16694	-0.14832	1.81945	1.83176
J1-6C	0.25502	0.26425	1.15039	1.15624	-0.20415	-0.18912	1.84782	1.85735
J2-1A	0.20059	0.23351	1.17382	1.19637	-0.21919	-0.16383	1.82369	1.86162
J2-1B	0.29343	0.31532	1.11340	1.12926	-0.12363	-0.08436	1.76572	1.79416
J2-1C	0.20697	0.24036	1.16649	1.18935	-0.20205	-0.14950	1.81595	1.85192
J2-2A	0.28275	0.29511	1.12614	1.13397	-0.16834	-0.14840	1.83399	1.84661
J2-2B	0.26636	0.28406	1.12966	1.13999	-0.29732	-0.26860	1.90625	1.92301
J2-2C	0.23124	0.25259	1.15167	1.16514	-0.27981	-0.24562	1.88508	1.90665
J2-3A	0.24283	0.26015	1.14863	1.16053	-0.16099	-0.13317	1.80577	1.82488
J2-3B	0.17154	0.20177	1.19505	1.21620	-0.23566	-0.19102	1.85188	1.88311
J2-3C	0.22823	0.25545	1.15335	1.17115	-0.25832	-0.20774	1.88873	1.92179
J2-4A	0.21563	0.24202	1.16896	1.18742	-0.14590	-0.10844	1.78918	1.81539
J2-4B	0.22166	0.23974	1.16529	1.17700	-0.20061	-0.17468	1.83592	1.85271
J2-4C	0.26273	0.27834	1.13444	1.14355	-0.25967	-0.23533	1.88696	1.90117
J2-5A	0.23312	0.25448	1.15203	1.16665	-0.16799	-0.13566	1.81547	1.83760
J2-5B	0.25873	0.27373	1.14032	1.14940	-0.25978	-0.23552	1.88158	1.89625
J2-5C	0.25401	0.26804	1.14572	1.15486	-0.18119	-0.16041	1.83835	1.85190
J2-6A	0.29544	0.30523	1.11983	1.12593	-0.16407	-0.14830	1.83766	1.84748
J2-6B	0.26478	0.27714	1.13900	1.14656	-0.31669	-0.29301	1.90635	1.92082
J2-6C	0.23355	0.24996	1.16228	1.17246	-0.25704	-0.22687	1.86489	1.88359
J3-1A	0.29626	0.32797	1.10129	1.12247	-0.12634	-0.06795	1.77304	1.81203
J3-1B	0.35535	0.38082	1.06410	1.08224	-0.12634	-0.06795	1.77017	1.80759
J3-1C	0.35535	0.38082	1.06410	1.08224	-0.13068	-0.07815	1.77017	1.80759
J3-2A	0.27704	0.30317	1.12054	1.13838	-0.14440	-0.10002	1.78549	1.81580
J3-2B	0.27251	0.29039	1.12732	1.13876	-0.18261	-0.15219	1.82279	1.84225
J3-2C	0.30609	0.33726	1.09460	1.11544	-0.12052	-0.06181	1.76862	1.80788
J3-3A	0.23587	0.25095	1.15651	1.16611	-0.15763	-0.13437	1.82164	1.83646
J3-3B	0.27171	0.28208	1.13850	1.14505	-0.19153	-0.17409	1.84208	1.85310
J3-3C	0.24398	0.26043	1.15112	1.16202	-0.15246	-0.12801	1.81571	1.83192
J3-4A	0.27707	0.29079	1.12964	1.13833	-0.16773	-0.14647	1.83609	1.84957
J3-4B	0.27224	0.28534	1.13212	1.14012	-0.22264	-0.20022	1.86638	1.88006
J3-4C	0.27153	0.28558	1.13217	1.14130	-0.13193	-0.10968	1.80466	1.81912
J3-5A	0.31462	0.32777	1.10270	1.11071	-0.22105	-0.19862	1.87101	1.88467
J3-5B	0.27413	0.29019	1.12932	1.13966	-0.17429	-0.14681	1.83381	1.85149
J3-5C	0.30774	0.31754	1.11260	1.11859	-0.25443	-0.23672	1.88764	1.89847
J3-6A	0.26924	0.28813	1.13032	1.14242	-0.20991	-0.18067	1.84925	1.86797
J3-6B	0.29800	0.30979	1.11588	1.12321	-0.22499	-0.20386	1.86421	1.87736
J3-6C	0.26500	0.28037	1.13717	1.14742	-0.13853	-0.11401	1.79892	1.81527

Appendix H

Fractal Analysis Results

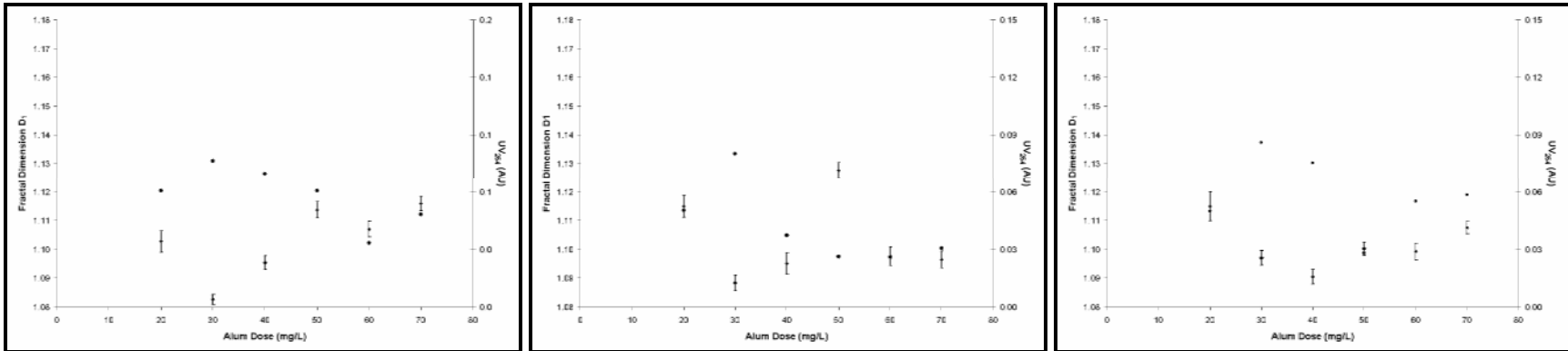


Figure H.1: Comparing aggregate D_1 to residual UV_{254} for alum coagulation at 5, 15 and 25 °C, respectively.

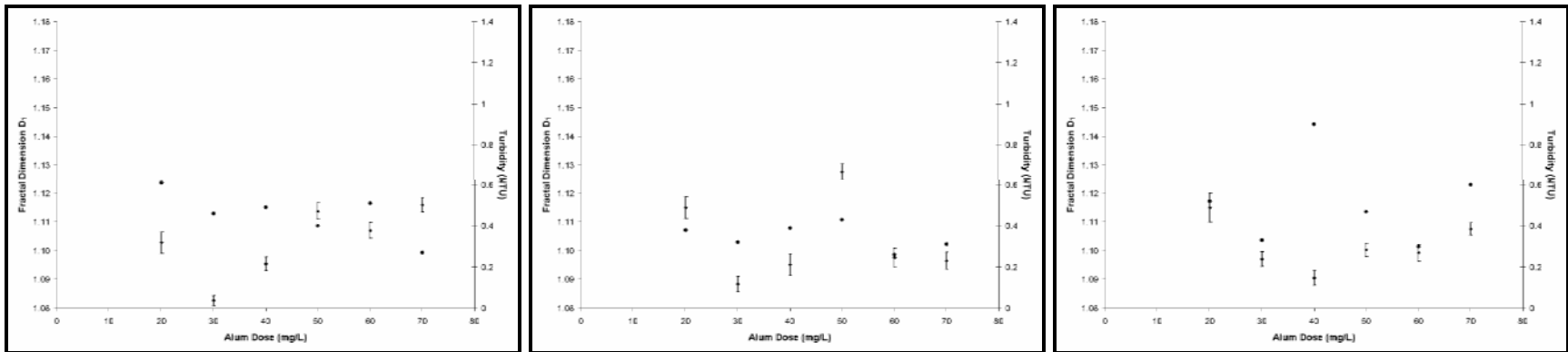


Figure H.2: Comparing aggregate D_1 to residual turbidity for alum coagulation at 5, 15 and 25 °C, respectively.

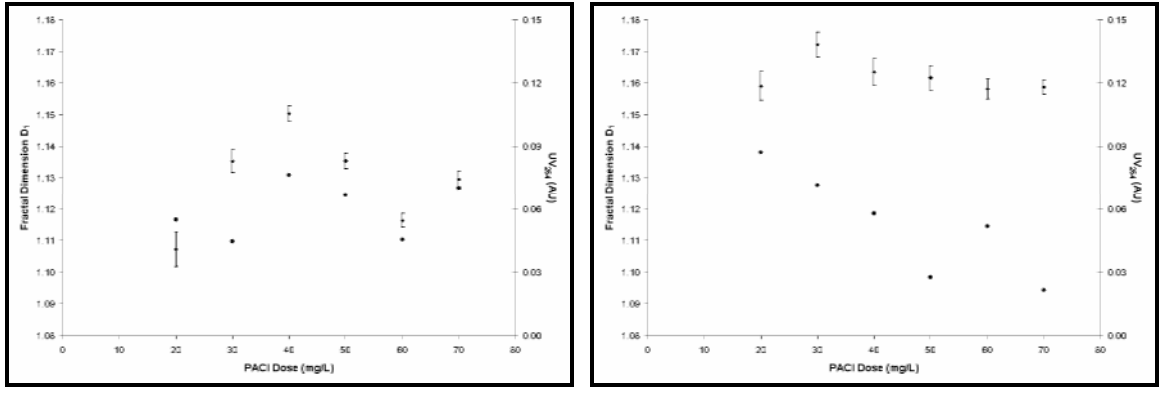


Figure H.3: Comparing aggregate D_1 to residual UV₂₅₄ for PACI coagulation at 5 and 25 °C, respectively.

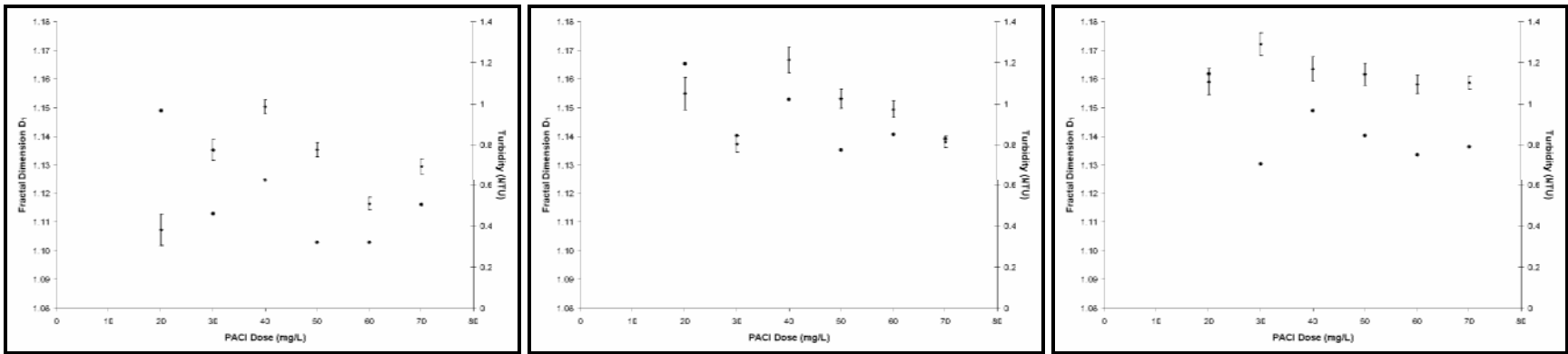


Figure H.4: Comparing aggregate D_1 to residual turbidity for PACI coagulation at 5, 15 and 25 °C, respectively.

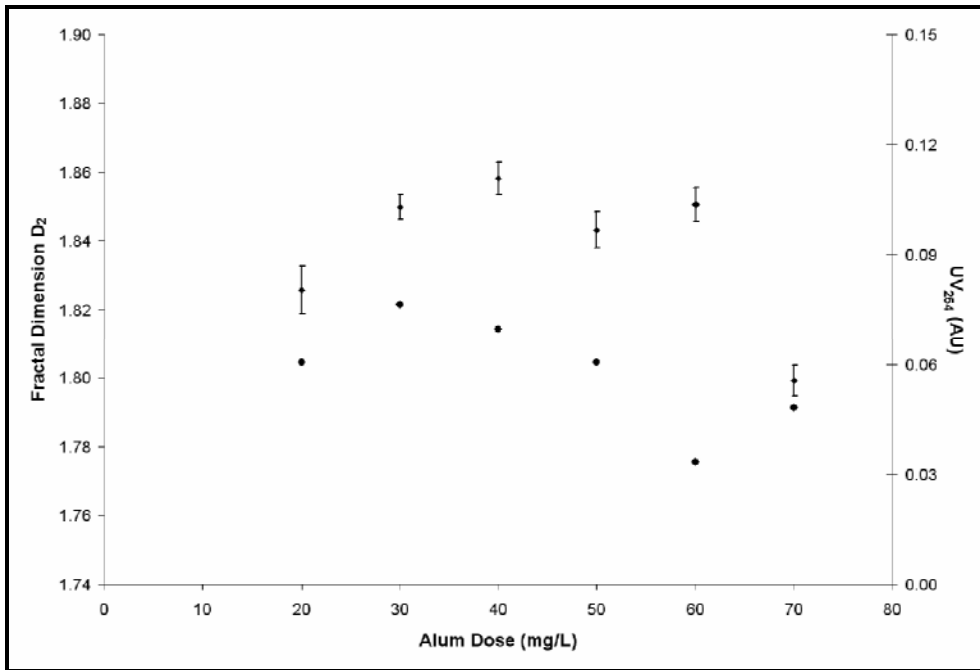


Figure H.5: Comparing aggregate D_2 to residual UV_{254} for alum coagulation at 5 °C.

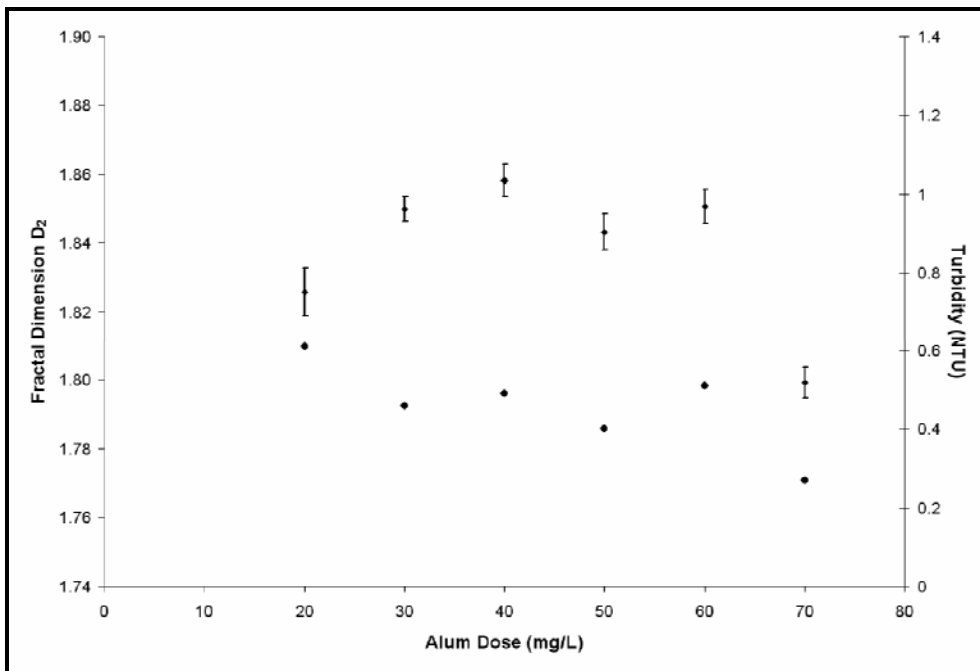


Figure H.6: Comparing aggregate D_2 to residual turbidity for alum coagulation at 5 °C.

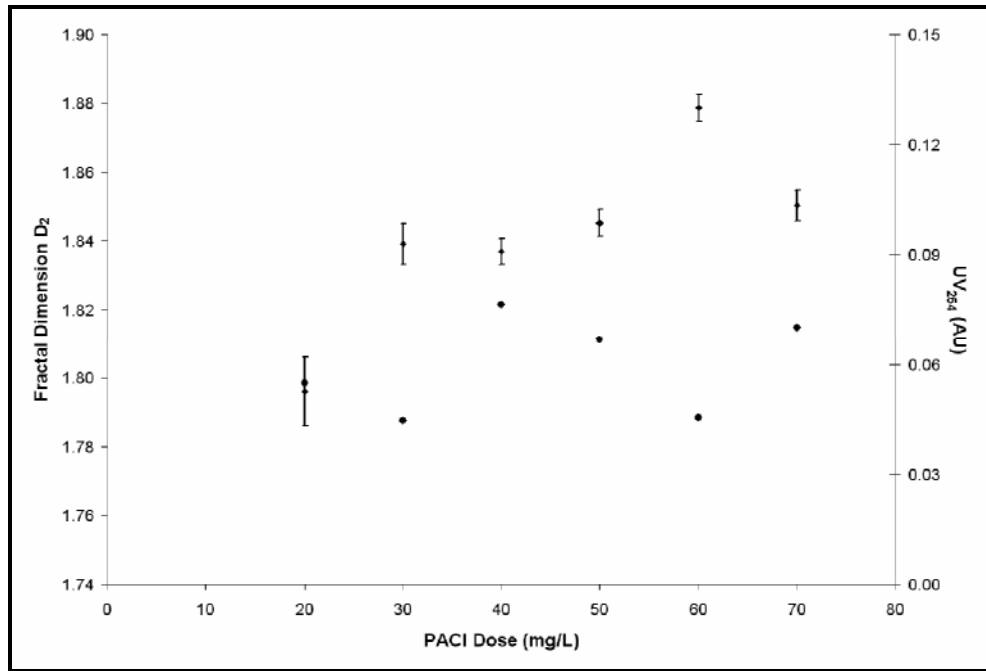


Figure H.7: Comparing aggregate D_2 to residual UV_{254} for PACI coagulation at 5 °C.

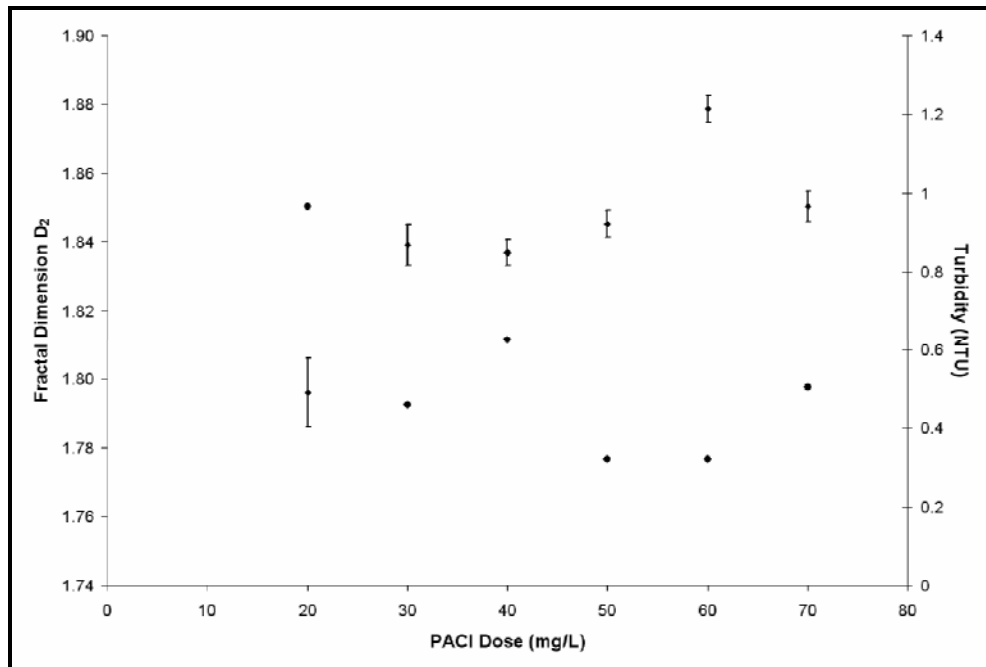


Figure H.8: Comparing aggregate D_2 to residual turbidity for PACI coagulation at 5 °C.

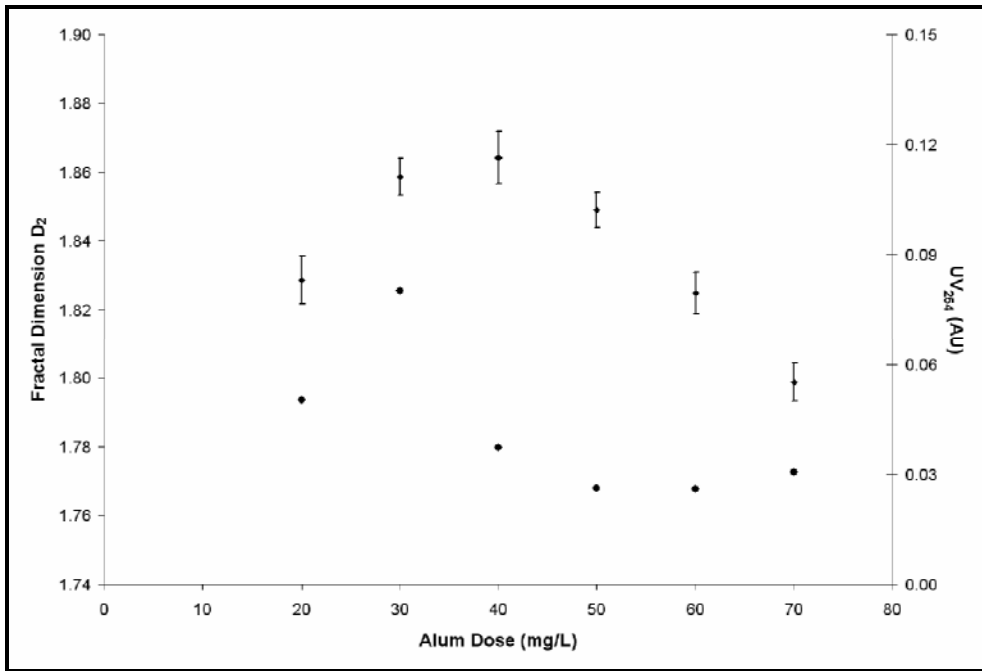


Figure H.9: Comparing aggregate D_2 to residual UV_{254} for alum coagulation at 15 °C.

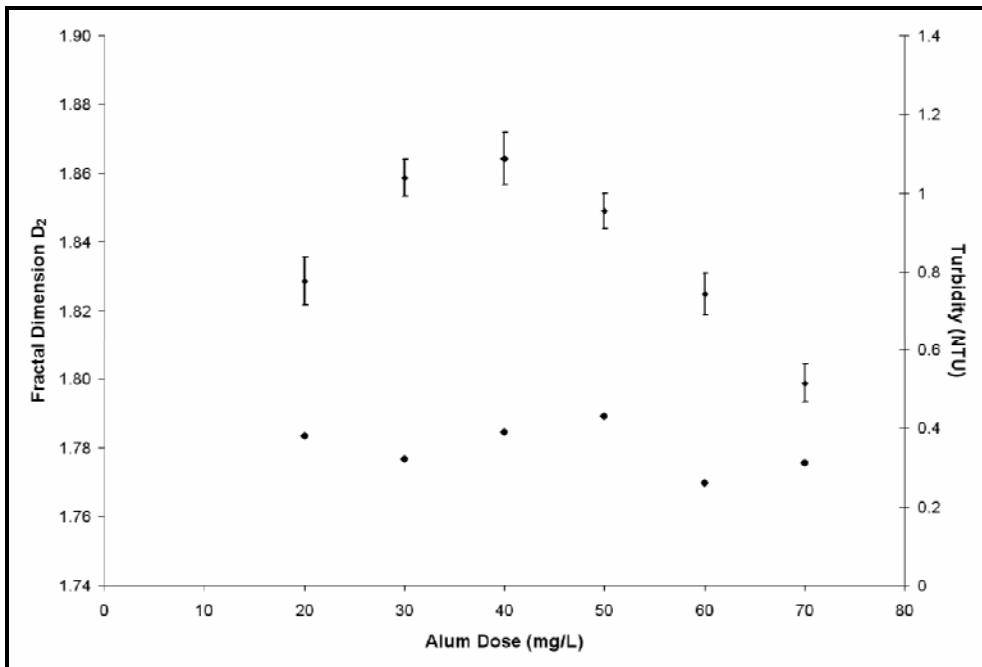


Figure H.10: Comparing aggregate D_2 to residual turbidity for alum coagulation at 15 °C.

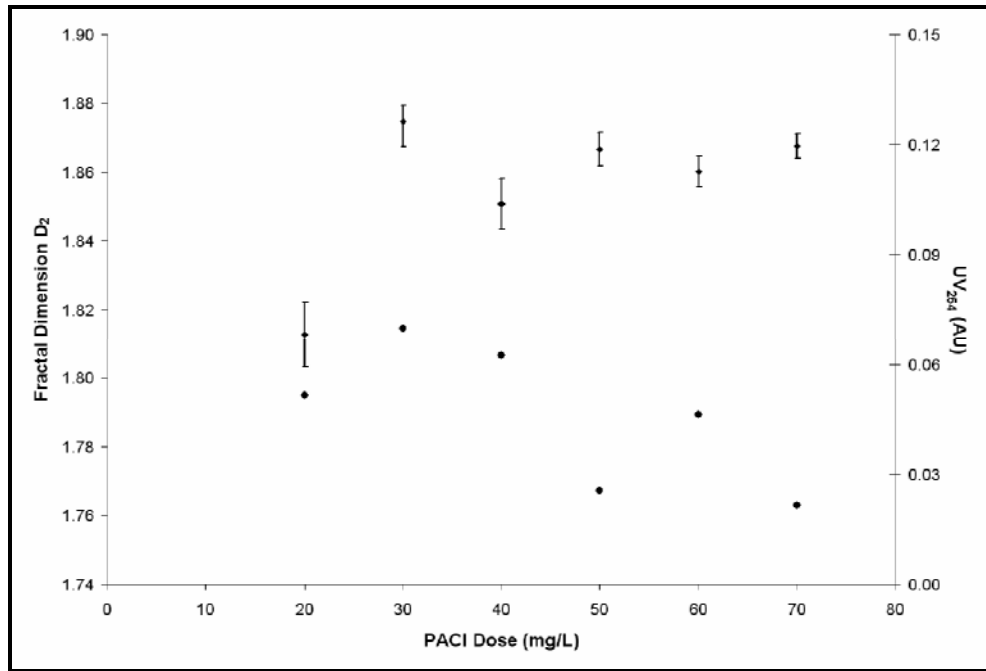


Figure H.11: Comparing aggregate D_2 to residual UV_{254} for PACI coagulation at 15 °C.

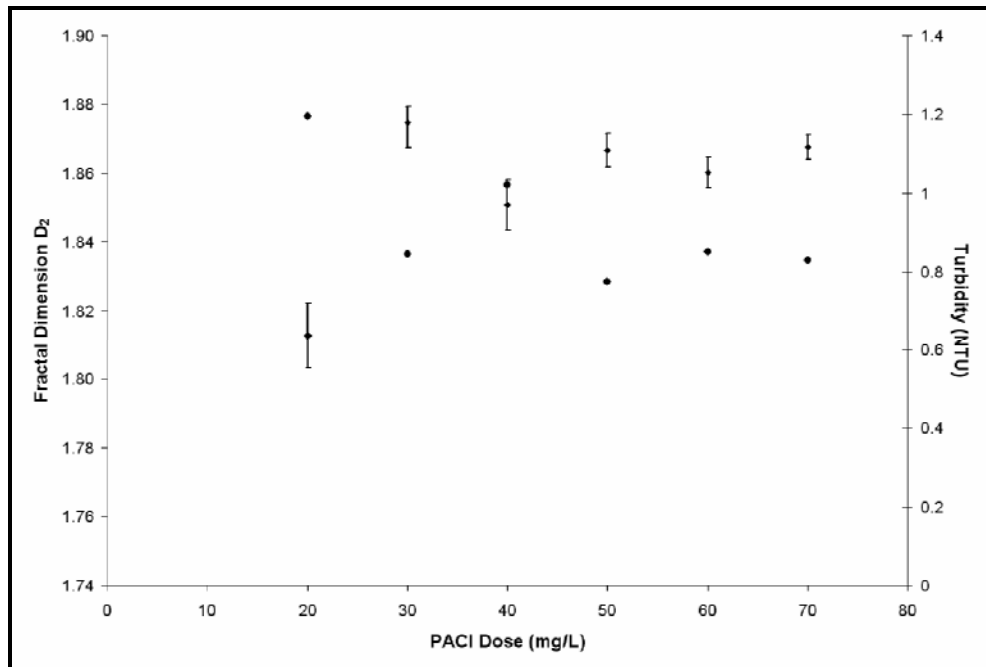


Figure H.12: Comparing aggregate D_2 to residual turbidity for PACI coagulation at 15 °C.

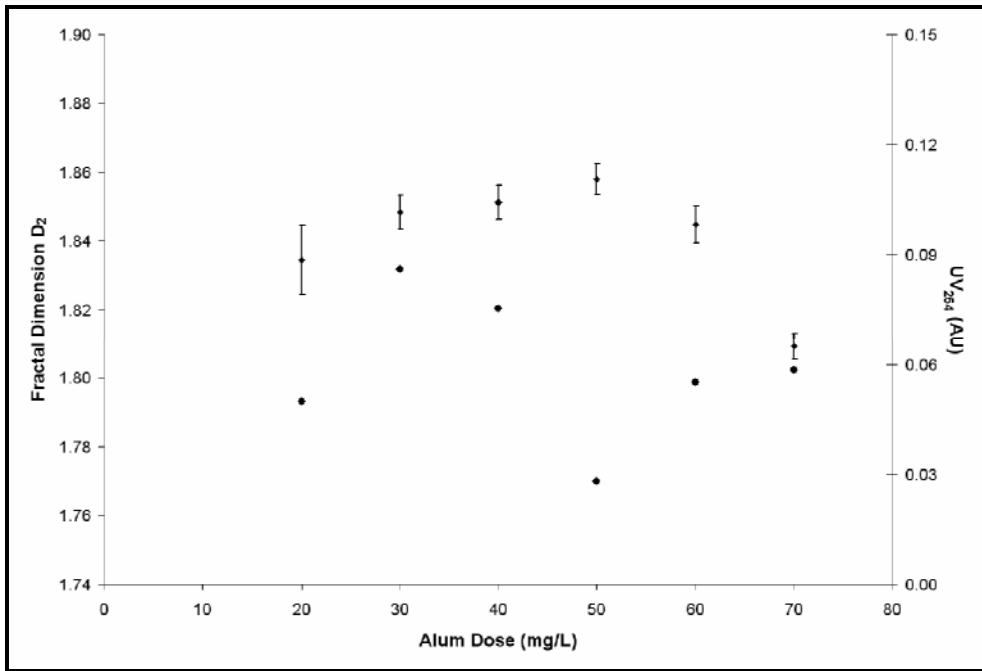


Figure H.13: Comparing aggregate D_2 to residual UV_{254} for alum coagulation at 25 °C.

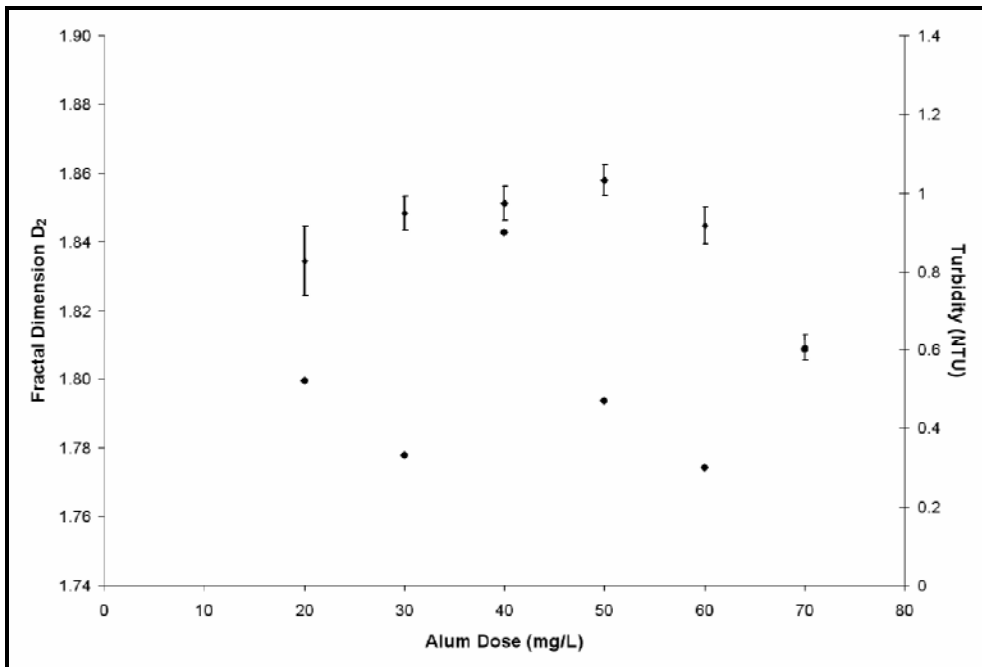


Figure H.14: Comparing aggregate D_2 to residual turbidity for alum coagulation at 25 °C.

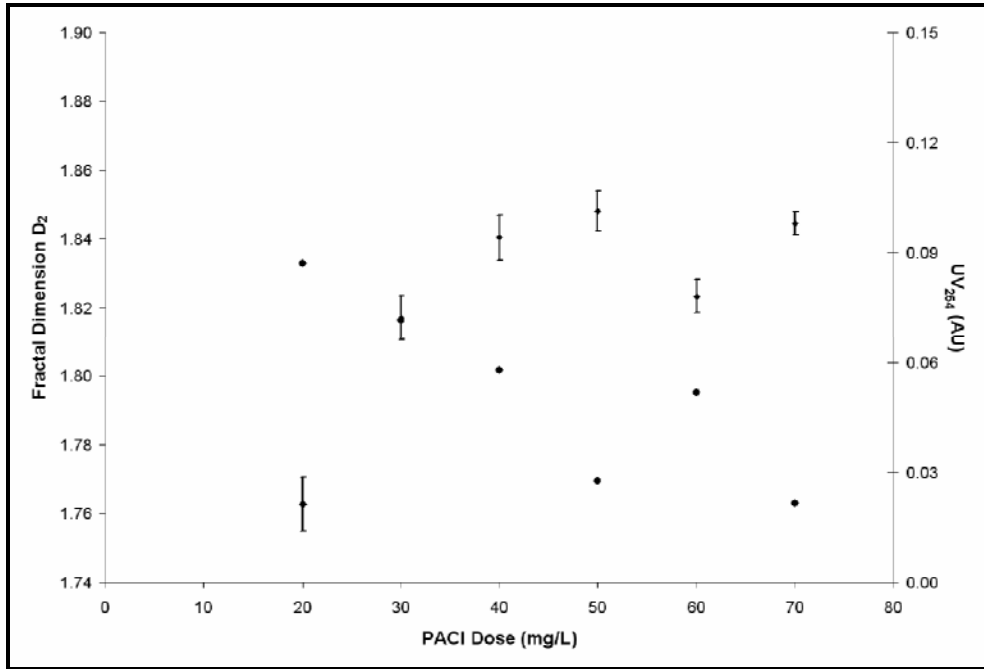


Figure H.15: Comparing aggregate D_2 to residual UV_{254} for PACI coagulation at 25 °C.

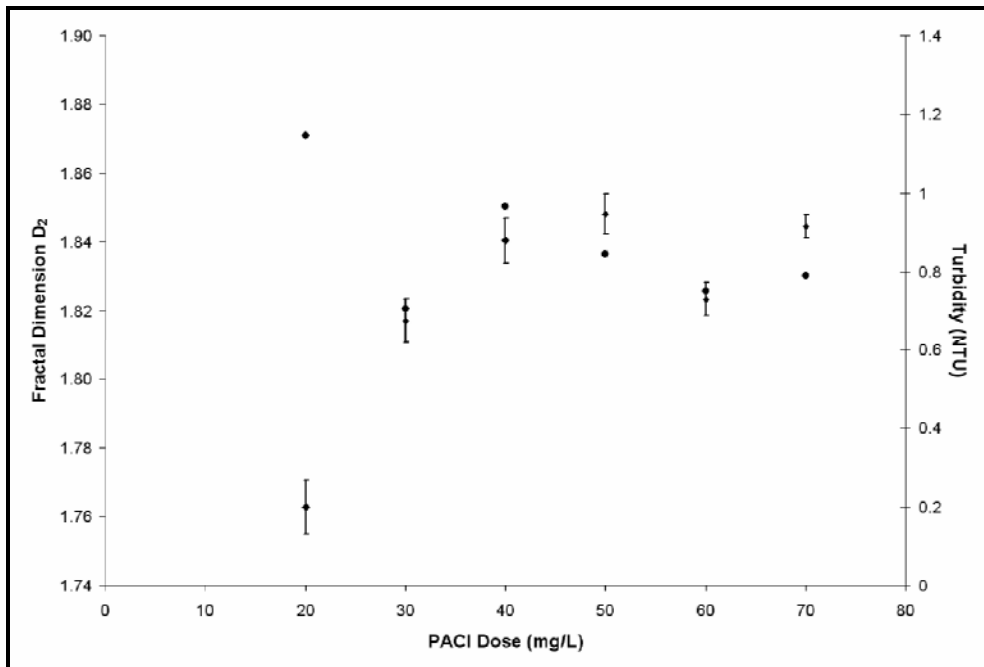


Figure H.16: Comparing aggregate D_2 to residual turbidity for PACI coagulation at 25 °C.

Appendix I

Statistical Assessment SPSS Output

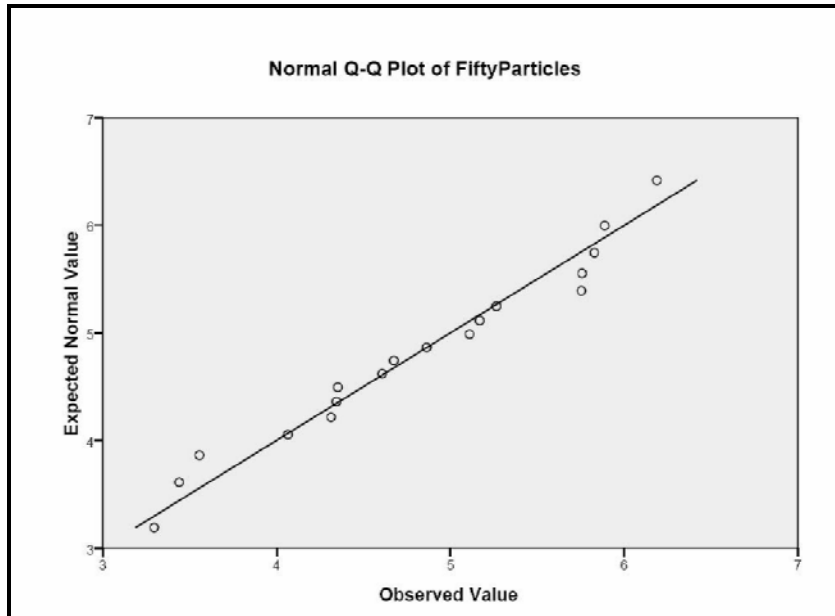


Figure I. 1: Q-Q plot of log-normally distributed engineered flocs and raw water particles (n=50).

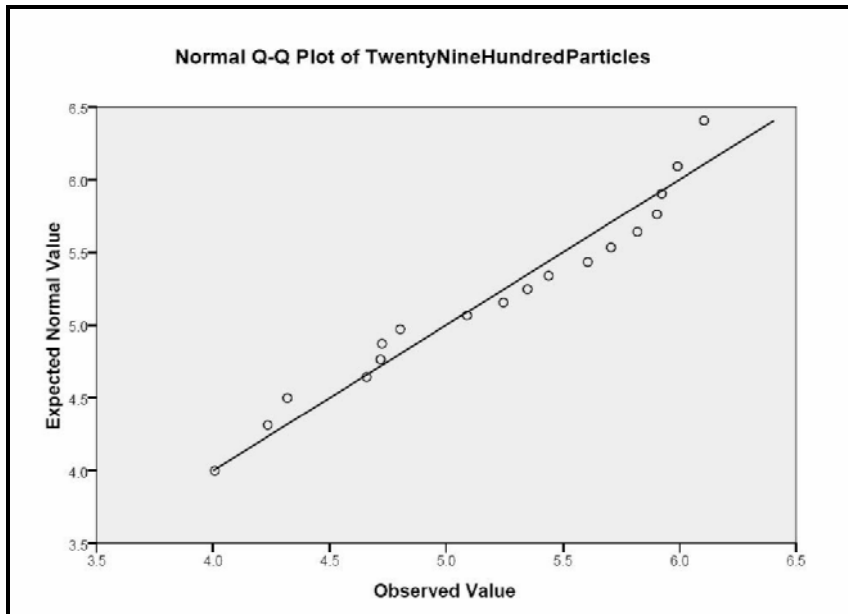


Figure I. 2: Q-Q plot of log-normally distributed engineered flocs and raw water particles (n=2900).

Multivariate Tests^d

Effect		Value	F	Hypothesis df	Error df	Sig.
Count	Pillai's Trace	.750	4.802 ^a	5.000	8.000	.025
	Wilks' Lambda	.250	4.802 ^a	5.000	8.000	.025
	Hotelling's Trace	3.001	4.802 ^a	5.000	8.000	.025
	Roy's Largest Root	3.001	4.802 ^a	5.000	8.000	.025
Count * Magnification	Pillai's Trace	.000	^a	.000	.000	.
	Wilks' Lambda	1.000	^a	.000	10.000	.
	Hotelling's Trace	.000	^a	.000	2.000	.
	Roy's Largest Root	.000	.000 ^a	5.000	7.000	1.000
Count * Matrix	Pillai's Trace	1.472	1.281	20.000	44.000	.242
	Wilks' Lambda	.135	1.140	20.000	27.483	.369
	Hotelling's Trace	2.913	.947	20.000	26.000	.544
	Roy's Largest Root	1.609	3.539 ^c	5.000	11.000	.038
Count * Magnification * Matrix	Pillai's Trace	.000	^a	.000	.000	.
	Wilks' Lambda	1.000	^a	.000	10.000	.
	Hotelling's Trace	.000	^a	.000	2.000	.
	Roy's Largest Root	.000	.000 ^a	5.000	7.000	1.000

a. Exact statistic

b. Computed using alpha = .05

c. The statistic is an upper bound on F that yields a lower bound on the significance level.

d. Design: Intercept + Magnification + Matrix + Magnification * Matrix
Within Subjects Design: Count

Tests of Within-Subjects Contrasts

Measure: MEASURE_1

Source	Count	Type III Sum of Squares	df	Mean Square	F	Sig.
Count	Level 2 vs. Level 1	.405	1	.405	9.882	.008
	Level 3 vs. Previous	1.778	1	1.778	8.926	.011
	Level 4 vs. Previous	1.371	1	1.371	13.190	.003
	Level 5 vs. Previous	.525	1	.525	8.339	.014
	Level 6 vs. Previous	.238	1	.238	7.486	.018
Count * Magnification	Level 2 vs. Level 1	.000	0	.	.	.
	Level 3 vs. Previous	.000	0	.	.	.
	Level 4 vs. Previous	.000	0	.	.	.
	Level 5 vs. Previous	.000	0	.	.	.
	Level 6 vs. Previous	.000	0	.	.	.
Count * Matrix	Level 2 vs. Level 1	.242	4	.061	1.480	.269

a. Computed using alpha = .05

Tests of Within-Subjects Contrasts

Measure: MEASURE_1

Source	Count	Type III Sum of Squares	df	Mean Square	F	Sig.
Count * Matrix	Level 3 vs. Previous	1.390	4	.348	1.745	.205
	Level 4 vs. Previous	.735	4	.184	1.769	.200
	Level 5 vs. Previous	.387	4	.097	1.536	.254
	Level 6 vs. Previous	.197	4	.049	1.548	.250
Count * Magnification * Matrix	Level 2 vs. Level 1	.000	0	.	.	.
	Level 3 vs. Previous	.000	0	.	.	.
	Level 4 vs. Previous	.000	0	.	.	.
	Level 5 vs. Previous	.000	0	.	.	.
	Level 6 vs. Previous	.000	0	.	.	.
Error(Count)	Level 2 vs. Level 1	.491	12	.041		
	Level 3 vs. Previous	2.390	12	.199		
	Level 4 vs. Previous	1.247	12	.104		
	Level 5 vs. Previous	.755	12	.063		
	Level 6 vs. Previous	.381	12	.032		

a. Computed using alpha = .05

Levene's Test of Equality of Error Variances^a

	F	df1	df2	Sig.
FiftyParticles	2.518	5	12	.088
OneHundredParticles	2.556	5	12	.085
FiveHundredParticles	1.093	5	12	.413
OneThousandParticles	3.967	5	12	.023
TwoThousandParticles	3.106	5	12	.050
TwentyNineHundred Particles	2.263	5	12	.114

Tests the null hypothesis that the error variance of the dependent variable is equal across groups.

a. Design: Intercept + Magnification + Matrix + Magnification * Matrix
Within Subjects Design: Count

Tests of Between-Subjects Effects

Measure: MEASURE_1

Transformed Variable: Average

Source	Type III Sum of Squares	df	Mean Square	F	Sig.	Noncent. Parameter
Intercept	469.222	1	469.222	10173.914	.000	10173.914
Magnification	.000	0000
Matrix	1.252	4	.313	6.785	.004	27.141

a. Computed using alpha = .05

Multiple Comparisons Tests				
Test	Matrix i	Matrix j	Significance	
Tamhane	F1	F2	1.000	
		F3	0.999	
		R1	0.002	
			R2	0.040
			R3	0.043
	F2	F3	1.000	
		R1	0.077	
		R2	0.384	
			R3	0.435
	F3	R1	0.060	
		R2	0.354	
		R3	0.387	
R1	R2	0.178		
	R3	0.057		
	R3	0.908		
Dunnnett T3	F1	F2	0.981	
		F3	0.950	
		R1	0.001	
			R2	0.014
			R3	0.022
	F2	F3	1.000	
		R1	0.032	
		R2	0.140	
			R3	0.215
	F3	R1	0.025	
		R2	0.128	
		R3	0.198	
R1	R2	0.066		
	R3	0.029		
	R3	0.566		
Games-Howell	F1	F2	0.920	
		F3	0.861	
		R1	0.001	
			R2	0.011
			R3	0.017
	F2	F3	1.000	
		R1	0.024	
		R2	0.113	
			R3	0.166
	F3	R1	0.019	
		R2	0.103	
		R3	0.152	
R1	R2	0.052		
	R3	0.022		
	R3	0.467		

Significance Level $\alpha = 0.05$

F = Engineered flocs, R = Raw water particles